Oxidative Medicine and Cellular Longevity

Oxidative Stress to Promote Cell Death or Survival

Guest Editors: Michela Battistelli, Manuela Malatesta, and Stefania Meschini

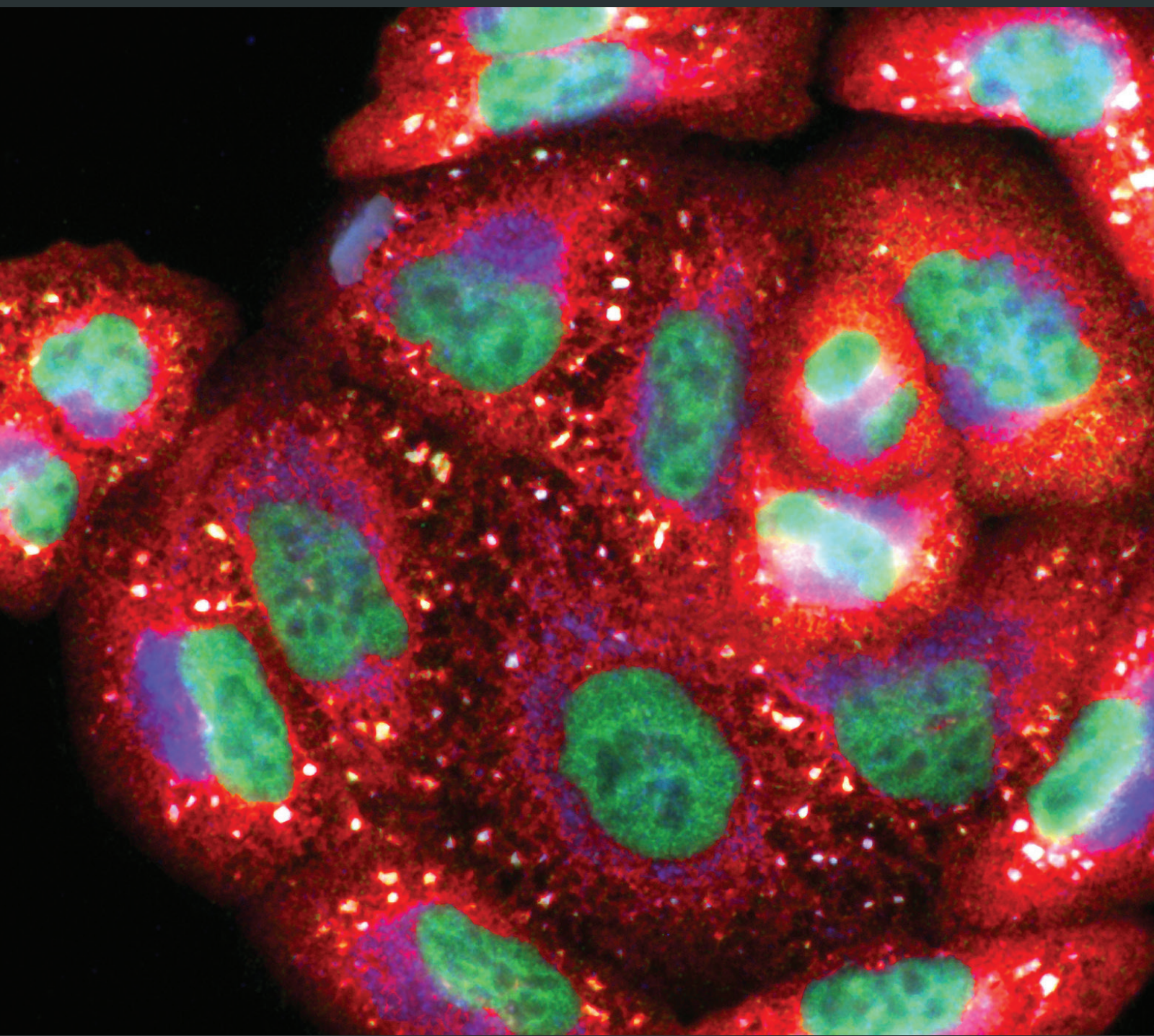

Oxidative Stress to Promote Cell Death or Survival

Oxidative Medicine and Cellular Longevity

Oxidative Stress to Promote Cell Death or Survival

Guest Editors: Michela Battistelli, Manuela Malatesta, and Stefania Meschini

Editorial Board

Contents

Hindawi Publishing Corporation
Oxidative Medicine and Cellular Longevity
Volume 2016, Article ID 2054650, 2 pages
http://dx.doi.org/10.1155/2016/2054650

Editorial

Oxidative Stress to Promote Cell Death or Survival

Michela Battistelli,[1] Manuela Malatesta,[2] and Stefania Meschini[3]

[1]*Department of Earth, Life and Environmental Sciences, University of Urbino Carlo Bo, Campus Scientifico "E. Mattei", Via Ca' le Suore 2, 61029 Urbino, Italy*
[2]*Department of Neurological and Movement Sciences, Anatomy and Histology Section, University of Verona, Strada le Grazie 8, 37134 Verona, Italy*
[3]*Department of Technology and Health, Istituto Superiore di Sanità, Viale Regina Elena 299, 00161 Rome, Italy*

Correspondence should be addressed to Michela Battistelli; michela.battistelli@uniurb.it

Received 22 October 2015; Accepted 4 November 2015

Oxidative stress is one of the mechanisms through which cells respond by activating pathways of cell survival or programmed cell death. The initial response of the cell to a stressful stimulus is activated for helping the cell to defend itself and respond positively to the insult. If the insult is very harmful and unresolved, it is the activation of programmed cell death by the cell itself with the aim of eliminating damaged cells without the presence of the inflammatory process.

The survival of a cell depends on the ability to activate an appropriate response to environmental and intracellular stimuli; this explains why the reaction is very conserved in evolution. In fact, the defense mechanisms of the cell through the activation of antioxidant systems against oxidative damage or stress proteins as the "heat shock proteins" occur both in lower organisms and in mammals.

The cells can be subjected to different types of stress and the response of the cells depends on the type and the level of insult.

For example, the attempt of survival is induced by a cell in the case of the heat shock response or the unfolded proteins response leading to activation of chaperone protein that increases the ability of the protein to fold, by counteracting induced stress and so promoting the cell survival. Thus, it is the adaptability of a cell to define its fate.

The cell is able to activate various cellular defense mechanisms and survival according to the level and mode of stress. If, however, these mechanisms are not activated successfully, then different types of cell death are promoted. The main mechanisms of cell death are apoptosis, necrosis, pyroptosis, and autophagic cell death. The activation of one mechanism of death or another depends on the cellular capacity to deal with the condition of suffering to which it is exposed. In this section, we wanted to learn about these topics:

(i) T. Yan et al. studied the effect of excessive alcohol consumption on brain tissue damage and cognitive dysfunction. They have shown that heavy drinking is associated with an earlier onset of neurodegenerative diseases such as Alzheimer's disease. They concluded that acetaldehyde induces cytotoxicity of SH-SY5Y cells via promotion of apoptotic signaling, inhibition of cell survival pathway, and induction of oxidative stress. So the inhibition of oxidative stress by antioxidants may be beneficial for preventing neuronal damage associated with acetaldehyde-induced cytotoxicity which could result from excessive alcohol consumption.

(ii) L. S. de Castro et al. analyzed the influence of oxidative status on spermatozoa by distinct mechanisms, from capacitation to fertilization.

They concluded that sperm, when exposed to oxidative environment, may present impaired motility traits, prooxidative status, and premature capacitation; such alterations resulting from embryo development fail, from the first cleavage to blastocyst.

(iii) T. Dou et al. assumed that herbicides and pesticides have been linked to nigrostriatal damage and the emergence of Parkinson symptoms in epidemiological and

animal studies and have investigated the oxidative stress effect of paraquat (PQ), a widely used herbicide in the world, on immortalized human embryonic neural progenitor cells (hNPCs).

They demonstrated that PQ exposure could significantly induce oxidative stress and cause oxidative imbalance.

(iv) S. Bekeschus et al. have studied the plasma composition and the beneficial role of cold plasmas in human pathologies such as wound healing. These studies demonstrated an effective antioxidant power by the cold blood cells subjected to inflammatory process.

(v) L. Dyugovskaya et al. wanted to elucidate the conditions and mechanisms involved in Gφ formation. Gφ formation may provide insights into basic neutrophil biology in inflammatory and atherogenic conditions or in the resolution of neutrophilic inflammation. Moreover, the a priori low yield of Gφ may indicate that they have a unique function and may represent a subgroup of progenitor cells.

(vi) X. Tang et al. assumed that the human Circadian Locomotor Output Cycle protein Kaput (CLOCK) gene was originally discovered as a regulator of essential human daily rhythms. They investigated the role of hCLOCK in the hypoxia-oxidative stress response system at the biochemical level.

They demonstrated that hypoxic states induced vascular oxidative damage and inflammation via hCLOCK-mediated production of ROS, with subsequent activation of the RhoA and NF-κB pathways.

This special issue treated, in a multidisciplinary way, the oxidative stress topic.

Michela Battistelli
Manuela Malatesta
Stefania Meschini

Hindawi Publishing Corporation
Oxidative Medicine and Cellular Longevity
Volume 2016, Article ID 8213071, 12 pages
http://dx.doi.org/10.1155/2016/8213071

Research Article

Sperm Oxidative Stress Is Detrimental to Embryo Development: A Dose-Dependent Study Model and a New and More Sensitive Oxidative Status Evaluation

Letícia S. de Castro,[1] Patrícia M. de Assis,[1] Adriano F. P. Siqueira,[1] Thais R. S. Hamilton,[1] Camilla M. Mendes,[1,2] João D. A. Losano,[3] Marcílio Nichi,[3] José A. Visintin,[1,2] and Mayra E. O. A. Assumpção[1]

[1]*Laboratory of Spermatozoa Biology, Department of Animal Reproduction, School of Veterinary Medicine and Animal Science, University of Sao Paulo, Avenida Prof. Dr. Orlando Marques de Paiva 87, Cidade Universitária, 05508-270 Sao Paulo, SP, Brazil*
[2]*Laboratory of In Vitro Fertilization, Cloning and Animal Transgenesis, Department of Animal Reproduction, School of Veterinary Medicine and Animal Science, University of Sao Paulo, Sao Paulo, Brazil*
[3]*Laboratory of Andrology, Department of Animal Reproduction, School of Veterinary Medicine and Animal Science, University of Sao Paulo, Sao Paulo, Brazil*

Correspondence should be addressed to Mayra E. O. A. Assumpção; meoaa@usp.br

Received 12 June 2015; Accepted 31 August 2015

Academic Editor: Manuela Malatesta

Our study aimed to assess the impact of sperm oxidative stress on embryo development by means of a dose-dependent model. In experiment 1, straws from five bulls were subjected to incubation with increasing H_2O_2 doses (0, 12.5, 25, and 50 μM). Motility parameters were evaluated by Computed Assisted System Analysis (CASA). Experiment 2 was designed to study a high (50 μM) and low dose (12.5 μM) of H_2O_2 compared to a control (0 μM). Samples were incubated and further used for *in vitro* fertilization. Analyses of motility (CASA), oxidative status (CellROX green and 2'-7' dichlorofluorescein diacetate), mitochondrial potential (JC-1), chromatin integrity (AO), and sperm capacitation status (chlortetracycline) were performed. Embryos were evaluated based on fast cleavage (30 h.p.i.), cleavage ($D = 3$), development ($D = 5$), and blastocyst rates ($D = 8$). We observed a dose-dependent deleterious effect of H_2O_2 on motility and increase on the percentages of positive cells for CellROX green, capacitated sperm, and AO. A decrease on cleavage and blastocyst rates was observed as H_2O_2 increased. Also, we detected a blockage on embryo development. We concluded that sperm when exposed to oxidative environment presents impaired motility traits, prooxidative status, and premature capacitation; such alterations resulting in embryo development fail.

1. Introduction

In vitro embryo production (IVP) in human represents an alternative for couples who are unable to naturally conceive, even after programmed intercourse or artificial insemination [1]. On the other hand, when focusing on animal reproduction, IVP is widely used with the main purpose of reducing the interval between generations, especially in cattle. In this scenario, Brazil stands out, responsible for 86% of *in vitro* produced embryos worldwide [2]. However, the extreme variability in IVP results limits the widespread use of this biotechnology.

One of the reasons for the inconsistent results of IVP is the individual effect of bull, known to strongly influence embryo development capacity [3, 4]. This may occur because spermatozoa may determine the moment [5] and the duration [6] of the first cleavage. In human, many studies have already demonstrated the influence of spermatozoa on embryo development, whether by extranuclear [7–9] or nuclear components [10–12].

In vitro and *in vivo* embryo production systems have some disparities with an important difference associated with oxygen concentrations. Values of approximately 20% of oxygen in the air normally used in IVP labs are superior to those found in the oviduct and uterus of most mammals [13]. The exposure of gametes and embryos to this excessive oxygen concentration during manipulations may lead to an inevitable increase in reactive oxygen species (ROS) production. A meta-analysis study in human has correlated increased ROS levels in the spermatozoa to subsequent impaired fertilization rate when using assisted reproduction techniques [14]. This result indicates that previous semen analysis for oxidative status may be essential towards attempts to predict IVP outcome and further course of procedures. In fact, previous study with primate oocytes undergoing intracytoplasmic sperm injection (ICSI) with spermatozoa exposed to oxidative stress revealed consequent fail in embryo development and high rates of blastomeric nuclear fragmentation [15]. Also, in bovine spermatozoa, Simões et al. [16] verified a negative correlation between sperm susceptibility to oxidative stress and cleavage and blastocyst rates. All these data suggest that spermatozoa when exposed to an oxidative environment may retain physical and chemical modifications potentially detrimental for embryo cytoplasmic and/or nuclear components, which may negatively affect embryo viability.

Another factor that may intensify sperm oxidative damage, influencing IVP results, is the process of cryopreservation, considering that the main source of male gametes for bovine *in vitro* fertilization is frozen semen. The process of cell cryopreservation has been related to ROS overproduction leading to cellular damage, especially due to lipid peroxidation, in different species including bovine sperm [17–20]. Also, during this process, the necessity of diluting or removing seminal plasma, the main source of antioxidant for spermatozoa, may increase the susceptibility of sperm to oxidative damage [21].

ROS generation in the spermatozoa can occur in the electron transport chain or though the NADPH oxidase activity [22]. Sperm energetic demand is extremely high and, therefore, mitochondrial activity is compensatively elevated. Probably, excessive mitochondrial ROS production may overcome the limited antioxidant machinery almost instantaneously. In sperm, ROS are known to participate in several physiological mechanisms such as capacitation, hyperactivation, and binding to the oocyte [23, 24]. Nevertheless, ROS are usually seen as a threat to cell integrity. Specific probes for ROS production show that free radicals may lead to membrane lipid peroxidation and decreased motility [25, 26]. Also, despite being highly compacted by protamine [27], sperm DNA is an important target for the attack of ROS, which leads to the formation of adducts between nitrogen bases, destabilizing the DNA molecule, resulting in DNA-strand breaks [28]. Studies indicate that even when DNA is damaged, sperm is still able to fertilize the oocyte; non-repaired chromatin alterations have serious consequences for further embryo development [29–31]. In this context, our hypothesis is that bovine cryopreserved spermatozoa, when exposed to an oxidative environment, suffer injuries that will impact motility patterns and mitochondrial and DNA integrity, impairing fertilization ability and further *in vitro* embryo development. We evaluated the effect of oxidative stress induced by hydrogen peroxide on bovine sperm attributes (motility, mitochondrial membrane potential, oxidative and capacitation status, and DNA integrity) and subsequent *in vitro* embryo development. Furthermore, we propose a new and more sensitive flow cytometry method (CellROX green) to assess oxidative status of bovine sperm prior fertilization.

2. Material and Methods

This study was carried at the Animal Reproduction Department from the School of Veterinary Medicine and Animal Science of the University of São Paulo (VRA/FMVZ/USP). All procedures were performed according to the Bioethics Committee of the previously mentioned institution (protocol number 2710/2012).

2.1. Reagent and Solutions. All chemical reagents and solutions used in this study were purchased from Sigma-Aldrich (St. Louis, MO, USA) unless otherwise stated.

2.2. Experiment 1: Effect of Oxidative Stress Induction on Sperm Motility Related Variables. For this first experiment, thawed straws of the same batch from five Nelore bulls ($n = 5$), donated from Reproduction Centers, were used. Bulls were selected according to post-Percoll motility of at least 70%. This experiment was conducted in four replicates comprehended in a period of 2 weeks.

2.2.1. Semen Processing. In order to maintain the same condition of semen processing prior to *in vitro* fertilization (IVF), experiment 1 was conducted as follows: each straw (0.25 mL) was thawed at 37°C for 30 seconds and subjected to Percoll gradient (45% and 90%) at 9000 G/5 minutes. Motile cells (pellet) were recovered and washed with 1 mL of Sp-TALP [32] at 9000 G/3 minutes. This final pellet was then resuspended to a final concentration of 25×10^6 sptz/mL in Fert-TALP [32], with no capacitation agents (heparin, penicillamine, epinephrine, and hypotaurine). The same semen sample was divided between the experimental groups and incubated during 1 hour at 38.5°C, 5% CO_2 in air, and high humidity.

2.2.2. Oxidative Challenge with Hydrogen Peroxide. For oxidative stress induction, we used hydrogen peroxide 30% (Perhydrol, MERCK Millipore) diluted in Fert-TALP, for a final solution of 625 μM. Hydrogen peroxide is not a free radical (i.e., one or more unpaired electrons); however, this peroxide is considered an important reactive oxygen species due to the high capacity to move across biological membranes and the high affinity with iron and copper ions to produce more unstable and reactive radicals such as the hydroxyl. Experimental groups were 0 (control), 12.5, 25, and 50 μM of hydrogen peroxide.

2.2.3. Computer Assisted Sperm Motility Analysis (CASA). Motility parameters were evaluated using the Computer

Assisted Sperm Analysis system (CASA; IVOS, v. 12.2, Hamilton Thorn Research, Beverly, MA). Settings used, previously described by Goovaerts et al. [33], were 30 frames at a frame rate of 60 frames/s; minimum contrast = 20; minimum cell size = 5 pixels; motility > 30 μm/s; progressive motility > 50 μm/s; straightness > 70%. In brief, each slide was heated at 37°C; 5 μL of sample was placed in the slide and covered by a coverslip. A minimum of six fields were selected for analysis. Motility related variables considered were VAP (velocity average path), VCL (curvilinear velocity), VSL (straight-line velocity), BCF (beat cross frequency), ALH (amplitude of lateral head displacement), total and progressive motility, and percentage of cells with fast, medium, slow, and static movement. Among the previously mentioned variables, total and progressive motility were selected as more relevant for the selection of the hydrogen peroxide concentrations used in the second experiment.

2.3. Experiment 2: Effects of Sperm Oxidative Stress Challenge on Embryo Development. In this second experiment, for IVF, we used semen samples subjected to only two concentrations of hydrogen peroxide, selected according to experiment 1 results: 50 μM (high concentration) and 12.5 μM (low concentration) and a control group (0 μM). This induction aimed to compare the impact of oxidative stress on cleavage, embryo development, and blastocyst rates. This experiment was conducted in 10 replicates, during two months, using 200 to 220 oocytes per replicate. For IVP control, semen samples with no H_2O_2 and not submitted to incubation were used and we considered only replicates with control blastocyst rate ≥20% (data not shown).

2.3.1. In Vitro Embryo Production. Ovaries obtained from a slaughterhouse were transported to the laboratory in saline solution 0.9% at 30°C. Cumulus-oocytes complexes (COCs) were aspirated with an 18-gauge needle from 2 to 8 mm follicles. Oocytes with homogeneous ooplasm surrounded by more than two layers of compacted cumulus cells were selected for *in vitro* maturation (IVM). COCs selected were washed 3X in holding medium (TCM199 Hepes supplemented with 10% FCS (Gibco), 22 μg/mL pyruvate, and 50 μg/mL gentamycin) and 3X in IVM medium (TCM199 Bicarbonate supplemented with 10% FCS, 22 μg/mL pyruvate, 50 μg/mL gentamycin, 0.5 μg/mL FSH Folltropin-V (Vetrepharm, Inc., Belleville, ON, Canada), 50 μg/mL human chorionic gonadotrophin (Vetecor Laboratories, Calier, Spain), and 1 μg/mL of 17β-estradiol) and placed for maturation in 90 μL microdroplets of IVM medium (20–30 oocytes/drop), covered with mineral oil, during 22 to 24 hours at 38.5°C, 5% (v/v) CO_2 in air, and high humidity.

For IVF, the same semen processing and induction protocol described in experiment 1 were performed (using only three concentrations of hydrogen peroxide, 0, 50, and 12.5 μM). However, after concentration adjustment, we performed a pool of 3 bulls (same number of cells of each bull), in order to eliminate sire effect, and then divided the same sample between experimental groups. Matured oocytes were washed 3X in pre-IVF medium (TCM199 Hepes supplemented with 0.003% of BSA-V (m/v), 22 μg/mL pyruvate, and 50 μg/mL gentamycin) and 3X in Fert-TALP and placed for fertilization in 90 μL microdroplets of Fert-TALP (20–30 oocytes/drop) covered with mineral oil. At the end of semen incubation, samples were washed with 550 μL of Fert-TALP (9000 G/90 seconds). The sediment with sperm was recovered and used to inseminate microdroplets with oocytes (±100.000 sptz/drop) and the rest of the sample was used in subsequent sperm evaluations.

After IVF (18 hours; $D = 1$), putative zygotes were mechanically denuded by pipetting in pre-IVF medium and cultured in KSOM medium (Millipore Corporation, New Bedford, MA, USA) during 8 days at 38.5°C, 5% CO_2, 5% O_2, and 90% N_2, under high humidity. On third day of culture ($D = 3$), KSOM was supplemented with FCS to a final drop concentration of 5%.

2.3.2. Sperm Attributes Evaluations. CASA was performed as described in experiment 1. In addition, in this second experiment, we performed epifluorescence microscopy (Olympus IX80, Olympus Corporation, Tokyo, Japan) and flow cytometry evaluations (Guava EasyCyte Mini System, Guava Technologies, Hayward, CA, USA). This latter equipment contains a blue laser, which operates at 488 nm and emits a 20 mW visible laser radiation. A total of 10,000 events per sample were analyzed and data corresponding to yellow (PM1 photodetector, 583 nm), red (PM2 photodetector, 680 nm), and green fluorescent signals (PM3 photodetector, 525 nm) were recorded after a logarithmic amplification. For data analysis, cell doublets and debris were excluded using PM3/FSC (forward scatter) and all data was analyzed by FlowJo v10.2 software, except DNA integrity, which was evaluated using FlowJo v8.7 software.

2.3.3. Mitochondrial Membrane Potential Evaluated by JC-1 Probe. Mitochondrial membrane potential was evaluated by JC-1 probe (5,5′,6,6′-tetrachloro-1,1′,3,3′-tetraethylbenzimidazolylcarbocyanine chloride) (Invitrogen, Eugene, OR, USA). This probe emits green or red-orange fluorescence for low (LMM) or high mitochondrial potential (HMP), respectively. The procedure was performed with 187,500 cells diluted in Fert-TALP and stained with JC-1 (76.5 μM in DMSO), in the dark at 37°C. Samples were analyzed by flow cytometry after 10 minutes, excited at 488 nm, and detected at 590 nm. For positive control, we used the protocol described by Celeghini et al. [34], with some modifications. A sample of semen submitted to 10 cycles of freezing and thawing in liquid nitrogen to disruption of membranes was used, and, for negative control, we used sperm sample processed as described in experiment 1.

2.3.4. Oxidative Status Evaluated by 2′,7′-Dichlorofluorescein Diacetate (DCFH). For this assay, 187,500 cells were stained with a solution containing DCFH and propidium iodide (PI) at a final concentration of 9.3 μM and 6 μM, respectively, in the dark at 37°C. Samples were analyzed by flow cytometry after 5 minutes, excited at 488 nm, and detected at 630–650 nm (PI) and 515–530 nm (DCFH). For data analysis, we selected the population of cells PI-DCFH+ (without membrane alteration and stressed).

2.3.5. Oxidative Status Evaluated by CellROX Green. CellROX green (Molecular Probes, Eugene, OR, USA) is a fluorescent probe that penetrates the cell and, when oxidized by intracellular free radicals, binds to DNA, emitting a more intense green fluorescence. For this assay, 187,500 cells were stained with CellROX green (final concentration of 5 μM) for 30 minutes at 37°C, and, in the last 10 minutes, PI was added to a final concentration of 6 μM. Samples were analyzed by flow cytometry, excited at 488 nm, and detected at 630–650 nm (PI) and 515–530 nm (CellROX green). For data analysis, we selected the population of cells PI-VD+ (without membrane alteration and stressed). For CellROX green validation, we used increasing concentrations of hydrogen peroxide (0, 12.5, 50, and 200 μM, during 1 hour at 38.5°C, 5% CO_2, and high humidity), and the same sample stained with CellROX green was also stained with DCFH, in order to compare the two techniques.

2.3.6. Chromatin Analysis. Chromatin stability assay was based on sperm chromatin structure assay (SCSA; [35], as described by Simões et al. [16]. This assay is based on an acid challenge that denatures DNA molecules from a susceptible chromatin structure, breaking hydrogen bounds and separating DNAs' strands, allowing acridine orange (AO) probe to intercalate and emit red (denatured single-strand DNA) or green (double-strand DNA) fluorescence. The procedure was performed with 375,000 cells. Samples were incubated with TNE buffer (Tris-HCl 0.01 M, NaCl 0.15 M, EDTA 1 mM, and distilled water, pH 7.4) and acid detergent (HCl 0.08 M, NaCl 0.15 M, and Triton X-100 0.1% in distilled water, pH 1.2). After 30 seconds, AO solution was added (citric acid 0.1 M, Na2HPO4 0.2 M, EDTA 0.001 M, NaCl 0.15 M, and AO stock 6 μg/mL in distilled water, pH 6), and each sample was analyzed by flow cytometry after 5 minutes of incubation at 37°C, excited at 488 nm, and detected at 630–650 nm (red) and 515–530 nm (green). For positive control, a sample was incubated with hydrochloric acid (1.2 M in acid detergent, pH 0.1) and, for negative control, samples processed as described in experiment 1 were used.

2.3.7. Capacitation Status Evaluated by Chlortetracycline Assay (CTC). Capacitation status was evaluated by CTC assay as described by Ward and Storey [36] with some modifications. CTC penetrates through cellular membranes, increasing the fluorescent intensity when it binds with free calcium. An aliquot containing 375,000 cells was added to 20 μL chlortetracycline solution, prepared in the same day of each replicate (CTC 38 μM; stock solution: TRIS 20 mM, NaCl 130 mM, and L-cystein 4 mM). Samples were then fixed with 5 μL paraformaldehyde 4%. An aliquot of this suspension was placed in a glass slide, mixed with DABCO solution (1,4-diazabicyclo[2.2.2]octane) and glycerol (1 : 9), covered with coverslip, and kept at −20°C, protected from light until the evaluation. Two hundred cells were examined, under epifluorescence microscope (Olympus IX80), using magnification of 1000x with mineral oil. Filters of 355 and 465 nm were used for excitation and emission, respectively. Three cellular categories were classified: noncapacitated (even distribution of yellow fluorescent over the head), capacitated (only acrosome region stained in yellow), and reacted (no yellow fluorescent in the head).

2.3.8. Embryo Development Evaluations. Fast cleavage rate assessment was performed 30 hours after insemination (30 h.p.i), counting the number of structures that already showed fist cleavage at this point. Cleavage rate was assessed in the third day of culture ($D = 3$). Development rate was performed at fifth day of culture ($D = 5$), and, at this moment, embryos were classified in three categories according to developmental stage: noncleaved (NC), 2–4 cells, or 8–16 cells. Finally, at day eight of culture ($D = 8$), blastocyst rate was assessed. All these evaluations were made in stereomicroscope (Olympus TH3, Olympus Corporation) with 63x of magnification and the percentage of all rates was made over the total number of oocytes.

2.4. Statistical Analysis. Statistical analysis was performed using the software Statistical Analysis System 9.3 (SAS Institute, Cary, NC, USA). Data were tested for residue normality and variance homogeneity. Variables that did not comply with these statistical premises were subjected to transformations. We used PROC GLM for polynomial regression model in both experiments, considering treatment as main effect. On experiment 2, Spearman correlations analysis was performed to verify the correlation between variables analyzed, using PROC CORR procedure. In this case, groups were analyzed separately as control or treated (data of groups treated with 12.5 and 50 μM of hydrogen peroxide were pooled). Results were reported as untransformed means ± SEM. All statistical analyses were calculated with a significance level of 5%.

3. Results

3.1. Experiment 1: Hydrogen Peroxide Promotes a Dose-Dependent Decrease in Sperm Motility Related Variables. In the first experiment, we observed a negative effect of increasing concentrations of hydrogen peroxide for all motility related variables. This effect was evident for the velocity patterns revealed by the variables VAP, VSL, and VCL, which significantly decreased for all hydrogen peroxide concentrations. This decrease also occurred for BCF, however, in a more moderate pattern (Figure 1(a)). Total and progressive motility were also impaired while hydrogen peroxide concentrations increased, being more intensive between the concentrations of 25 and 50 μM (Figure 1(b)). Similarly, for sperm populations with fast, medium, slow, and static movement, there was a decrease in sperm population with fast movement with a consequent increase in the remaining populations according to the increase in hydrogen peroxide concentrations (Figure 1(c)). Media values, straight-line equation, and r^2 values of all variables with treatment effect ($p < 0.05$) are present in Supplementary Material available online at http://dx.doi.org/10.1155/2016/8213071 (Table S1).

Based on the straight-line equation generated for total and progressive motility (Table S1), we chose, for experiment 2, 12.5 and 50 μM concentrations of hydrogen peroxide. The criterion for such selection was a concentration that caused considerable oxidative damage but with acceptable motility

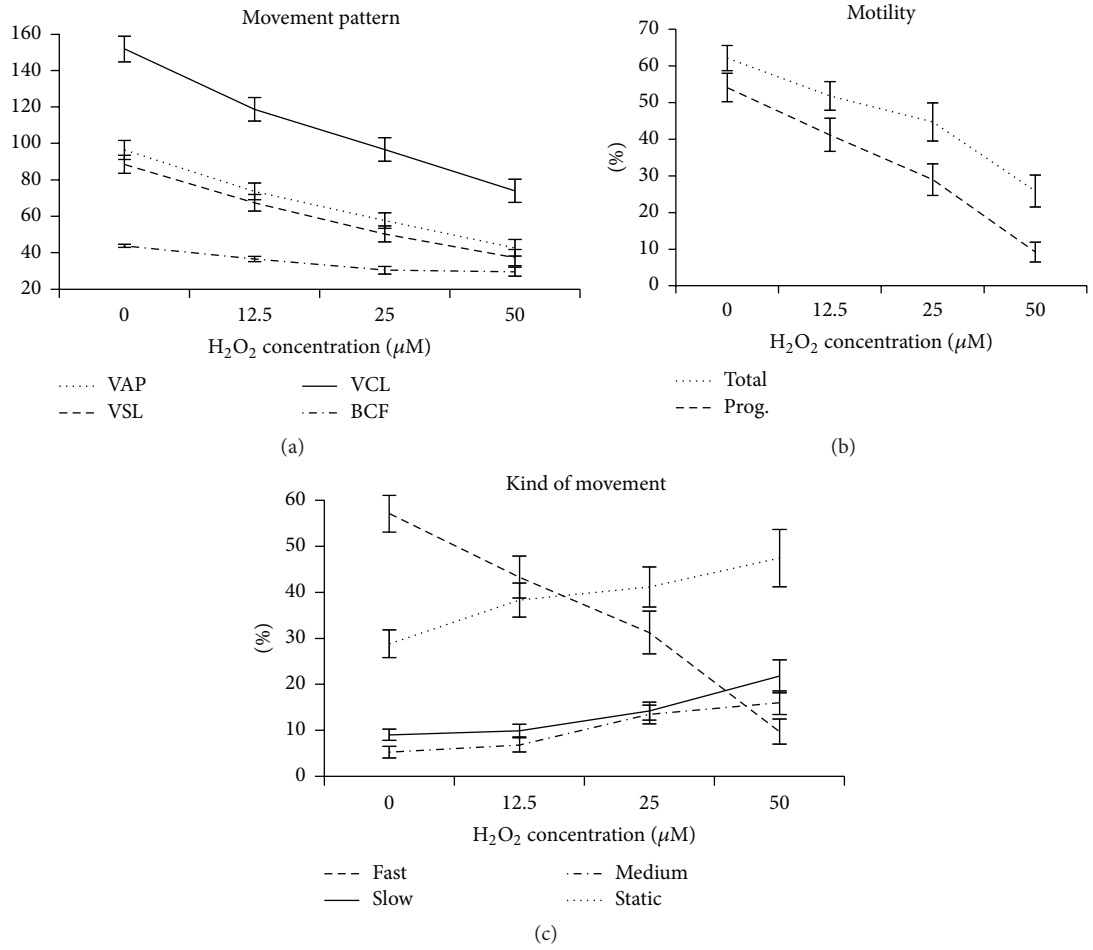

Figure 1: Spermatozoa motility parameters with treatment effect for hydrogen peroxide. (a) Units of VAP, VSL, and VCL = μm/s and BCF = hertz; (b) Total: total motility and Prog.: progressive motility.

for IVF (53% and 26% for total motility; and 41.7% and 8% for progressive motility, for the low and the high concentrations, resp.).

3.2. Experiment 2: Spermatozoa When Exposed to Hydrogen Peroxide Promote a Dose-Dependent Decrease in Embryo Development

3.2.1. CellROX Green Validation. In this validation, our results show more sensibility of CellROX green to detect increasing concentrations of hydrogen peroxide when compared to DCFH (Figure 2(a)). The same did not occur for DCFH (Figure 2(b)), since all concentrations have the same fluorescence intensity detected. We considered as more relevant, for both probes, the population of stressed cells with no membrane alteration (PI-DCFH+ or PI-VD+), once we speculate that these are the cells that still have the ability to fertilize the oocyte.

3.2.2. Sperm Evaluations. The dose-dependent effect of oxidative stress on sperm motility occurred in the second experiment, similarly to the first experiment (Figures 3(a) and 3(b)). However, with additional sperm analyses, we observed this dose-dependent effect on oxidative and capacitation status, as evaluated by CellROX green and chlortetracycline assay, respectively. No treatment effect was observed for mitochondrial membrane potential ($p = 0.13$) nor oxidative status analyzed by DCFH ($p = 0.09$).

We observed an increase in the percentage of cells with no membrane alteration and stressed (PI-VD+; Figure 2(c)) and capacitated cells (Figure 3(d)) according to the increase of hydrogen peroxide concentrations. There was no effect of treatment for other categories related to capacitation status as evaluated by CTC assay (noncapacitated and reacted). Finally, Figure 3(e) shows the increase in the percentage of cells positive for AO (i.e., chromatin alteration), with increasing doses of hydrogen peroxide.

3.2.3. Embryo Development. For IVP, all parameters related to embryo development showed treatment effect, except for the fast cleavage rate ($p = 0.15$). Figures 4(a) and 4(c) show, respectively, the negative effect of hydrogen peroxide concentration on both cleavage and blastocyst rates. Figure 4(b) illustrates embryo development rate, evaluated on the fifth

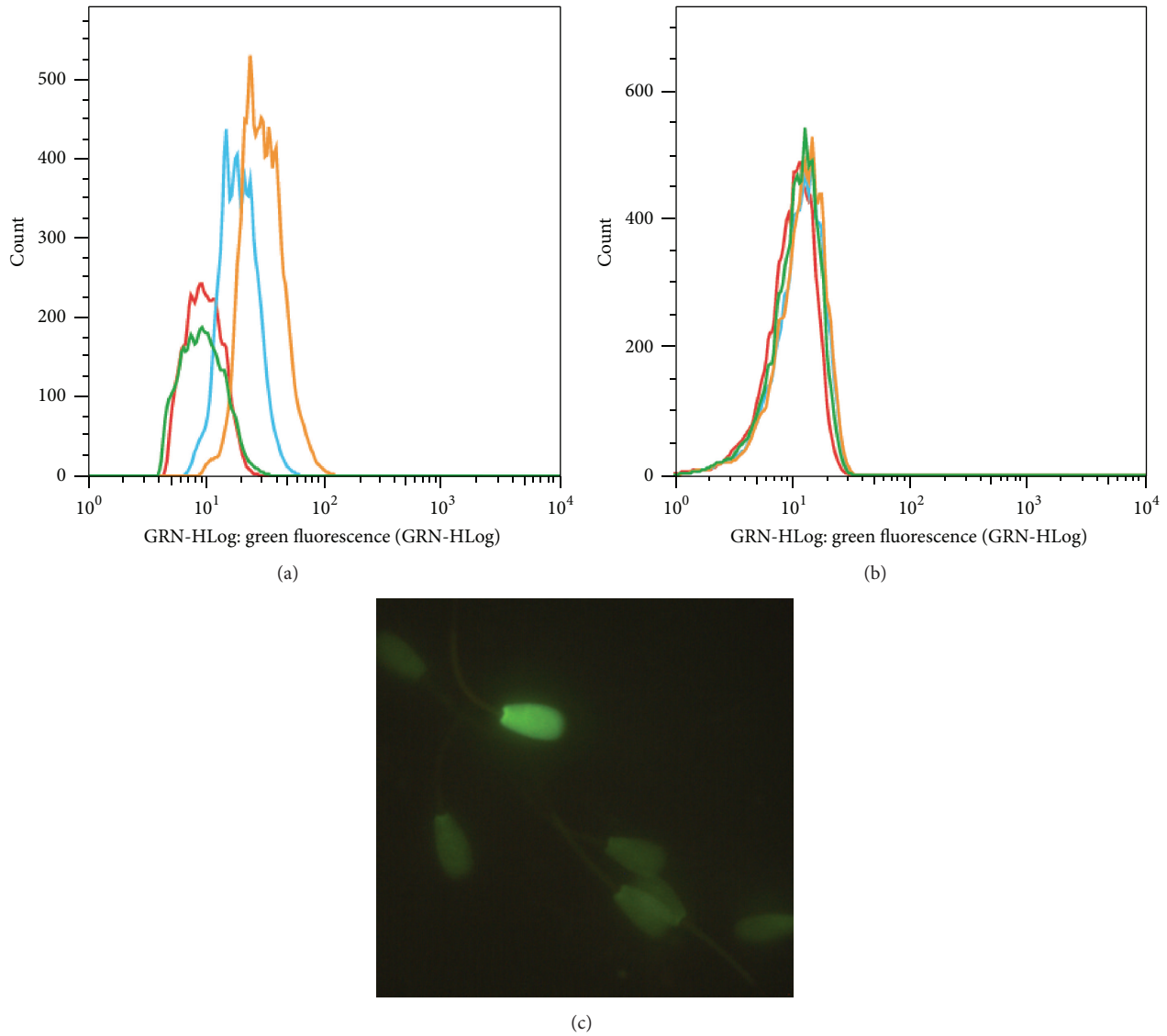

Figure 2: Histogram of green fluorescent intensity for CellROX green and DCFH probes and epifluorescence microscopy of spermatozoa stained with CellROX green. Histogram of green fluorescent intensity for CellROX green (a) and DCFH (b), wherein green lines correspond to control (without H_2O_2); red = 12,5 μM H_2O_2; blue = 50 μM H_2O_2; and orange = 200 μM H_2O_2. Spermatozoa stained with CellROX green (c), positive (intense green) and negative cells (weak green), 1000x magnification with mineral oil.

day of culture. We observed an increase in the percentage of noncleaved (NC) and 2–4 cells embryos according to increase hydrogen peroxide concentrations. Contrarily, the number of 8–16 cells embryos decreased under the same hydrogen peroxide incubation protocol.

With these results, we verified that oxidative stress suffered by the sperm prior to IVF has a dose-dependent effect on both early (cleavage rate) and late (development rate and blastocyst) embryo development.

3.2.4. Correlation between Sperm Parameters and Embryo Development. Correlation data are shown in Supplementary Material (Table S4). When sperm was treated with hydrogen peroxide, there was a positive correlation between the percentage of cells with high mitochondrial membrane potential and cells PI-VD+, and a negative correlation between the percentage of cells with high mitochondrial potential and movement pattern (VAP, VSL, VCL, and BCF).

For the oxidative status related variables, also in treated group, there was a negative correlation between stressed cells with no membrane alteration (PI-VD+ and PI-DCFH+) with movement pattern, and the percentage of cells PI-DCFH+ also correlates negatively with the total and progressive motility.

Finally, in the treated group, cleavage rate correlates positively with total and progressive motility, and blastocyst

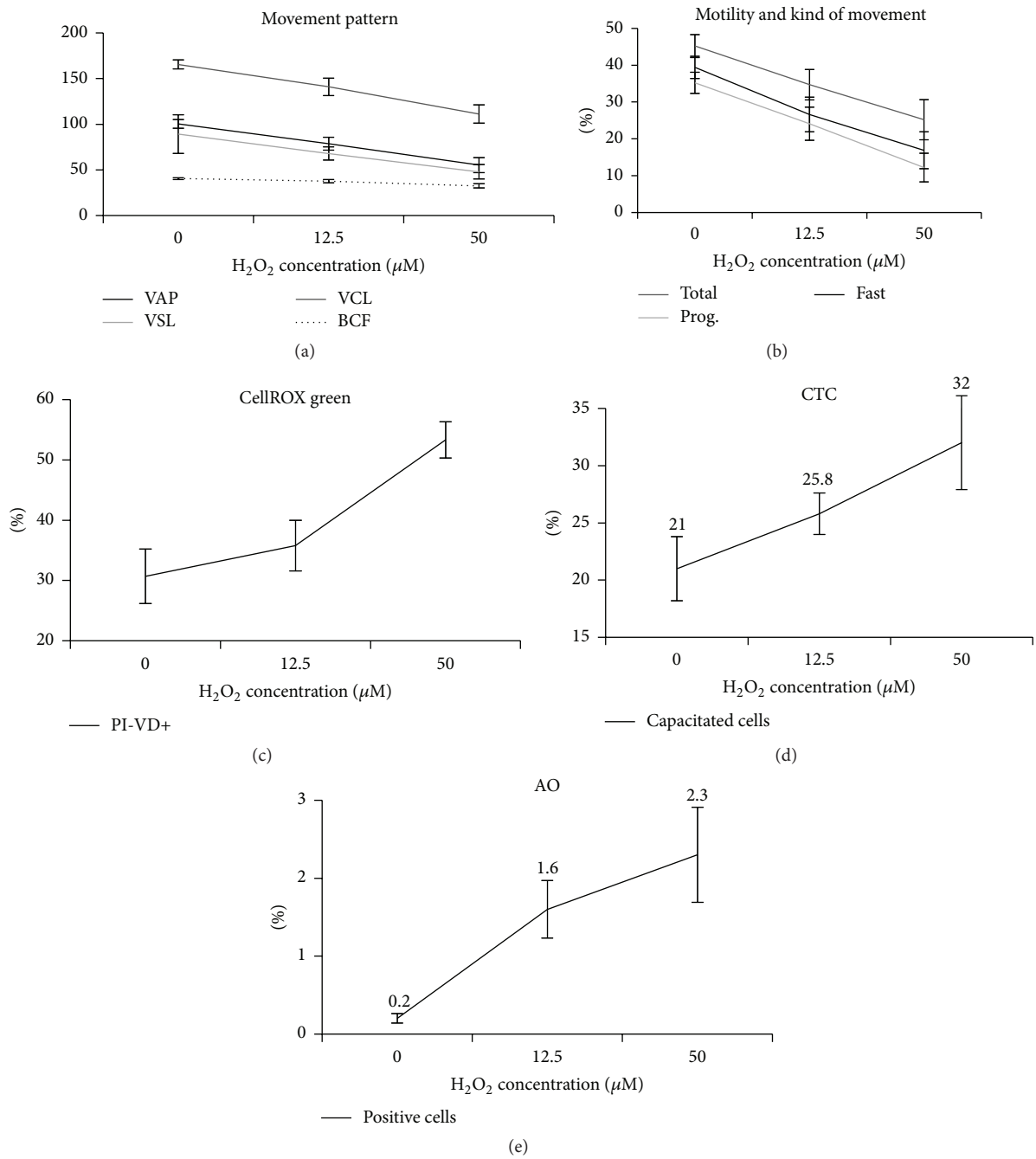

Figure 3: Spermatozoa evaluations with treatment effect for hydrogen peroxide. Units for VAP, VSL, and VCL = μm/s and BCF = hertz (a); Total: total motility and Prog.: progressive motility (b); oxidative status evaluated by CellROX green represented by percentage of cells without membrane alterations and stressed (PI-VD+) (c); sperm capacitation evaluated by chlortetracycline assay (CTC) (d); and positive cells for AO (e).

rate correlates negatively with the percentage of cells PI-VD+ and positively with velocity pattern (VAP, VSL, and VCL).

4. Discussion

In our study, we verified that sperm submitted to an oxidative environment negatively influence embryo development when used for *in vitro* fertilization. The severity of such effect is dependent on the intensity of the oxidative challenge. Interestingly, this impact can be observed not only on cleavage stage but also during the development to blastocyst. In addition, we verified the dose-dependent detrimental effect of oxidative stress on sperm motility, capacitation, and chromatin integrity. The regression model used in the preset work enables more inferences than studies which performed only mean comparisons. We can also consider the

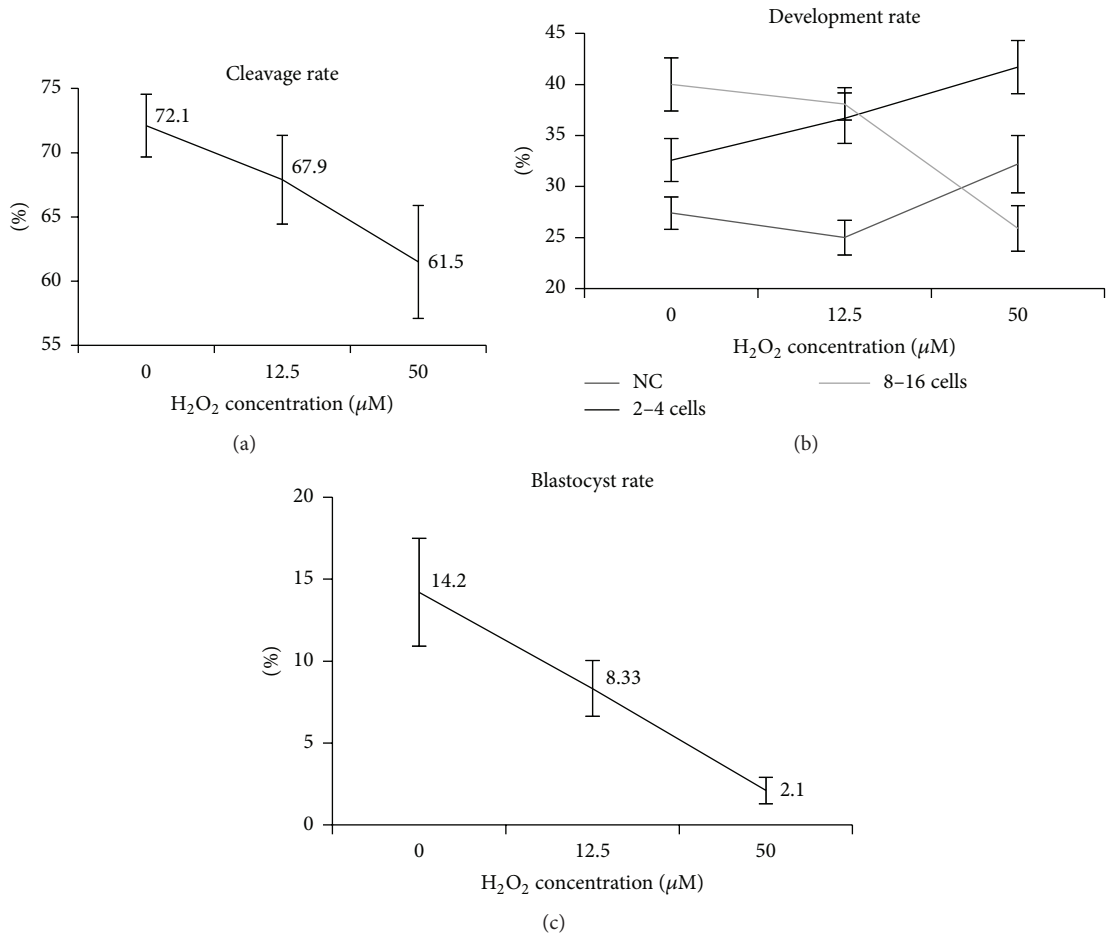

Figure 4: Embryo development evaluations. Cleavage rate evaluates on 3rd day of culture (a); development rate evaluates on 5th day of culture, wherein NC is noncleavage (b); and blastocyst rate evaluates on 8th day of culture (c).

functioning of our treatment (hydrogen peroxide as oxidative stress promoter) over different biological sperm functions (motility, capacitation, embryo development, etc.), inferring over the effect of other doses not used in the present study, once the model generates a straight-line equation. Based on such equation, we may calculate the ideal hydrogen peroxide concentration for different desired effects (minimum effect on IVP, DNA damage, influence on motility, etc.). Also, for the first time, we reported the use of a new fluorescent probe, more efficient and sensible, to evaluate oxidative status by flow cytometry on bovine spermatozoa.

4.1. Oxidative Stress Impaired Sperm Motility, without Affecting Mitochondrial Membrane Potential. In experiment 1, we proposed a model to evaluate the effect of induced oxidative stress on bovine sperm motility patterns. Even though we used low concentrations of hydrogen peroxide in a short incubation period when compared to those previously used [37–39], our data suggests that bovine sperm motility is highly sensitive to oxidative stress induced by hydrogen peroxide. Furthermore, in treated group, the negative correlations between oxidative status (percentage of cells PI-VD+ and PI-DCFH+), sperm movement pattern (VAP, VSL, VCL, and BCF), and percentage of total and progressive motility reinforce the deleterious influence of the oxidative environment created by hydrogen peroxide on motility.

Hydrogen peroxide promotes a negative effect on motility patterns, but this effect apparently is not related to alteration on mitochondrial membrane potential. In boar sperm, hydrogen peroxide induces similar effect; reduction on sperm motility is not accompanied by impaired mitochondrial membrane potential or ATP concentrations [40]. These authors suggest that decreased motility caused by hydrogen peroxide is probably due to the action of the ROS in the contractility mechanisms of the sperm tail rather than impaired mitochondrial function. Another possibility is that the effect of hydrogen peroxide on mitochondrial membrane potential may be observed in a subsequent moment, as verified in other studies [20, 22, 26]. At this later stage, sperm is already dead, with impaired membrane integrity, and then the decreased mitochondrial membrane potential should be observed, similarly to cells submitted to the cryopreservation process [41].

The positive correlation between the percentage of sperm showing high mitochondrial membrane potential and those with signs of stress and no membrane alteration (PI-VD+)

found in the treated group suggests that, in stressful conditions, intact and metabolically active cells would exhibit greater potential to release prooxidative substances. Similar relationship between mitochondrial membrane potential and ROS has been demonstrated in other cell types [42, 43]. Studies on heart and kidney cells hypothesize that mitochondrial membrane potential could be controlled by ATP/ADP production, since ATP synthesis is maximum in low membrane potential and ROS formation increases exponentially under high membrane potential (>140 mV) [44]. In fact, in our study, under the influence of hydrogen peroxide, samples showing higher percentages of sperm with high mitochondrial membrane potential presented impaired sperm movement pattern (VAP, VSL, VCL, and BCF). According to these results, we could speculate that, under stressful situations, intermediary to low mitochondrial membrane potential may be more favorable to motility, because in these conditions such cells would feature decreased potential to release intramitochondrial prooxidative factors.

4.2. Oxidative Stress and Sperm Capacitation. An important biological function of ROS on sperm physiology occurs in the capacitation process [45]. The action mechanism of hydrogen peroxide on sperm capacitation is still a matter of debate. However, previous studies demonstrated that, for bovine sperm, low concentrations of hydrogen peroxide (up to 50 μM) promote a time- and dose-dependent effect on tyrosine phosphorylation of some proteins related to capacitation, with opposite effect under high concentrations (5 mM) [24]. In our study, oxidative stress induced by hydrogen peroxide also promoted a dose-dependent increase in the percentage of capacitated sperm. However, this increased number of capacitated sperm had no influence on sperm fertilization ability, evaluated indirectly by cleavage rate. Probably, under the challenge with hydrogen peroxide, such capacitation would occur prematurely, being actually an indication that these cells are dying, resulting in decreased sperm motility. Sperm cryopreservation, as well as successive washes, could anticipate the capacitation process by altering membrane's permeability and removing capacitation inhibition factors [46, 47]. In our study, hydrogen peroxide on higher concentrations probably exacerbated the premature capacitation, already initiated by the cryopreservation/thawing process, reducing the sperm limited lifespan and decreasing the ability to fertilize the oocyte. This is probably one of the reasons for the decreased cleavage rates on higher hydrogen peroxide concentrations.

4.3. CellROX Green Is More Efficient for Oxidative Status Evaluation on Bovine Spermatozoa. In our study, oxidative status was assessed by two fluorescent probes: 2′,7′-dichlorofluorescein diacetate (DCFH) and CellROX green. We observed differences in oxidative status detection between these two fluorescent probes. While, for DCFH, no dose-dependent effect for hydrogen peroxide was detected, for CellROX green, we could clearly observe an effect of increasing concentrations of hydrogen peroxide, indicating a difference of sensibility between these two probes to assess oxidative status.

To our knowledge, there is no previous report regarding the use of CellROX green in bovine sperm. A recent study validated CellROX deep red to detect oxidative status in ovine sperm [48], but in contrast to CellROX green that binds to DNA when it oxidizes, CellROX deep red detects cytoplasmic free radicals.

Both DCFH and CellROX green are considered nonspecific to the type of free radical detected, although some studies still use DCFH as a specific probe to detect hydrogen peroxide production [49]. In addition, these probes act in different cellular compartments. The signal generated by DCFH is most effective when the oxidizing agent is generated in the cytoplasm or near the plasma membrane [50]. On the other hand, CellROX green is considered primarily a nuclear probe. According to manufacture instructions, this probe has a weak basal fluorescence and, when oxidized, binds to DNA showing a bright and intense green fluorescence, which may also indicate a greater fluorescent stability.

The different sensibility of these two probes was observed in the validation for flow cytometry (Figure 2). When we used CellROX green, we could identify difference on green fluorescence intensity as hydrogen peroxide concentration increases. Such effect was not observed for DCFH; once it was independent of concentration, the green fluorescent was the same for all hydrogen peroxide concentrations. However, we must consider that samples used in the present study were frozen-thawed, subjected to many centrifugations (Percoll gradient and washes), and already highly susceptible to the oxidative stress [51]. Maybe this oxidative stress, inherent to this particular sample, was sufficient to generate positive signal for most of the cells evaluated using the DCFH. Also, some studies report the difficulty to work with this probe due to instability and photooxidation [52]. Under these experimental conditions, CellROX green proved to be more sensitive to and efficient in detecting oxidative status on bovine cryopreserved sperm cell submitted to an oxidative challenge.

4.4. Impact of Sperm Oxidative Status on In Vitro Embryo Development. In our experiment, we verified that sperm, when exposed to an oxidative environment, induce a dose-dependent effect on embryo development, from the first cleavage until blastocyst stage. The diminished cleavage rate probably occurred due to the lower percentage of motile cells as the concentration of the induction agent increased, which would then lead to impaired fertilization rates. In fact, the correlations found between motility and cleavage rate would agree with this hypothesis. In the control group, no correlation was found between motility and cleavage rate probably because, in this situation, sperm motility would remain high due to the Percoll gradient. However, in the treated group, there was a positive correlation between these two variables, suggesting that only under oxidative stressful conditions (the presence of hydrogen peroxide) sperm motility would strongly influence cleavage rates.

Embryo development rates evaluated on the fifth day of culture demonstrated that most embryos block the development at the 2–4 cells stage; at this moment, embryos should normally be at 8–16 cells stage. The influence of such

developmental block would result in lower blastocyst rates. We can speculate two possible causes: (1) sperm that experienced an oxidative environment, after fertilization, may carry metabolites that would promote oocyte intracellular damage such as lipid peroxidation and antioxidant depletion, which would then impair initial embryo development (2–4 cells); (2) sperm DNA abnormalities induced by oxidative stress block embryo development even before embryo genome activation, leading to cellular division failure. The first hypothesis is very difficult to prove, once techniques currently available to assess zygotes' intracellular damage compromise further embryo development. Results of previous studies [29–31] give indications that sperm chromatin abnormalities are probably the most important reason for embryo development blockage.

In our study, we verified the effect of oxidative stress increasing the percentage of cells with chromatin alteration (AO+). Chromatin alterations in bovine sperm are relatively rare when compared to other species [16, 53, 54]. Despite the reduced percentage of cells positive for AO (2.3% for 50 μM), hydrogen peroxide was capable of promoting a dose-dependent increase in the percentage of positive cells. Shaman and Ward [55] described that most of the DNA breaks, identified by the SCSA test, are located in the toroid linker regions. These chromatin regions can be more sensitive to oxidizing agents. As oxidation mechanism is dynamic, the DNA lesions started by hydrogen peroxide can be perpetuated within the cell even after fertilization, in these sensible regions and also on histone rich regions.

The retained histones on sperm DNA are not accidental. In an interesting study, Hammoud et al. [56] identified that retained histones are bound to developmental promoters, regions in *HOX* clusters, noncoding RNAs, and paternally expressed imprinted loci. This strategic localization of histones is considered important epigenetic markers of paternal DNA, indicating genes related to early embryo development that must be immediately activated after fertilization [57, 58]. However, the DNA attached to histones can be more susceptible to damage [55], exposing important epigenetic markers that, if damaged, may lead to embryo development arrest. Therefore, even under low percentage of cells with chromatin alteration, we can assume that the reason for embryo development block of our study is chromatin damage.

Embryo development fails due to spermatozoa exposed to oxidative stress which has been previously observed in primate [15]. In this study, authors attribute embryo development arrest before embryo genome activation to alterations during cellular division and high levels of nuclear fragmentation. In mouse, another study verified that spermatozoa exposed to hydrogen peroxide promote delay in embryo development and decrease in implantation rates [59]. Similar to our study, Simões et al. [16] identified lower cleavage rates in bovine sperm samples more susceptible to oxidative stress, but no effect was observed for blastocyst rate. Authors speculate that embryos that were able to surpass blocking phase are capable of reaching blastocyst stage. However, an increase in apoptotic blastomeres was observed. More studies directed to the early development period (between fist cleavage until 8–16 cells stage, when bovine embryo genome is activated) and epigenetic mechanisms may elucidate the dynamic of embryo development arrest caused by spermatozoa previously submitted to oxidative damage.

With the advances in transcriptome research, several studies have identified the presence of RNAs on spermatozoa [60–62]. Some of these RNAs have been reported as functional, necessary for important physiological events such as the first cleavage of zygotes [63]. RNA molecule is more unstable than DNA and also prone to damage due to ROS attack [64]. When oxidized, it can lead to formation of dysfunctional proteins, truncated or with incorrect folding [65]. In this context, we can speculate that some of these sperm RNAs can also be target of ROS oxidation, and once they are necessary for embryo development, this could be deleterious even before embryo genome activation.

5. Conclusion

We concluded that an oxidative environment can significantly impair bovine sperm motility pattern, oxidative and capacitation status, and DNA integrity. These changes would then reflect negatively on embryonic development from cleavage to blastocyst stage. Also, our study validated a new method to evaluate oxidative stress, CellROX green, which is more sensitive and efficient when compared to another assay normally used for sperm. More studies focusing on the moments between first cleavage and embryonic genome activation should be conducted aiming to better understand the deleterious effect of oxidized sperm in this particular period.

Conflict of Interests

The authors declare that there is no conflict of interests regarding the publication of this paper.

Acknowledgments

This study was supported by São Paulo Research Foundation (FAPESP), Process no. 2012/22915-8, and National Board for Scientific and Technological Development (CNPq), Process no. 480760/2012-8.

References

[1] R. J. Aitken and B. Nixon, "Sperm capacitation: a distant landscape glimpsed but unexplored," *Molecular Human Reproduction*, vol. 19, no. 12, Article ID gat067, pp. 785–793, 2013.

[2] R. Mapletoft, "History and perspectives on bovine embryo transfer," *Animal Reproduction*, vol. 10, pp. 168–173, 2013.

[3] G. A. Palma and F. Sinowatz, "Male and female effects on the in vitro production of bovine embryos," *Anatomia, Histologia, Embryologia*, vol. 33, no. 5, pp. 257–262, 2004.

[4] J. Xu, Z. Guo, L. Su et al., "Developmental potential of vitrified Holstein cattle embryos fertilized in vitro with sex-sorted sperm," *Journal of Dairy Science*, vol. 89, no. 7, pp. 2510–2518, 2006.

[5] F. Ward, D. Rizos, D. Corridan, K. Quinn, M. Boland, and P. Lonergan, "Paternal influence on the time of first embryonic cleavage post insemination and the implications for subsequent bovine embryo development in vitro and fertility in vivo," *Molecular Reproduction and Development*, vol. 60, no. 1, pp. 47–55, 2001.

[6] P. Comizzoli, B. Marquant-Le Guienne, Y. Heyman, and J. P. Renard, "Onset of the first S-phase is determined by a paternal effect during the G1-phase in bovine zygotes," *Biology of Reproduction*, vol. 62, no. 6, pp. 1677–1684, 2000.

[7] R. Asch, C. Simerly, T. Ord, V. A. Ord, and G. Schatten, "The stages at which human fertilization arrests: microtubule and chromosome configurations in inseminated oocytes which failed to complete fertilization and development in humans," *Human Reproduction*, vol. 10, no. 7, pp. 1897–1906, 1995.

[8] V. Y. Rawe, S. B. Olmedo, F. N. Nodar, G. D. Doncel, A. A. Acosta, and A. D. Vitullo, "Cytoskeletal organization defects and abortive activation in human oocytes after IVF and ICSI failure," *Molecular Human Reproduction*, vol. 6, no. 6, pp. 510–516, 2000.

[9] S.-Y. Yoon, T. Jellerette, A. M. Salicioni et al., "Human sperm devoid of PLC, zeta 1 fail to induce Ca^{2+} release and are unable to initiate the first step of embryo development," *The Journal of Clinical Investigation*, vol. 118, no. 11, pp. 3671–3681, 2008.

[10] J.-G. Sun, A. Jurisicova, and R. F. Casper, "Detection of deoxyribonucleic acid fragmentation in human sperm: correlation with fertilization in vitro," *Biology of Reproduction*, vol. 56, no. 3, pp. 602–607, 1997.

[11] R. A. Saleh, A. Agarwal, E. A. Nada et al., "Negative effects of increased sperm DNA damage in relation to seminal oxidative stress in men with idiopathic and male factor infertility," *Fertility and Sterility*, vol. 79, no. 3, pp. 1597–1605, 2003.

[12] R. J. Aitken and C. Krausz, "Oxidative stress, DNA damage and the Y chromosome," *Reproduction*, vol. 122, no. 4, pp. 497–506, 2001.

[13] S. Bontekoe, E. Mantikou, M. van Wely, S. Seshadri, S. Repping, and S. Mastenbroek, "Low oxygen concentrations for embryo culture in assisted reproductive technologies," *Cochrane Database of Systematic Reviews*, vol. 7, Article ID CD008950, 2012.

[14] A. Agarwal, S. S. R. Allamaneni, K. P. Nallella, A. T. George, and E. Mascha, "Correlation of reactive oxygen species levels with the fertilization rate after in vitro fertilization: a qualified meta-analysis," *Fertility and Sterility*, vol. 84, no. 1, pp. 228–231, 2005.

[15] V. Burruel, K. L. Klooster, J. Chitwood, P. J. Ross, and S. A. Meyers, "Oxidative damage to rhesus macaque spermatozoa results in mitotic arrest and transcript abundance changes in early embryos," *Biology of Reproduction*, vol. 89, no. 3, article 72, 2013.

[16] R. Simões, W. B. Feitosa, A. F. P. Siqueira et al., "Influence of bovine sperm DNA fragmentation and oxidative stress on early embryo in vitro development outcome," *Reproduction*, vol. 146, no. 5, pp. 433–441, 2013.

[17] M. N. Bucak, P. B. Tuncer, S. Sariözkan et al., "Effects of antioxidants on post-thawed bovine sperm and oxidative stress parameters: antioxidants protect DNA integrity against cryodamage," *Cryobiology*, vol. 61, no. 3, pp. 248–253, 2010.

[18] A. Partyka, E. Łukaszewicz, W. Nizański, and J. Twardoń, "Detection of lipid peroxidation in frozen-thawed avian spermatozoa using C(11)-BODIPY(581/591)," *Theriogenology*, vol. 75, no. 9, pp. 1623–1629, 2011.

[19] M. Mata-Campuzano, M. Álvarez-Rodríguez, E. del Olmo, M. R. Fernández-Santos, J. J. Garde, and F. Martínez-Pastor, "Quality, oxidative markers and DNA damage (DNA) fragmentation of red deer thawed spermatozoa after incubation at 37 °C in presence of several antioxidants," *Theriogenology*, vol. 78, no. 5, pp. 1005–1019, 2012.

[20] A. Amaral, B. Lourenço, M. Marques, and J. Ramalho-Santos, "Mitochondria functionality and sperm quality," *Reproduction*, vol. 146, no. 5, pp. R163–R174, 2013.

[21] J.-F. Bilodeau, S. Chatterjee, M.-A. Sirard, and C. Gagnon, "Levels of antioxidant defenses are decreased in bovine spermatozoa after a cycle of freezing and thawing," *Molecular Reproduction and Development*, vol. 55, no. 3, pp. 282–288, 2000.

[22] A. J. Koppers, G. N. De Iuliis, J. M. Finnie, E. A. McLaughlin, and R. J. Aitken, "Significance of mitochondrial reactive oxygen species in the generation of oxidative stress in spermatozoa," *Journal of Clinical Endocrinology and Metabolism*, vol. 93, no. 8, pp. 3199–3207, 2008.

[23] C. M. O'Flaherty, N. B. Beorlegui, and M. T. Beconi, "Reactive oxygen species requirements for bovine sperm capacitation and acrosome reaction," *Theriogenology*, vol. 52, no. 2, pp. 289–301, 1999.

[24] J. Rivlin, J. Mendel, S. Rubinstein, N. Etkovitz, and H. Breitbart, "Role of hydrogen peroxide in sperm capacitation and acrosome reaction," *Biology of Reproduction*, vol. 70, no. 2, pp. 518–522, 2004.

[25] S. S. du Plessis, D. A. McAllister, A. Luu, J. Savia, A. Agarwal, and F. Lampiao, "Effects of H_2O_2 exposure on human sperm motility parameters, reactive oxygen species levels and nitric oxide levels," *Andrologia*, vol. 42, no. 3, pp. 206–210, 2010.

[26] R. J. Aitken, G. N. De Iuliis, Z. Gibb, and M. A. Baker, "The simmet lecture: new horizons on an old landscape—oxidative stress, DNA damage and apoptosis in the male germ line," *Reproduction in Domestic Animals*, vol. 47, supplement 4, pp. 7–14, 2012.

[27] A. Zini and A. Agarwal, *Sperm Chromatin*, Springer, New York, NY, USA, 2011.

[28] R. J. Aitken and G. N. De Iuliis, "On the possible origins of DNA damage in human spermatozoa," *Molecular Human Reproduction*, vol. 16, no. 1, Article ID gap059, pp. 3–13, 2009.

[29] J. Tesarik, E. Greco, and C. Mendoza, "Late, but not early, paternal effect on human embryo development is related to sperm DNA fragmentation," *Human Reproduction*, vol. 19, no. 3, pp. 611–615, 2004.

[30] M. R. Virro, K. L. Larson-Cook, and D. P. Evenson, "Sperm chromatin structure assay (SCSA) parameters are related to fertilization, blastocyst development, and ongoing pregnancy in in vitro fertilization and intracytoplasmic sperm injection cycles," *Fertility and Sterility*, vol. 81, no. 5, pp. 1289–1295, 2004.

[31] A. N. Fatehi, M. M. Bevers, E. Schoevers, B. A. J. Roelen, B. Colenbrander, and B. M. Gadella, "DNA damage in bovine sperm does not block fertilization and early embryonic development but induces apoptosis after the first cleavages," *Journal of Andrology*, vol. 27, no. 2, pp. 176–188, 2006.

[32] J. J. Parrish, J. Susko-Parrish, M. A. Winer, and N. L. First, "Capacitation of bovine sperm by heparin," *Biology of Reproduction*, vol. 38, no. 5, pp. 1171–1180, 1988.

[33] G. F. Goovaerts, G. G. Hoflack, A. Van Soom et al., "Evaluation of epididymal semen quality using the Hamilton-Thorne analyser indicates variation between the two caudae epididymides of the same bull," *Theriogenology*, vol. 66, no. 2, pp. 323–330, 2006.

[34] E. C. C. Celeghini, R. P. de Arruda, A. F. C. de Andrade, J. Nascimento, and C. F. Raphael, "Practical techniques for bovine sperm simultaneous fluorimetric assessment of plasma, acrosomal and mitochondrial membranes," *Reproduction in Domestic Animals*, vol. 42, no. 5, pp. 479–488, 2007.

[35] D. Evenson and L. Jost, "Sperm chromatin structure assay is useful for fertility assessment," *Methods in Cell Science*, vol. 22, no. 2-3, pp. 169–189, 2000.

[36] C. R. Ward and B. T. Storey, "Determination of the time course of capacitation in mouse spermatozoa using a chlortetracycline fluorescence assay," *Developmental Biology*, vol. 104, no. 2, pp. 287–296, 1984.

[37] R. J. Aitken, E. Gordon, D. Harkiss et al., "Relative impact of oxidative stress on the functional competence and genomic integrity of human spermatozoa," *Biology of Reproduction*, vol. 59, no. 5, pp. 1037–1046, 1998.

[38] P. F. N. Silva, B. M. Gadella, B. Colenbrander, and B. A. J. Roelen, "Exposure of bovine sperm to pro-oxidants impairs the developmental competence of the embryo after the first cleavage," *Theriogenology*, vol. 67, no. 3, pp. 609–619, 2007.

[39] M. B. Rahman, L. Vandaele, T. Rijsselaere et al., "Oocyte quality determines bovine embryo development after fertilisation with hydrogen peroxide-stressed spermatozoa," *Reproduction, Fertility and Development*, vol. 24, no. 4, pp. 608–618, 2012.

[40] H. D. Guthrie, G. R. Welch, and J. A. Long, "Mitochondrial function and reactive oxygen species action in relation to boar motility," *Theriogenology*, vol. 70, no. 8, pp. 1209–1215, 2008.

[41] D. Schober, C. Aurich, H. Nohl, and L. Gille, "Influence of cryopreservation on mitochondrial functions in equine spermatozoa," *Theriogenology*, vol. 68, no. 5, pp. 745–754, 2007.

[42] R. G. Hansford, B. A. Hogue, and V. Mildaziene, "Dependence of H_2O_2 formation by rat heart mitochondria on substrate availability and donor age," *Journal of Bioenergetics and Biomembranes*, vol. 29, no. 1, pp. 89–95, 1997.

[43] I. Lee, E. Bender, and B. Kadenbach, "Control of mitochondrial membrane potential and ROS formation by reversible phosphorylation of cytochrome c oxidase," *Molecular and Cellular Biochemistry*, vol. 234-235, no. 1-2, pp. 63–70, 2002.

[44] I. Lee, E. Bender, S. Arnold, and B. Kadenbach, "New control of mitochondrial membrane potential and ROS formation—a hypothesis," *Biological Chemistry*, vol. 382, no. 12, pp. 1629–1636, 2001.

[45] E. de Lamirande, H. Jiang, A. Zini, H. Kodama, and C. Gagnon, "Reactive oxygen species and sperm physiology," *Reviews of Reproduction*, vol. 2, no. 1, pp. 48–54, 1997.

[46] N. Cormier, M.-A. Sirard, and J. L. Bailey, "Premature capacitation of bovine spermatozoa is initiated by cryopreservation," *Journal of Andrology*, vol. 18, no. 4, pp. 461–468, 1997.

[47] T. Leahy and B. M. Gadella, "Sperm surface changes and physiological consequences induced by sperm handling and storage," *Reproduction*, vol. 142, no. 6, pp. 759–778, 2011.

[48] M. B. R. Alves, A. F. C. Andrade, R. P. Arruda et al., "An efficient technique to detect sperm reactive oxygen species: the CellRox deep red fluorescent probe," *Biochemistry & Physiology*, vol. 4, no. 2, Article ID 1000157, 2015.

[49] A. Gomes, E. Fernandes, and J. L. F. C. Lima, "Fluorescence probes used for detection of reactive oxygen species," *Journal of Biochemical and Biophysical Methods*, vol. 65, no. 2-3, pp. 45–80, 2005.

[50] R. J. Aitken, T. B. Smith, T. Lord et al., "On methods for the detection of reactive oxygen species generation by human spermatozoa: analysis of the cellular responses to catechol oestrogen, lipid aldehyde, menadione and arachidonic acid," *Andrology*, vol. 1, no. 2, pp. 192–205, 2013.

[51] A. Agarwal, I. Ikemoto, and K. R. Loughlin, "Effect of sperm washing on levels of reactive oxygen species in semen," *Archives of Andrology*, vol. 33, no. 3, pp. 157–162, 1994.

[52] H. Wang and J. A. Joseph, "Quantifying cellular oxidative stress by dichlorofluorescein assay using microplate reader," *Free Radical Biology and Medicine*, vol. 27, no. 5-6, pp. 612–616, 1999.

[53] K. E. Waterhouse, A. Gjeldnes, A. Tverdal et al., "Alterations of sperm DNA integrity during cryopreservation procedure and in vitro incubation of bull semen," *Animal Reproduction Science*, vol. 117, no. 1-2, pp. 34–42, 2010.

[54] E. Malama, E. Kiossis, T. Theodosiou, C. Boscos, and H. Bollwein, "Lag effect of microclimatic conditions on DNA integrity of frozen-thawed bovine sperm," *Animal Reproduction Science*, vol. 136, no. 1-2, pp. 33–41, 2012.

[55] J. A. Shaman and W. S. Ward, "Sperm chromatin stability and susceptibility to damage in relation to its structure," in *The Sperm Cell: Production, Maturation, Fertilization, Regeneration*, pp. 31–48, Cambridge University Press, 1st edition, 2006.

[56] S. S. Hammoud, D. A. Nix, H. Zhang, J. Purwar, D. T. Carrell, and B. R. Cairns, "Distinctive chromatin in human sperm packages genes for embryo development," *Nature*, vol. 460, no. 7254, pp. 473–478, 2009.

[57] D. Miller, M. Brinkworth, and D. Iles, "Paternal DNA packaging in spermatozoa: more than the sum of its parts? DNA, histones, protamines and epigenetics," *Reproduction*, vol. 139, no. 2, pp. 287–301, 2010.

[58] D. T. Carrell, "Epigenetics of the male gamete," *Fertility and Sterility*, vol. 97, no. 2, pp. 267–274, 2012.

[59] M. Lane, N. O. McPherson, T. Fullston et al., "Oxidative stress in mouse sperm impairs embryo development, fetal growth and alters adiposity and glucose regulation in female offspring," *PLoS ONE*, vol. 9, no. 7, Article ID e100832, 2014.

[60] J.-P. Dadoune, "Spermatozoal RNAs: what about their functions?" *Microscopy Research and Technique*, vol. 72, no. 8, pp. 536–551, 2009.

[61] C. Lalancette, D. Miller, Y. Li, and S. A. Krawetz, "Paternal contributions: new functional insights for spermatozoal RNA," *Journal of Cellular Biochemistry*, vol. 104, no. 5, pp. 1570–1579, 2008.

[62] J. M. Feugang, N. Rodriguez-Osorio, A. Kaya et al., "Transcriptome analysis of bull spermatozoa: implications for male fertility," *Reproductive BioMedicine Online*, vol. 21, no. 3, pp. 312–324, 2010.

[63] W.-M. Liu, R. T. K. Pang, P. C. N. Chiu et al., "Sperm-borne microRNA-34c is required for the first cleavage division in mouse," *Proceedings of the National Academy of Sciences of the United States of America*, vol. 109, no. 2, pp. 490–494, 2012.

[64] Q. Kong and C.-L. G. Lin, "Oxidative damage to RNA: mechanisms, consequences, and diseases," *Cellular and Molecular Life Sciences*, vol. 67, no. 11, pp. 1817–1829, 2010.

[65] H. E. Poulsen, E. Specht, K. Broedbaek et al., "RNA modifications by oxidation: a novel disease mechanism?" *Free Radical Biology and Medicine*, vol. 52, no. 8, pp. 1353–1361, 2012.

Hindawi Publishing Corporation
Oxidative Medicine and Cellular Longevity
Volume 2016, Article ID 4512309, 9 pages
http://dx.doi.org/10.1155/2016/4512309

Research Article

Acetaldehyde Induces Cytotoxicity of SH-SY5Y Cells via Inhibition of Akt Activation and Induction of Oxidative Stress

Tingting Yan, Yan Zhao, and Xia Zhang

Department of Bioengineering, Harbin Institute of Technology, Weihai, Shandong 264209, China

Correspondence should be addressed to Yan Zhao; zhaoyan@hitwh.edu.cn

Received 13 June 2015; Accepted 14 July 2015

Academic Editor: Michela Battistelli

Excessive alcohol consumption can lead to brain tissue damage and cognitive dysfunction. It has been shown that heavy drinking is associated with an earlier onset of neurodegenerative diseases such as Alzheimer's disease. Acetaldehyde, the most toxic metabolite of ethanol, is speculated to mediate the brain tissue damage and cognitive dysfunction induced by the chronic excessive consumption of alcohol. However, the exact mechanisms by which acetaldehyde induces neurotoxicity are not totally understood. In this study, we investigated the cytotoxic effects of acetaldehyde in SH-SY5Y cells and found that acetaldehyde induced apoptosis of SH-SY5Y cells by downregulating the expression of antiapoptotic *Bcl-2* and *Bcl-xL* and upregulating the expression of proapoptotic *Bax*. Acetaldehyde treatment led to a significant decrease in the levels of activated Akt and cyclic AMP-responsive element binding protein (CREB). In addition, acetaldehyde induced the activation of p38 mitogen-activated protein kinase (MAPK) while inhibiting the activation of extracellular signal-regulated kinases (ERKs, p44/p42MAPK). Meanwhile, acetaldehyde treatment caused an increase in the production of reactive oxygen species and elevated the oxidative stress in SH-SY5Y cells. Therefore, acetaldehyde induces cytotoxicity of SH-SY5Y cells via promotion of apoptotic signaling, inhibition of cell survival pathway, and induction of oxidative stress.

1. Introduction

Excessive alcohol consumption can cause brain tissue damage and cognitive dysfunction [1]. It has been reported that heavy drinking is associated with an earlier onset of neurodegenerative diseases such as Alzheimer's disease (AD) [2]. Acetaldehyde, the most toxic metabolite of ethanol, is speculated to mediate the brain tissue damage and cognitive dysfunction induced by the chronic excessive consumption of alcohol. The major enzyme that generates acetaldehyde during ethanol metabolism in liver is alcohol dehydrogenase. Catalase and cytochrome p450 2E1 are additional enzymes that are important for the local formation of acetaldehyde in the brain [3]. Acetaldehyde can also be directly ingested from foods such as alcohol beverages, fruit juice, and yogurt or from tobacco smoke [4]. The principle enzyme responsible for the detoxification and metabolism of acetaldehyde into acetate is aldehyde dehydrogenase (ALDH) 2. Thus, the local accumulation of acetaldehyde depends on the amount of exposure and the rates of its formation and clearance. Indeed, it has been found that the levels of acetaldehyde in blood are much higher in individuals with defective ALDH2 in comparison with normal individuals after alcohol ingestion [5].

The generation and accumulation of acetaldehyde by local metabolism in brain may contribute to the synaptic dysfunction. It has been demonstrated that acetaldehyde mediates the acute inhibition of long-term potentiation by ethanol in the CA1 region of rat hippocampal slices [6]. The tissue damage caused by acetaldehyde is largely mediated by the direct cytotoxicity caused by acetaldehyde. In rat embryos, acetaldehyde treatment induces marked cell death in several tissues including neuroepithelium, correlating to the malformations seen in fetal alcohol syndrome (FAS) [7]. Similarly, exposure to acetaldehyde inhibits cell growth in primary cultures of rat astrocytes, presumably via apoptotic pathway [8]. Induction of mitochondria dysfunction and overproduction of reactive oxygen species (ROS) have been linked to the action of acetaldehyde [9, 10]. The redox imbalance induced by acetaldehyde is accompanied by a transient

reduction in the protein content of mitochondrial superoxide dismutase SOD2 [11]. In rat cerebellar neuron cultures, acetaldehyde treatment causes decrease in cell viability while impairing mitochondrial function and significantly elevating markers of oxidative stress including 4-hydroxy-2-nonenal and 8-hydroxydeoxyguanosine [12]. In addition, it has been shown that acetaldehyde induces cytotoxic effects of neuronal cells by activating apoptotic signals such as cytochrome c release and caspase 3 activation [13].

Above evidence suggests acetaldehyde may cause neurotoxic effects by promoting oxidative stress and apoptotic signals. However, the exact molecular mechanisms of acetaldehyde-induced neurotoxicity are not totally understood. There are few studies on whether acetaldehyde affects pathways that are essential for cell survival such as the activation of Akt (a serine/threonine kinase or protein kinase, PKB) and cyclic AMP-responsive element binding protein (CREB). In this study, we investigated the cytotoxic effects of acetaldehyde in SH-SY5Y cells and found that acetaldehyde induced apoptosis of SH-SY5Y cells by downregulating the expression of antiapoptotic *Bcl-2* and *Bcl-xL* and upregulating the expression of proapoptotic *Bax*. Acetaldehyde treatment led to a significant decrease in the levels of activated Akt and CREB. In addition, acetaldehyde induced the activation of p38 mitogen-activated protein kinase (MAPK) while inhibiting the activation of extracellular signal-regulated kinases (ERKs, p44/p42MAPK). Meanwhile, acetaldehyde treatment led to elevated production of ROS and oxidative stress in SH-SY5Y cells. Therefore, acetaldehyde induces cytotoxicity of SH-SY5Y cells via promotion of apoptotic signaling, inhibition of cell survival pathway, and induction of oxidative stress.

2. Materials and Methods

2.1. Materials. Fetal bovine serum (FBS), streptomycin, and penicillin were purchased from Thermo Scientific (Rockford, IL, USA). Dulbecco's modified Eagle's medium (DMEM), trypsin, and reverse-transcription reaction system were purchased from Invitrogen (Eugene, OR, USA). Caspase 3 activity kit, BCA protein assay kit, DMSO, BeyoECL plus Western blotting detection system, anti-Akt, and goat antirabbit IgG (H+L) antibodies were purchased from Beyotime Institute of Biotechnology (Haimen, China). MDA assay kit and GSH assay kit were purchased from Nanjing Jiancheng Bioengineering Institute (Nanjing, China). Brandford protein assay kit, anti-phospho-Akt (Ser 473) antibody, agarose, primers, and PCR reaction system were purchased from Sangon Biotech (Shanghai, China). $2'$, $7'$-Dichlorofluorescin diacetate (DCFH-DA) was purchased from Sigma Chemical (St. Louis, MO, USA). Antibodies for CREB, phospho-CREB (Ser 133), p38MAPK, phospho-p38MAPK (Thr180/Tyr182), JNK, phospho-JNK (Thr183/Tyr185), p44/p42 MAPK, and phospho-p44/p42MAPK (Thr202/Tyr204) were purchased from Cell Signaling Technology (Beverly, MA, USA).

2.2. Cell Viability Assay. Human neuroblastoma SH-SY5Y cells were maintained in DMEM with 10% FBS and 1% streptomycin/penicillin in a CO_2 incubator at 37°C, with 5% CO_2 and 95% air. Cells were seeded in 12-well plates with a density of 4×10^4 per well. The viability of cells was checked by trypan blue exclusion assay.

2.3. Hoechst 33258 Nuclear Staining Assay. Apoptotic cells were detected by Hoechst 33258 nuclear staining assay. Cells were fixed in 4% paraformaldehyde in PBS for 10 min at room temperature after 24 h treatment of acetaldehyde. The fixed cells were incubated with Hoechst 33258 for 5 min at room temperature and subsequently washed with PBS for three times. The fluorescence was examined using an Olympus BX53 fluorescence microscope.

2.4. Caspase 3 Activity. The activity of caspase 3 was determined using a caspase 3 activity kit according to the manufacturer's instructions. After treatments, cells were harvested by digesting with trypsin and the cell lysates were prepared. To evaluate the activity of caspase 3, cell lysates were incubated with Ac-DEVD-pNA and reaction buffer for 10 h at 37°C. Substrate cleavage was then measured using a spectrometer at 405 nm.

2.5. Measurement of Intracellular Oxidation Stress. Fluorescent probe DCFH-DA was used to determine the intracellular generation of ROS. After 1 h treatment with 10 mM acetaldehyde, cells were rinsed three times with PBS and incubated with 5 μM DCFH-DA at 37°C for 30 min. The fluorescence was examined using an Olympus BX53 fluorescence microscope. The concentrations of malondialdehyde (MDA) and glutathione (GSH) were determined using commercial available kits according to the manufacturer's instructions.

2.6. RT-PCR. Total RNA was isolated using RNAiso Plus reagent (Takara Biotechnology (Dalian) Co., Ltd.) and converted to cDNA using reverse-transcription reaction system. PCR was then performed to determine the expression of *Bcl-2*, *Bcl-xL*, and *Bax*. The housekeeping gene *GAPDH* was used as the internal control. The sequences of forward and reverse primers used were ACC ACA GTC CAT GCC ATC AC and ACC TTG CCC ACA GCC TTG for *GAPDH*; CCA GCT GCC TTG GAC TGT GT and GGT TTA TTA CCC CCT CAA GAC CAC for *Bax*; GGA GGA TTG TGG CCT TCT TG and GG TGC CGG TTC AGG TAC TCA for *Bcl-2*; and TTG GAC AAT GGA CTG GTT A and GTA TAG TGG ATG GTC AGT G for *Bcl-xL*. The PCR conditions were 95°C for 5 min followed by 35 cycles at 95°C for 1 min, 55°C for 1 min, and 72°C for 1 min followed by final extension at 72°C for 10 min for *GAPDH*; 94°C for 3 min followed by 25 cycles at 94°C for 30 s, 54°C for 30 s, and 72°C for 1 min followed by final extension at 72°C for 5 min for *Bcl-2*; 95°C for 5 min followed by 40 cycles at 95°C for 1 min, 55°C for 1 min, and 72°C for 1 min followed by final extension at 72°C for 10 min for *Bcl-xL*; and 94°C for 5 min followed by 30 cycles at 94°C for 30 s, 54°C for 30 s, and 72°C for 1 min followed by final extension at 72°C for 5 min for *Bax*. The PCR products were electrophoresed on 1.5% agarose gel, stained with ethidium bromide, and photographed under ultraviolet light.

2.7. Western Blot Analysis. After treatments, cells were washed twice with PBS and the cell lysates were prepared in cell lysis buffer (Tris 20 mM, NaCl 150 mM, EDTA 1 mM, sodium pyrophosphate 2.5 mM, NaF 20 mM, β-glycerophosphoric acid 1 mM, and sodium orthovanadate 1 mM). The supernatants were collected after centrifugation at 14000 ×g for 10 min at 4°C and the protein concentration of the supernatants was measured. 20 μg of protein extracts was resolved by SDS-polyacrylamide gel electrophoresis and then transferred to polyvinylidene difluoride (PVDF) membrane and subsequently incubated with specific primary antibodies. PVDF membrane was washed by Tris buffered saline (TBS) containing 0.1% Tween-20 for three times. For detection, the PVDF membrane was incubated with a horseradish peroxidase-coupled secondary antibody, followed by an enhanced chemiluminescence substrate reaction using BeyoECL plus Western blotting detection system.

2.8. Statistical Analysis. All the experiments were carried out in triplicates. Quantitative data are represented as the mean ± SD. Student's t-test was used to compare the difference between the control and treatment groups. P values of 0.05 were considered statistically significant.

3. Results

3.1. Acetaldehyde Induces Apoptosis and Affects the Gene Expression of Bcl-2 Family Proteins. We first examined the effect of acetaldehyde on the cell viability of SH-SY5Y cells. As shown in Figure 1(a), acetaldehyde decreased the viability of SH-SY5Y cells significantly and in a concentration-dependent manner, suggesting that acetaldehyde induced cytotoxicity of SH-SY5Y cells. Hoechst 33528 staining of cells treated with 10 mM of acetaldehyde for 24 h demonstrated that acetaldehyde induced apoptosis of SH-SY5Y cells (Figure 1(b)).

Proapoptotic protein Bax and antiapoptotic proteins, Bcl-2 and Bcl-xL, are Bcl-2 family proteins that regulate apoptotic pathway via affecting the permeability of the mitochondrial outer membrane [14]. We next examined the effect of acetaldehyde on the expression of these Bcl-2 family proteins. As shown in Figure 1(c), exposure of SH-SY5Y cells to acetaldehyde for 24 h resulted in the decrease in *Bcl-2* and *Bcl-xL* mRNA levels, which were concomitant with the increase in the level of *Bax*. Thus, acetaldehyde treatment might promote apoptosis by decreasing the expression of antiapoptotic proteins *Bcl-2* and *Bcl-xL* and inducing the expression of proapoptic protein *Bax*. Caspase 3 is a hallmark of the late apoptotic events. As shown in Figure 1(d), acetaldehyde treatment significantly increased the activity of caspase 3 and the elevation of caspase 3 activities by acetaldehyde had a dose-response effect. These data indicated that acetaldehyde treatment induced cytotoxicity and apoptosis of SH-SY5Y cells.

3.2. Effect of Acetaldehyde on the Activation of Akt and CREB Pathway. Akt/CREB pathway is important for the survival of neuronal cells [15]. To find out whether acetaldehyde affects cell survival pathway, the activation of Akt and CREB was examined by Western blot analysis. As shown in Figure 2(a), treatment of acetaldehyde (10 and 25 mM) for 24 h induced a significant decrease in the levels of activated Akt. Similarly, levels of activated CREB were also decreased by the treatment of acetaldehyde (Figure 2(b)). These data suggested that acetaldehyde may decrease cell viability and promote apoptosis by inhibiting the activation of Akt and CREB.

3.3. Effect of Acetaldehyde on the Activation of MAPKs. MAPKs have been shown to have important roles in promotion or inhibition of apoptosis. We next examined the effect of acetaldehyde on the activation of p38MAPK/ERK/JNK pathway by Western blot analysis. Treatment of acetaldehyde increased the levels of activated p38MAPK in a dose-dependent manner (Figure 3(a)). In contrast, acetaldehyde treatment caused a downregulation of the levels of activated ERK (Figure 3(b)). There was only a slight change in the activation of JNK after 24 h treatment of acetaldehyde (Figure 3(c)).

3.4. Acetaldehyde Increases Oxidative Stress in SH-SY5Y Cells. To further study the underlying mechanism of the cytotoxic effects of acetaldehyde, the effects of acetaldehyde on the redox status of the cells were studied. As shown in Figure 4(a), exposure of acetaldehyde caused a quick and dramatic increase in the production of ROS in SH-SY5Y cells. In addition, acetaldehyde treatment also induced a decrease in the concentration of tripeptide GSH (Figure 4(b)), which plays important function in the detoxification of ROS. MDA, which is a breakdown product of the oxidative degradation of cell membrane lipids, is generally considered as the marker of intracellular oxidative stress and an indicator of lipid peroxidation [16]. Thus, we next determined the concentration of MDA in acetaldehyde treated SH-SY5Y cells. As shown in Figure 4(c), MDA levels increased significantly by acetaldehyde treatment in a concentration-dependent manner. The increase of ROS and MDA levels and the decreased GSH concentration suggested that the oxidative stress was induced by the acetaldehyde treatment, which might subsequently lead to the cytotoxicity and apoptosis of SH-SY5Y cells.

4. Discussion

Excessive accumulation of acetaldehyde in brain could lead to neurotoxicity and perhaps contribute to the acceleration of the development of neurodegenerative diseases; however, the exact molecular mechanisms of acetaldehyde-induced neurotoxicity are not totally understood. Here we studied the cytotoxic effects of acetaldehyde in SH-SY5Y cells and found that acetaldehyde induced cytotoxicity by promoting apoptosis and inhibiting cell survival pathways.

The role of mitochondria in the apoptotic process has been well established. Mitochondria apoptotic pathway is mainly regulated by Bcl-2 family proteins, including proapoptotic protein Bax and antiapoptotic proteins, Bcl-2

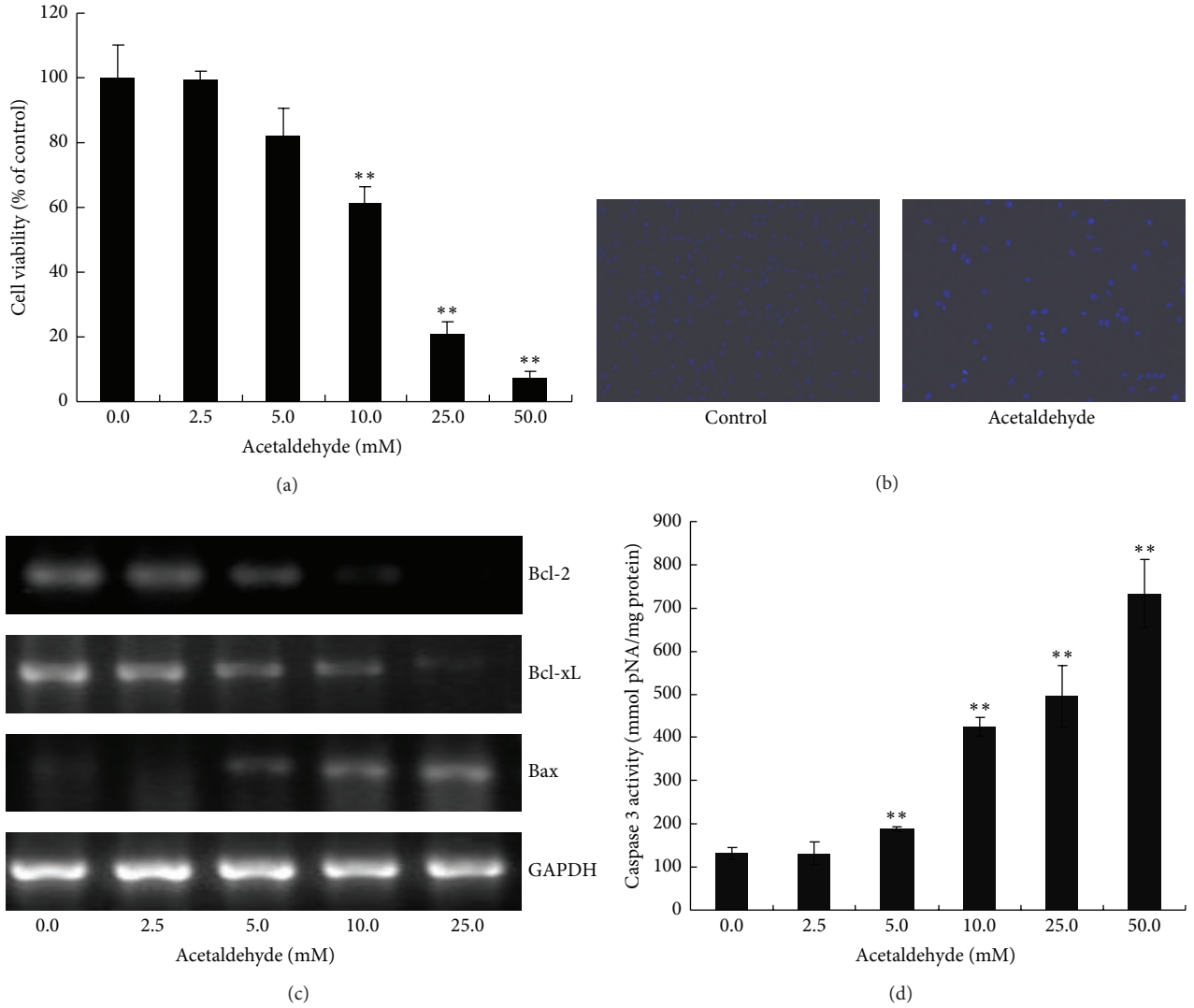

Figure 1: Effects of acetaldehyde on the cell viability and apoptosis of SH-SY5Y cells. Cells were incubated with various concentrations of acetaldehyde for 24 h. (a) Cell viability was determined with trypan blue assay. The number of cells in control group is set to 100%. (b) The cells were fixed and stained with Hoechst 33258. (c) SH-SY5Y cells were treated with different concentration of acetaldehyde for 24 h. Total RNA was isolated after the treatment and the expression of *Bcl-2*, *Bcl-xL*, and *Bax* genes was assessed by RT-PCR. The expression of GAPDH was used as an internal control. (d) Total lysates of cells were collected and the caspase 3 activities were determined. Data are expressed as the values of concentration of pNA. Values are means ± SD, $n = 3$. $**$, significantly different from untreated cells ($P < 0.01$).

and Bcl-xL, via affecting the permeability of the mitochondrial outer membrane [14]. The balance between antiapoptotic and proapoptotic Bcl-2 family proteins determines the fate of cells including the survival of individual neurons [17–19]. Our results showed that the expression of *Bcl-xL* and *Bcl-2* was decreased while the expression of *Bax* was upregulated by acetaldehyde treatment in SH-SY5Y cells. These results suggested that acetaldehyde induced apoptosis of SH-SY5Y cells though mitochondria apoptotic pathway.

The serine/threonine kinase Akt, also known as protein kinase B (PKB), is a key player in regulating cell signals that are important for cell death and survival [20]. Multiple apoptotic/survival regulating molecules are downstream substrates of Akt, for examples, Bcl-2-associated death protein (Bad) [21], caspase 9 [22], glycogen synthase kinase 3β (GSK3β) [23], and CREB [24]. The reduction of Akt activation by augmented acetaldehyde exposure has been shown in alcohol-induced myocardial dysfunction and hepatic apoptosis [25–27]. In this study, acetaldehyde treatment caused a dose-dependent inhibition of the activation of Akt in SH-SY5Y cells, suggesting that acetaldehyde might decrease the cell survival and promote apoptotic signaling by suppressing Akt activation. The phosphorylation of transcription factor CREB by Akt on Ser133 results in its transcriptional activation. Our data also showed that the levels of activated CREB were decreased by acetaldehyde treatment. CREB promotes cell survival via a transcription-dependent mechanism, upregulating the expression of antiapoptotic genes such as *Bcl-2* [28, 29]. Thus, it is possible that the decrease of *Bcl-2* gene expression by acetaldehyde treatment seen in our study

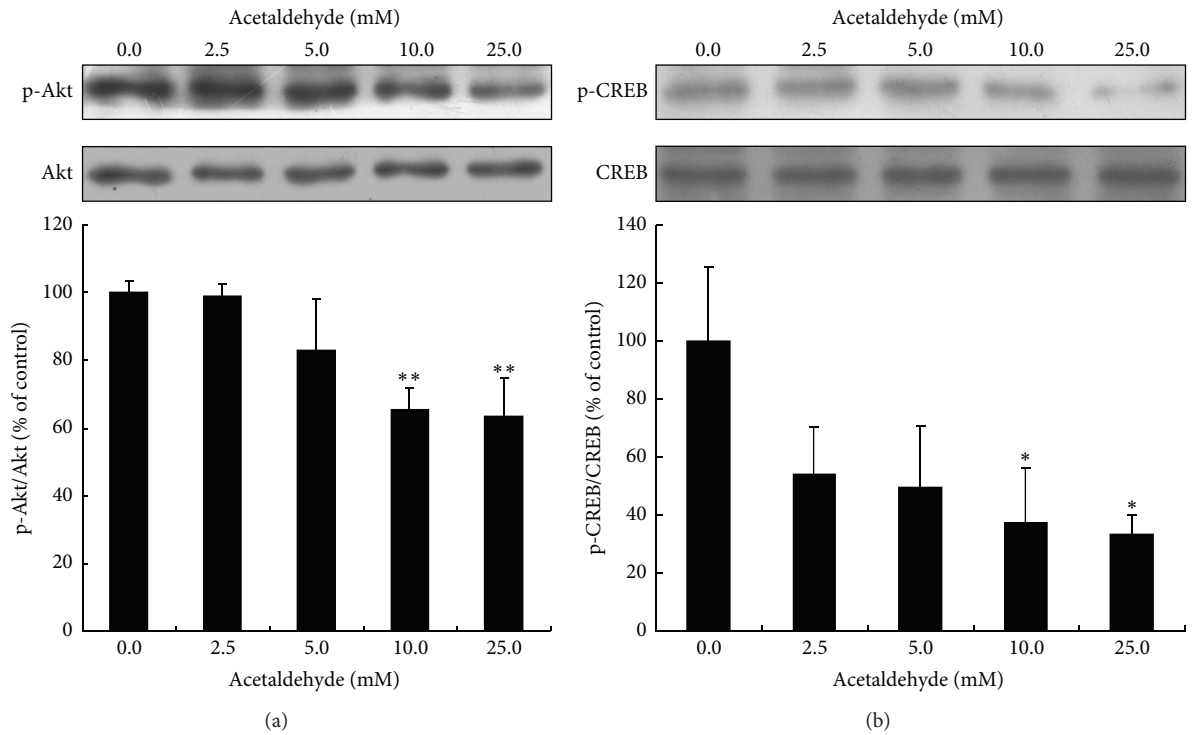

Figure 2: Effects of acetaldehyde treatment on the activation of Akt and CREB in SH-SY5Y cells. SH-SY5Y cells were treated with different concentrations of acetaldehyde for 24 h. Total cell lysates were collected and the amount of Akt, phospho-Akt (Ser473) (a), CREB, and phospho-CREB (Ser 133) (b) was determined by Western blot analysis. The intensities of the bands were quantified by densitometric analyses and normalized by the amount of Akt or CREB. Values are means ± SD from three independent experiments. ∗, significantly different from control ($P < 0.05$); ∗∗, significantly different from control ($P < 0.01$).

resulted from the inhibition of acetaldehyde on Akt/CREB pathway.

MAPKs are important cell signals that are involved in both apoptosis and cell survival. It has been shown that the activation of p38MAPK and c-Jun N-terminal kinases (JNKs) promotes apoptosis [30, 31] while ERKs inhibit apoptosis [32]. There are few studies on how acetaldehyde affects the activation of MAPKs in neuronal cells. In this study, 24 h treatment of SH-SY5Y cells with acetaldehyde activated p38MAPK while inhibiting ERKs in a dose-dependent manner. The suppression of ERKs activation has been associated with the decrease of Bcl-2 expression or the ratio of Bcl-2/Bax that leads to the activation of caspase 3 [33, 34]. It is also reported that ERKs suppress the apoptosis of osteosarcoma cells induced by an acidic polysaccharide via activating Bcl-xL [35]. Thus, the inhibition of acetaldehyde on ERK activation may play a role in its modulation of the expression of Bcl-2 family proteins. As p38MAPK was shown to inhibit CREB activated Bcl-2 expression [36], the activation of p38MAPK by acetaldehyde may also contribute to the downregulation of *Bcl-2* expression, potentially mediated by the inhibitory effect of p38MAPK on CREB activation. Furthermore, previous studies have shown that treating cells with ERKs inhibitor attenuates the activation of Akt [37, 38] while the activation of p38MAPK may be involved in the inactivation of PI3K/Akt signaling pathway [39]. Collectively, the evidence suggests that there may be a crosstalk between Akt-CREB and p38/ERKs pathways, and Akt/CREB may be located in the downstream of p38/ERK signaling pathway in acetaldehyde-induced apoptotic event, with p38MAPK playing a role as proapoptotic factor while ERKs acting as an antiapoptotic factor.

Activated JNKs have been shown to suppress the expression of Bcl-2, leading to the release of cytochrome c and triggering apoptosis [40]. In our study, we only found a slight increase in the activation of JNKs after 24 h exposure of acetaldehyde (5 mM). It is possible that acetaldehyde induces the activation of JNKs within short period after the treatment, as reported in the study of Lee and Shukla [41]. This is currently under investigation and the preliminary results showed that the elevation of activated JNK occurred after a short exposure (<1 h) of acetaldehyde (data not shown). And this short term activation of JNK could contribute to the downregulation of Bcl-2 expression and apoptosis induced by acetaldehyde. Overall, these data suggested that the modulation of MAPKs by acetaldehyde plays important roles in acetaldehyde-induced apoptosis in SH-SY5Y cells.

Oxidative stress has emerged as one of the important factors in neuronal cell death in neurodegenerative diseases such as AD. Accumulating evidence has shown that ethanol and acetaldehyde exposure could lead to elevated production of ROS and oxidative stress [42, 43]. Our results also showed that ROS production was significantly elevated in SH-SY5Y cells after a short time exposure of acetaldehyde.

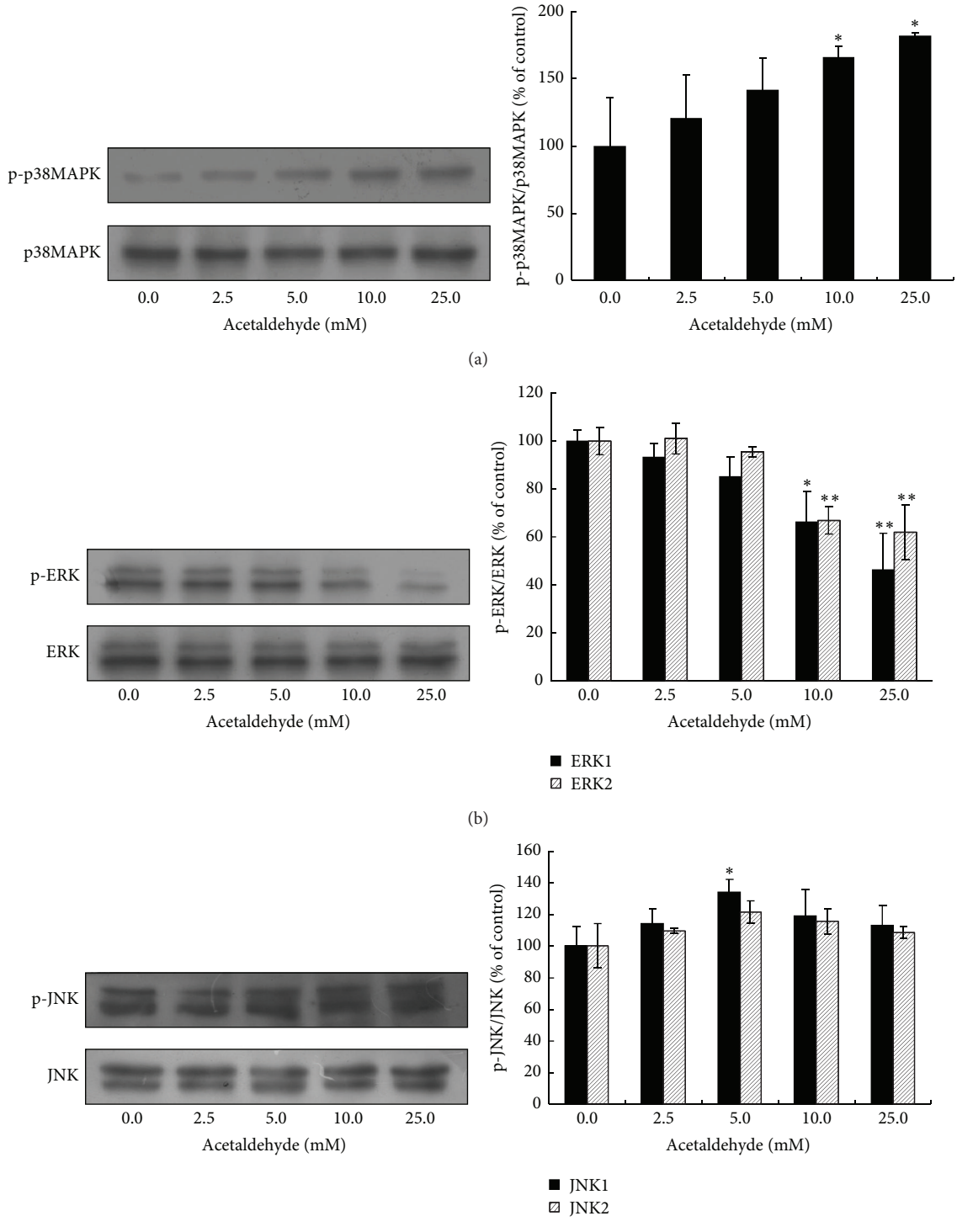

Figure 3: Effects of acetaldehyde on the activation of p38MAPK/ERK/JNK in SH-SY5Y cells. SH-SY5Y cells were treated with different concentrations of acetaldehyde for 24 h. Total cell lysates were collected and the protein levels of p38MAPK, phosho-p38MAPK (Thr180/Tyr182) (a), ERK (p44/p42) MAPK and phospho-ERK (Thr202/Tyr204) (b), and JNK and phospho-JNK (Thr183/Tyr185) (c) were determined by Western blot analyses. The intensities of the bands were quantified by densitometric analyses and normalized by the amount of p38MAPK, JNK, or ERK. Values are means ± SD from three independent experiments. $*$, significantly different from control ($P < 0.05$); $**$, significantly different from control ($P < 0.01$).

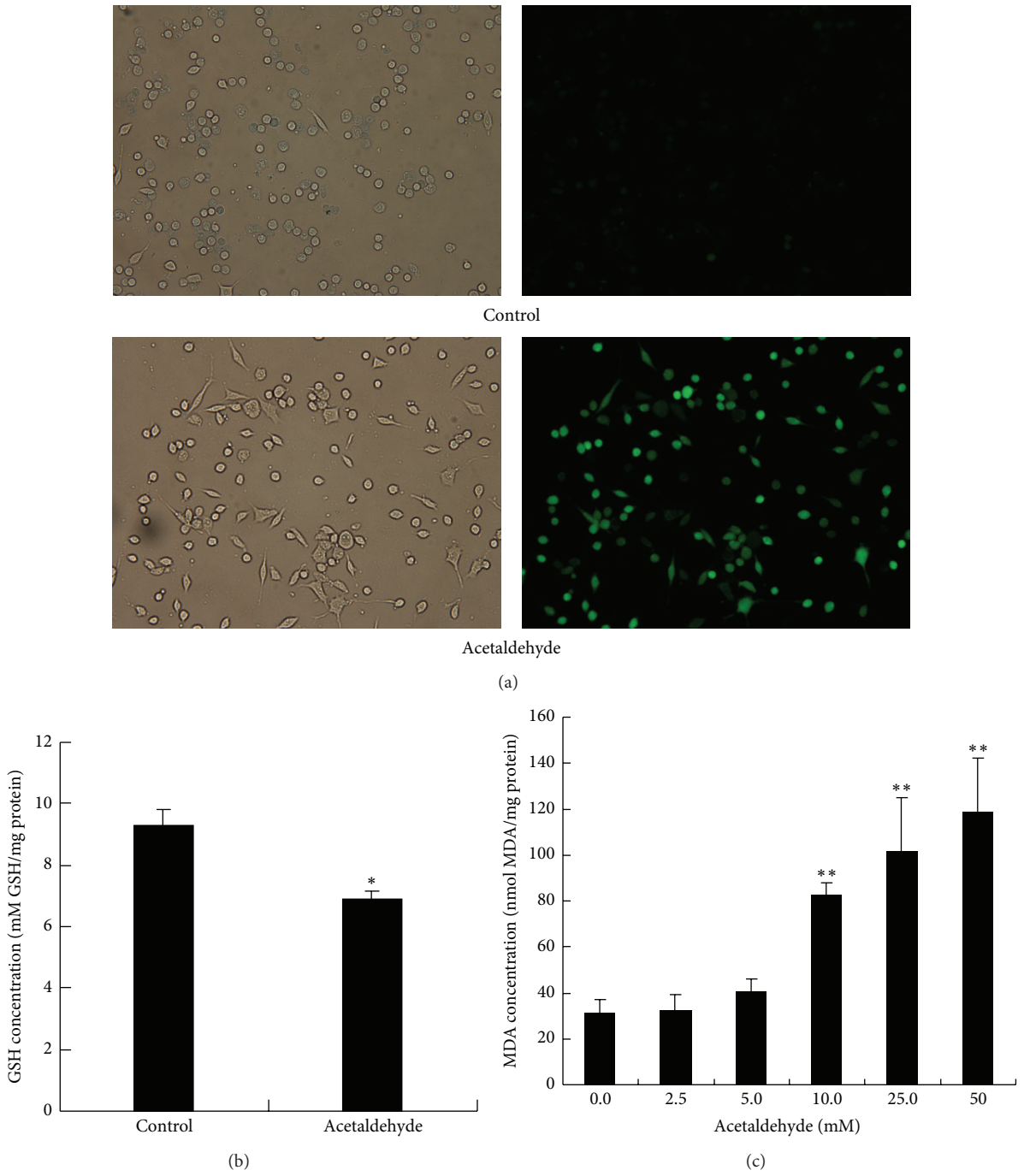

Figure 4: Acetaldehyde increases oxidative stress in SH-SY5Y cells. (a) SH-SY5Y cells were treated with 10 mM of acetaldehyde for 1 h. Cells were then stained with DCFH-DA to determine the production of ROS. Images on the left side are the phase images of the cells. (b) SH-SY5Y cells were treated with 5 mM of acetaldehyde for 2 h. The levels of reduced GSH were determined in the cell lysates. (c) SH-SY5Y cells were treated with different concentration of acetaldehyde for 24 h. MDA production was measured in the cell lysates. Values are means ± SD. $*$, significantly different from control cells ($P < 0.05$); $**$, significantly different from control cells ($P < 0.01$).

The induction of oxidative stress was also indicated by the decreased intracellular GSH content and the increased levels of MDA after acetaldehyde treatment. These data suggest that oxidative stress is one of the early events induced by acetaldehyde in the cell, and the cytotoxicity of acetaldehyde is at least partly caused by its induction of intracellular oxidative stress.

In summary, our results suggest that a complex crosstalk between signaling pathways, such as MAPKs and Akt/CREB, may act together in acetaldehyde-induced apoptotic event.

And acetaldehyde induced cytotoxicity of SH-SY5Y cells via promotion of apoptotic signaling, inhibition of cell survival pathway, and induction of oxidative stress. The study also provides evidence that inhibition of oxidative stress by antioxidants may be beneficial for preventing neuronal damage associated with acetaldehyde-induced cytotoxicity which could be resulting from excessive alcohol consumption.

Abbreviations

ALDH: Aldehyde dehydrogenase
AD: Alzheimer's disease
CREB: Cyclic AMP-responsive element binding protein
ERKs: Extracellular signal-regulated kinases
JNKs: c-Jun N-terminal kinases
MDA: Malondialdehyde
MAPK: Mitogen-activated protein kinase
ROS: Reactive oxygen species.

Conflict of Interests

The authors declare that there is no conflict of interests regarding the publication of this paper.

Acknowledgments

This work is supported by grants from the National Natural Science Foundation of China (31371082) and research fund from Harbin Institute of Technology at Weihai (HIT (WH) Y200902).

References

[1] C. Harper, "The neuropathology of alcohol-related brain damage," *Alcohol and Alcoholism*, vol. 44, no. 2, pp. 136–140, 2009.

[2] D. G. Harwood, A. Kalechstein, W. W. Barker et al., "The effect of alcohol and tobacco consumption, and apolipoprotein E genotype, on the age of onset in Alzheimer's disease," *International Journal of Geriatric Psychiatry*, vol. 25, no. 5, pp. 511–518, 2010.

[3] D. W. Crabb and S. Liangpunsakul, "Acetaldehyde generating enzyme systems: roles of alcohol dehydrogenase, CYP2E1 and catalase, and speculations on the role of other enzymes and processes," *Novartis Foundation Symposium*, vol. 285, pp. 4–22, 2007.

[4] T. Miyake and T. Shibamoto, "Quantitative analysis of acetaldehyde in foods and beverages," *Journal of Agricultural and Food Chemistry*, vol. 41, no. 11, pp. 1968–1970, 1993.

[5] G.-S. Peng and S.-J. Yin, "Effect of the allelic variants of aldehyde dehydrogenase *ALDH2*2* and alcohol dehydrogenase *ADH1B*2* on blood acetaldehyde concentrations," *Human Genomics*, vol. 3, no. 2, pp. 121–127, 2009.

[6] K. Tokuda, Y. Izumi, and C. F. Zorumski, "Locally-generated acetaldehyde is involved in ethanol-mediated LTP inhibition in the hippocampus," *Neuroscience Letters*, vol. 537, pp. 40–43, 2013.

[7] E. Menegola, M. L. Broccia, F. Di Renzo, and E. Giavini, "Acetaldehyde in vitro exposure and apoptosis: a possible mechanism of teratogenesis," *Alcohol*, vol. 23, no. 1, pp. 35–39, 2001.

[8] A. Holownia, M. Ledig, J. J. Braszko, and J.-F. Ménez, "Acetaldehyde cytotoxicity in cultured rat astrocytes," *Brain Research*, vol. 833, no. 2, pp. 202–208, 1999.

[9] L. Gómez-Quiroz, L. Bucio, V. Souza et al., "Interleukin 8 response and oxidative stress in HepG2 cells treated with ethanol, acetaldehyde or lipopolysaccharide," *Hepatology Research*, vol. 26, no. 2, pp. 134–141, 2003.

[10] B. E. Farfán Labonne, M. Gutiérrez, L. E. Gómez-Quiroz et al., "Acetaldehyde-induced mitochondrial dysfunction sensitizes hepatocytes to oxidative damage," *Cell Biology and Toxicology*, vol. 25, no. 6, pp. 599–609, 2009.

[11] D. Clavijo-Cornejo, M. Gutiérrez-Carrera, M. Palestino-Domínguez et al., "Acetaldehyde targets superoxide dismutase 2 in liver cancer cells inducing transient enzyme impairment and a rapid transcriptional recovery," *Food and Chemical Toxicology*, vol. 69, pp. 102–108, 2014.

[12] M. Tong, L. Longato, Q.-G. Nguyen, W. C. Chen, A. Spaisman, and S. M. De La Monte, "Acetaldehyde-mediated neurotoxicity: relevance to fetal alcohol spectrum disorders," *Oxidative Medicine and Cellular Longevity*, vol. 2011, Article ID 213286, 13 pages, 2011.

[13] T. W. Jung, J. Y. Lee, W. S. Shim et al., "Adiponectin protects human neuroblastoma SH-SY5Y cells against acetaldehyde-induced cytotoxicity," *Biochemical Pharmacology*, vol. 72, no. 5, pp. 616–623, 2006.

[14] A. Gross, J. M. McDonnell, and S. J. Korsmeyer, "BCL-2 family members and the mitochondria in apoptosis," *Genes and Development*, vol. 13, no. 15, pp. 1899–1911, 1999.

[15] M. Tang, S. Shi, Y. Guo et al., "GSK-3/CREB pathway involved in the gx-50's effect on Alzheimer's disease," *Neuropharmacology*, vol. 81, pp. 256–266, 2014.

[16] H. Esterbauer, R. J. Schaur, and H. Zollner, "Chemistry and biochemistry of 4-hydroxynonenal, malonaldehyde and related aldehydes," *Free Radical Biology and Medicine*, vol. 11, no. 1, pp. 81–128, 1991.

[17] D. M. Finucane, E. Bossy-Wetzel, N. J. Waterhouse, T. G. Cotter, and D. R. Green, "Bax-induced caspase activation and apoptosis via cytochrome c release from mitochondria is inhibitable by Bcl-xL," *The Journal of Biological Chemistry*, vol. 274, no. 4, pp. 2225–2233, 1999.

[18] C. Xu, A. Wu, H. Zhu et al., "Melatonin is involved in the apoptosis and necrosis of pancreatic cancer cell line SW-1990 via modulating of Bcl-2/Bax balance," *Biomedicine & Pharmacotherapy*, vol. 67, no. 2, pp. 133–139, 2013.

[19] D. Y. Yang, X. Liu, R. F. Zhang et al., "Increased apoptosis and different regulation of pro-apoptosis protein bax and anti-apoptosis protein bcl-2 in the olfactory bulb of a rat model of depression," *Neuroscience Letters*, vol. 504, no. 1, pp. 18–22, 2011.

[20] Y.-Y. Hsu, C.-M. Liu, H.-H. Tsai, Y.-J. Jong, I.-J. Chen, and Y.-C. Lo, "KMUP-1 attenuates serum deprivation-induced neurotoxicity in SH-SY5Y cells: roles of PKG, PI3K/Akt and Bcl-2/Bax pathways," *Toxicology*, vol. 268, no. 1-2, pp. 46–54, 2010.

[21] F. Yu, T. Sugawara, C. M. Maier, L. B. Hsieh, and P. H. Chan, "Akt/Bad signaling and motor neuron survival after spinal cord injury," *Neurobiology of Disease*, vol. 20, no. 2, pp. 491–499, 2005.

[22] M. V. Chuenkova and M. A. Pereira, "PDNF, a human parasite-derived mimic of neurotrophic factors, prevents caspase activation, free radical formation, and death of dopaminergic cells exposed to the Parkinsonism-inducing neurotoxin MPP^+," *Molecular Brain Research*, vol. 119, no. 1, pp. 50–61, 2003.

[23] B. A. Stoica, V. A. Movsesyan, P. M. Lea IV, and A. I. Faden, "Ceramide-induced neuronal apoptosis is associated

with dephosphorylation of Akt, BAD, FKHR, GSK-3β, and induction of the mitochondrial-dependent intrinsic caspase pathway," *Molecular and Cellular Neuroscience*, vol. 22, no. 3, pp. 365–382, 2003.

[24] L. Zhang, H. Zhao, X. Zhang et al., "Nobiletin protects against cerebral ischemia via activating the p-Akt, p-CREB, BDNF and Bcl-2 pathway and ameliorating BBB permeability in rat," *Brain Research Bulletin*, vol. 96, pp. 45–53, 2013.

[25] S.-Y. Li and J. Ren, "Cardiac overexpression of alcohol dehydrogenase exacerbates chronic ethanol ingestion-induced myocardial dysfunction and hypertrophy: role of insulin signaling and ER stress," *Journal of Molecular and Cellular Cardiology*, vol. 44, no. 6, pp. 992–1001, 2008.

[26] S.-Y. Li, S. A. B. Gilbert, Q. Li, and J. Ren, "Aldehyde dehydrogenase-2 (ALDH2) ameliorates chronic alcohol ingestion-induced myocardial insulin resistance and endoplasmic reticulum stress," *Journal of Molecular and Cellular Cardiology*, vol. 47, no. 2, pp. 247–255, 2009.

[27] R. Guo, L. Zhong, and J. Ren, "Overexpression of aldehyde dehydrogenase-2 attenuates chronic alcohol exposure-induced apoptosis, change in akt and pim signalling in liver," *Clinical and Experimental Pharmacology and Physiology*, vol. 36, no. 5-6, pp. 463–468, 2009.

[28] S. Finkbeiner, "CREB couples neurotrophin signals to survival messages," *Neuron*, vol. 25, no. 1, pp. 11–14, 2000.

[29] J. Zhou, F.-F. Ping, W.-T. Lv, J.-Y. Feng, and J. Shang, "Interleukin-18 directly protects cortical neurons by activating PI3K/AKT/NF-κB/CREB pathways," *Cytokine*, vol. 69, no. 1, pp. 29–38, 2014.

[30] H. Zhang, F. Li, Z. Y. Pan, Z. J. Wu, Y. H. Wang, and Y. D. Cui, "Activation of PI3K/Akt pathway limits JNK-mediated apoptosis during EV71 infection," *Virus Research*, vol. 192, pp. 74–84, 2014.

[31] J. Evans, Y. Ko, W. Mata et al., "Arachidonic acid induces brain endothelial cell apoptosis via p38-MAPK and intracellular calcium signaling," *Microvascular Research*, vol. 98, pp. 145–158, 2015.

[32] G. Y. Wang, C. Y. Jin, Y. Y. Hou et al., "Overexpression of Shp-2 attenuates apoptosis in neonatal rat cardiac myocytes through the ERK pathway," *Experimental and Molecular Pathology*, vol. 93, no. 1, pp. 50–55, 2012.

[33] W. Pang, X. Leng, H. Lu et al., "Depletion of intracellular zinc induces apoptosis of cultured hippocampal neurons through suppression of ERK signaling pathway and activation of caspase-3," *Neuroscience Letters*, vol. 552, pp. 140–145, 2013.

[34] J. P. Yan, Q. B. Liu, Y. Dou et al., "Activating glucocorticoid receptor-ERK signaling pathway contributes to ginsenoside Rg1 protection against beta-amyloid peptide-induced human endothelial cells apoptosis," *Journal of Ethnopharmacology*, vol. 147, no. 2, pp. 456–466, 2013.

[35] Z. Z. Zhang, Y. Zheng, R. Zhu et al., "The ERK/eIF4F/Bcl-XL pathway mediates SGP-2 induced osteosarcoma cells apoptosis in vitro and in vivo," *Cancer Letters*, vol. 352, no. 2, pp. 203–213, 2014.

[36] K. Hui, Y. Yang, K. Shi et al., "The p38 MAPK-regulated PKD1/CREB/Bcl-2 pathway contributes to selenite-induced colorectal cancer cell apoptosis in vitro and in vivo," *Cancer Letters*, vol. 354, no. 1, pp. 189–199, 2014.

[37] X. Wang, J. Z. Liu, J. X. Hu et al., "ROS-activated p38 MAPK/ERK-Akt cascade plays a central role in palmitic acid-stimulated hepatocyte proliferation," *Free Radical Biology and Medicine*, vol. 51, no. 2, pp. 539–551, 2011.

[38] X.-H. Guan, Q.-C. Fu, D. Shi et al., "Activation of spinal chemokine receptor CXCR3 mediates bone cancer pain through an Akt-ERK crosstalk pathway in rats," *Experimental Neurology*, vol. 263, pp. 39–49, 2015.

[39] H. J. Kim, J. E. Oh, S. W. Kim, Y. J. Chun, and M. Y. Kim, "Ceramide induces p38 MAPK-dependent apoptosis and Bax translocation via inhibition of Akt in HL-60 cells," *Cancer Letters*, vol. 260, no. 1-2, pp. 88–95, 2008.

[40] J. Xu, X. Qin, X. Cai et al., "Mitochondrial JNK activation triggers autophagy and apoptosis and aggravates myocardial injury following ischemia/reperfusion," *Biochimica et Biophysica Acta*, vol. 1852, no. 2, pp. 262–270, 2015.

[41] Y. J. Lee and S. D. Shukla, "Pro- and anti-apoptotic roles of c-Jun N-terminal kinase (JNK) in ethanol and acetaldehyde exposed rat hepatocytes," *European Journal of Pharmacology*, vol. 508, no. 1–3, pp. 31–45, 2005.

[42] M. C. Gutiérrez-Ruiz, S. C. Quiroz, V. Souza et al., "Cytokines, growth factors, and oxidative stress in HepG2 cells treated with ethanol, acetaldehyde, and LPS," *Toxicology*, vol. 134, no. 2-3, pp. 197–207, 1999.

[43] M. V. Apte, P. A. Phillips, R. G. Fahmy et al., "Does alcohol directly stimulate pancreatic fibrogenesis? Studies with rat pancreatic stellate cells," *Gastroenterology*, vol. 118, no. 4, pp. 780–794, 2000.

Hindawi Publishing Corporation
Oxidative Medicine and Cellular Longevity
Volume 2016, Article ID 8923860, 8 pages
http://dx.doi.org/10.1155/2016/8923860

Research Article

Nrf2/ARE Pathway Involved in Oxidative Stress Induced by Paraquat in Human Neural Progenitor Cells

Tingting Dou, Mengling Yan, Xinjin Wang, Wen Lu, Lina Zhao, Dan Lou, Chunhua Wu, Xiuli Chang, and Zhijun Zhou

School of Public Health and Key Laboratory of Public Health Safety of the Ministry of Education, Fudan University, Shanghai 200032, China

Correspondence should be addressed to Xiuli Chang; xlchang@fudan.edu.cn and Zhijun Zhou; zjzhou@shmu.edu.cn

Received 11 June 2015; Accepted 8 July 2015

Academic Editor: Michela Battistelli

Compelling evidences have shown that diverse environmental insults arising during early life can either directly lead to a reduction in the number of dopaminergic neurons or cause an increased susceptibility to neurons degeneration with subsequent environmental insults or with aging alone. Oxidative stress is considered the main effect of neurotoxins exposure. In this study, we investigated the oxidative stress effect of Paraquat (PQ) on immortalized human embryonic neural progenitor cells by treating them with various concentrations of PQ. We show that PQ can decrease the activity of SOD and CAT but increase MDA and LDH level. Furthermore, the activities of Cyc and caspase-9 were found increased significantly at 10 μM of PQ treatment. The cytoplasmic Nrf2 protein expressions were upregulated at 10 μM but fell back at 100 μM. The nuclear Nrf2 protein expressions were upregulated as well as the downstream mRNA expressions of HO-1 and NQO1 in a dose-dependent manner. In addition, the proteins expression of PKC and CKII was also increased significantly even at 1 μM. The results suggested that Nrf2/ARE pathway is involved in mild to moderate PQ-induced oxidative stress which is evident from dampened Nrf2 activity and low expression of antioxidant genes in PQ induced oxidative damage.

1. Introduction

Agricultural chemicals are becoming increasingly potent environmental threats. Paraquat (PQ; 1,1′-dimethyl-4,4′-bipyridium) is a widely used fast-acting and nonselective contact herbicide, which is mainly accumulated in the lung, resulting in widespread reports for its pulmonary toxicity [1]. PQ has also been shown to cross the blood-brain barrier and enter the brain through a neutral amino acid carrier due to its structural homology to amino acids [2, 3]. Animal experiments demonstrate that prolonged PQ exposure can result in its accumulation in different brain regions [4]. Extensive evidence demonstrates that PQ is linked to nigrostriatal damage and the emergence of Parkinson symptoms in epidemiological investigations and animal studies [5]. Importantly, compelling evidence from animal models has shown that diverse environmental factors arising during early life may either directly lead to a reduction in the number of dopamine neurons in substantia nigra or cause an increased susceptibility to degeneration of these neurons with subsequent environmental insults or with aging alone [6, 7]. Moreover, some direct evidence shows that PQ has the ability to cross the placenta and it was found in higher concentrations in the placenta than in the mother's blood [8]. Exposure to PQ in the early life can produce progressive, permanent, and cumulative neurotoxicity of the nigrostriatal dopamine system and enhance vulnerability to subsequent environmental insults [6, 7]. Our previous study in vitro suggested that PQ could reduce viability of human embryonic neural progenitor cells (hNPCs) by inducing oxidative stress and apoptosis [9]. Taken together, the persistence developmental neurotoxicity of PQ which may contribute to later-in-life adverse effects needs more attention.

Although the mechanism of PQ neurotoxicity has not been completely clear, the importance of oxidative stress in it has been generally proved [10–12]. PQ can induce oxidative damage to various neurocytes like neurons and hippocampus cells [13–15]. PQ induces oxidative stress through producing

reactive oxygen species (ROS), including hydrogen peroxide, superoxide anion, and hydroxyl radicals, and consuming nicotinamide adenine dinucleotide phosphate (NADPH), an important intracellular reducing agent to exert its toxicity. In addition, ROS is an important second messenger involved in activation or regulation of cell apoptosis. In the apoptosis pathway, caspase-dependent mitochondria pathway plays a decisive role. Divergent cellular stresses promote the release of caspase-activating factors, notably cytochrome c (Cyc) from mitochondrial intermembrane space, to cytoplasm to combine with apoptotic protease activating factor-1 (Apaf-1) and adenosine triphosphate (ATP) to form apoptosome assembly, activating caspase-9 to further activate caspase-3, driving caspase cascade in cytoplasm, causing substrate proteolysis and cellular collapse to induce cell apoptosis [16, 17].

Therefore, the identification of the potential antioxidant pathway against oxidative damage had attracted intense interest. Among the multiple mechanisms, Nrf2-Keap1/ARE signal pathway is the most important endogenous antioxidant pathway discovered to date. While being attacked by ROS or other exogenous toxicant, the cytoplasm nuclear factor erythroid 2-related factor 2 (Nrf2) which was activated by dissociation with kelch-like ECH-associated protein (Keap1) entered the nucleus, binding to antioxidant reactive element (ARE), starting the transcription of corresponding downstream antioxidant molecules including phase II detoxifying enzymes [18] and antioxidative proteins [19, 20], to suppress the oxidative stress and maintain the redox balance. Several antioxidative enzymes and detoxifying enzymes levels had been downregulated in Nrf2 knockout mouse, which made the mouse more susceptive to toxin damage [21].

In addition, the developing brain is much more susceptible to being injured than the adult's brain [22, 23]. Neural stem cells' self-renewal and multipotent differentiation capacity makes it an ideal model in studying neurodevelopmental toxicological mechanism [24, 25]. In this study, we investigate the effects caused by PQ on the imbalance of oxidation and antioxidation and the role of the antioxidation pathway—the Nrf2/ARE pathway in PQ induced neurotoxicity in hNPCs.

2. Material and Methods

2.1. Chemicals and Solution. PQ was purchased from Sigma Chemical Co. (Sigma-Aldrich, Milan, Italy). ReNcell NSC Maintenance Medium and accutase were obtained commercially from Millipore (Temecula, CA). Epidermal growth factor (EGF) and basic fibroblast growth factor (FGF-2) were purchased from PeproTech. Laminin was purchased from Invitrogen (Carlsbad, CA, USA). Catalase Assay Kit, Malondialdehyde Assay Kit, Lactate Dehydrogenase Assay Kit, BCA Protein Assay Kit, Cell Lysis Buffer for Western and IP, goat anti-rabbit IgG-HRP, and goat anti-mouse IgG-HRP were obtained from Beyotime (Jiangsu, China). Total Superoxide Dismutase Assay Kit was purchased from Dojindo Molecular Technologies (Kumamoto, Japan). Tripure was obtained from Roche (Basel, Switzerland). The AMV first strand cDNA Synthesis Kit was purchased from MBI (Fermentas, Canada). Real-time PCR Kit was obtained from Tiangen Biotech (Beijing, China). Rabbit anti-Nrf2 polyclonal antibody, rabbit anti-Keap1 polyclonal antibody, rabbit anti-PKC polyclonal antibody, and rabbit anti-CKII polyclonal antibody were purchased from GeneTex (San Antonio, USA). Mouse anti-β-tubulin polyclonal antibody was purchased from Boster (Wuhan, China).

2.2. Cell Culture and PQ Treatment. Human neural progenitor cells (hNPCs) were obtained from Millipore (Temecula, CA). Frozen cells were thawed and expanded on laminin-coated 100 mm diameter dish (Corning, Inc., Corning, NY) in complete medium containing fresh EGF (20 ng/mL) and FGF-2 (20 ng/mL). Cells were passaged when they were 80% confluent. After accutase dissociation and centrifugation at 300 g for 3 min, cells were resuspended in complete medium and plated in laminin-coated dish (Corning, Inc., Corning, NY). The cultures were incubated at 37°C in 5% CO_2. The medium was replaced every 24 h.

The cells were plated at a density of 1×10^5/mL in laminin-coated plates. When the cells are approximately 70%–80% confluent, PQ dissolved in PBS was added at concentrations ranging from 0, 1, and 10 to 100 μM and the cultures were maintained for 24 h.

2.3. Measurement of Biomarkers of Oxidative Stress. After treatment of PQ for 24 h, the levels of methane dicarboxylic aldehyde (MDA) were determined as an indicator of lipid peroxidation. And the activities of superoxide dismutase (SOD), catalase (CAT), and MDA were measured using qualified kits [26, 27]. The absorbance was obtained using a Microplate Reader (Biotek, USA) reading at corresponding wavelength.

2.4. Lactate Dehydrogenase (LDH) Leakage Assay. Oxidative stress-induced cytotoxicity was determined in a colorimetric assay based on the measurement of LDH released into the supernatant, which was determined using an LDH cytotoxicity assay kit according to the manufacturer's instructions [28]. The absorbance was obtained using a Microplate Reader (Biotek, USA) reading at 450 nm.

2.5. RNA Purification, Reverse Transcription, and Quantitative Real-Time PCR. Cell samples were collected after being exposed to PQ for 24 h. Total RNA was first extracted by Tripure following manufacturer instructions. The synthesis of the cDNA was performed utilizing an oligo(DT) primer and reverse transcriptase. All the primers were designed and synthesized based on Primer Premier Software 5.0 (PREMIER Biosoft International) by Sangon Biotech (Shanghai) Co., Ltd. The β-actin primers were 5′-CTCCATCCTGGCCTCGCTGT-3′ (sense) and 5′-GCTGTCACCTTCACCGTTCC-3′ (antisense; NM_001101). The HO-1 primers were 5′-TCGCCCCTGTCTACTTCC-3′ (sense) and 5′-GCAGCTCCTGCAACTCCT-3′ (antisense; NM_002133). The NQO-1 primers were 5′-GCCTAGCACAAGTACCACTCTTGGTC-3′ (sense) and 5′-CTGAGGCAGGAGAATTGCTGGAACC-3′ (antisense; NM_001025434). β-actin was used

as the housekeeping gene. The real-time PCR was done using 2 μL of cDNA, 0.5 μL of each primer, and 2 μL SYBR Green PCR Master Mix in a 10 μL reaction volume. PCR program was a 10 min activation step at 95°C, followed by 40 cycles of 94°C for 15 s, 55°C for 30 s, and finally 72°C for 1 min. Every sample was done in triplicate. The ΔΔCt method was applied for RNA relative expression quantification [9].

2.6. Western Blot Analysis of Cytoplasmic Nrf2, Nuclear Nrf2, Protein Kinase C (PKC), Casein Kinase II (CKII), Cyc, and Caspase-9. After treatment with 0, 1, 10, and 100 μmol/L PQ for 24 h, the protein extraction and western blot process were operated according to the previous study [9]. The immunoreactive proteins were detected by enhanced chemiluminescence using hyperfilm and enhanced chemiluminescence reagent (GE Healthcare, Little Chalfont, Buckinghamshire, UK) according to the manufacturer's instructions. Band intensities were quantified by densitometer analysis system and expressed as IOD (integrated optical density). Target protein densitometry values were adjusted to β-tubulin intensity and normalized to expression from the control sample.

2.7. Statistical Analysis. Data were analyzed with the SPSS 17.0 statistic program and expressed as means ± standard deviations (SD). All data were analyzed by one-way analysis of variance (one-way ANOVA), followed by LSD-*t* test for variance homogeneity and Kruskal-Wallis *H* test for variance heterogeneity. Data obtained at each chemical concentration were compared with the controls. p-value < 0.05 was considered significant.

3. Results

3.1. The Oxidative Damages Induced by PQ in hNPCs. Previous reports from our laboratory indicated that PQ can significantly reduce cells viability to 69% at concentration of 100 μM while it had no effect at 0, 1, and 10 μM [9]; we chose 0, 1 and 10 μM PQ which were no significant cytotoxic and 100 μM PQ which was significant cytotoxic as the exposure concentration in this study. Considering the ROS generation induced by PQ at 10 μM [9] and the balance between oxidation and antioxidation in normal circumstance, we first investigated the antioxidative molecules' SOD and CAT activity to research the oxidative mechanism after treatment with various concentrations of PQ. The two antioxidant enzyme activities both had a dose-dependent decrease with the significant decrease at 100 μM PQ exposure compared to untreated group ($p < 0.05$) (Figure 1).

As the final metabolite of lipid peroxidation, MDA can change the construction and function of cell membrane, leading to the membrane breakage [29]. Besides, LDH which was released when the membrane damaged is considered a kind of sensitive markers of membrane breakage. Therefore, we detected the PQ induced oxidative damage via measuring the intracellular MDA and LDH activity. After treatment with various concentrations of PQ, we found a significant dose-dependent increase of MDA and LDH activity with PQ concentrations as low as 10 μM compared to untreated group ($p < 0.05$) (Figure 2), which were accordant with ROS [9].

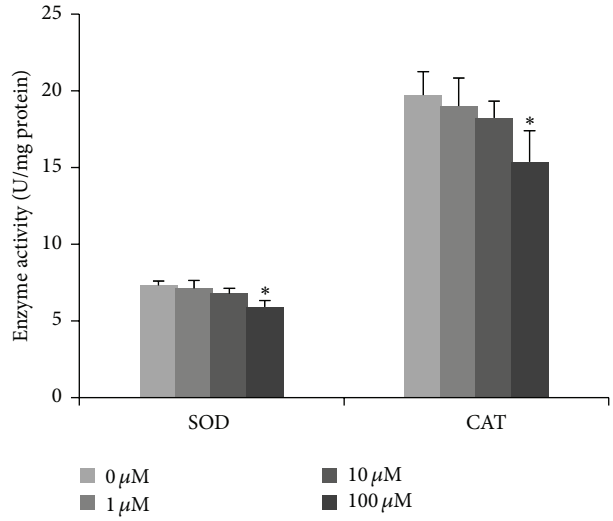

Figure 1: SOD and CAT activity in hNPCs upon exposure to different concentrations of PQ for 24 hr. Results are expressed as means ± S.D. ($n = 3$). * means $p < 0.05$ when compared with the corresponding control group (0 μM).

3.2. Nrf2/ARE Pathway Involved in Oxidative Stress Induced by PQ in hNPCs. Nrf2-ARE-driven genes coordinately function to protect cells from H_2O_2-induced apoptosis in cell studies [30]. Toxic doses of H_2O_2 vary with the cell density, components in culture media, and the cell type studied. The following oxidative stress may result in apoptotic and/or necrotic cell death depending on a variety of factors. To examine the potential role of Nrf2 signaling pathway in preventing PQ induced oxidative stress in hNPCs, we detected the cytoplasmic and nuclear Nrf2 protein expression by western blot. As Figure 3 showed, the cytoplasmic Nrf2 expression was significantly upregulated to 181% at 10 μM of PQ ($p < 0.05$) but fell back to 116% at 100 μM ($p > 0.05$). The nuclear Nrf2 expression was significantly upregulated to 178% and 218% at 10 and 100 μM ($p < 0.05$).

As a result of nuclear Nrf2 increase, we examine Nrf2-ARE-driven genes using real-time PCR after PQ treatment for 24 h. HO-1 mRNA expression was slightly increased to 117% at 1 μM and significantly increased to 175% and 221% at 10 and 100 μM ($p < 0.05$), respectively. NQO1 expression was slightly increased to 111% at 1 μM and significantly increased to 215% and 220% at 10 and 100 μM ($p < 0.01$) (Figure 4).

3.3. Activation of Protein Kinase (PKC and CKII) Induced by PQ in hNPCs. Previous studies had discovered the involvement of protein kinase in phosphorylating Nrf2 and triggering its nuclear translocation in response to oxidative stress [31]. In our study, we used western blot to detect the intracellular PKC and CKII proteins expression after treatment with different concentrations of PQ for 24 h to observe the role of protein kinases in PQ induced Nrf2 activation. As Figure 5 showed, the intracellular PKC and CKII expressions were both significantly upregulated at even 1 μM of PQ ($p < 0.01$).

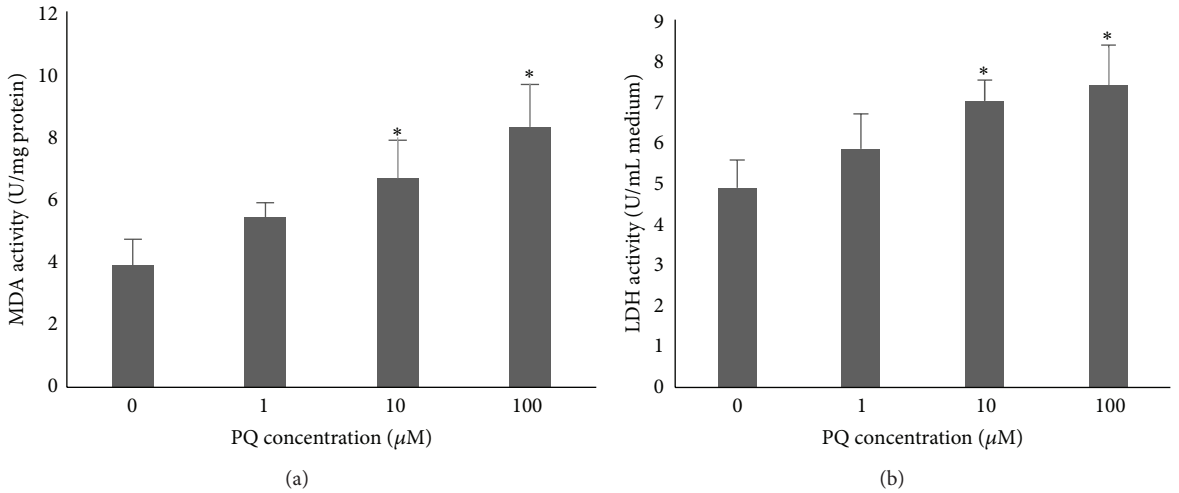

Figure 2: The oxidative damage of hNPCs induced by PQ treatment. (a) The intracellular MDA activity in hNPCs upon exposure to different concentrations of PQ. (b) The released LDH level of hNPCs upon exposure to different concentrations of PQ. Results are expressed as means ± S.D. ($n = 3$). ∗ means $p < 0.05$ when compared with the corresponding control group (0 μM).

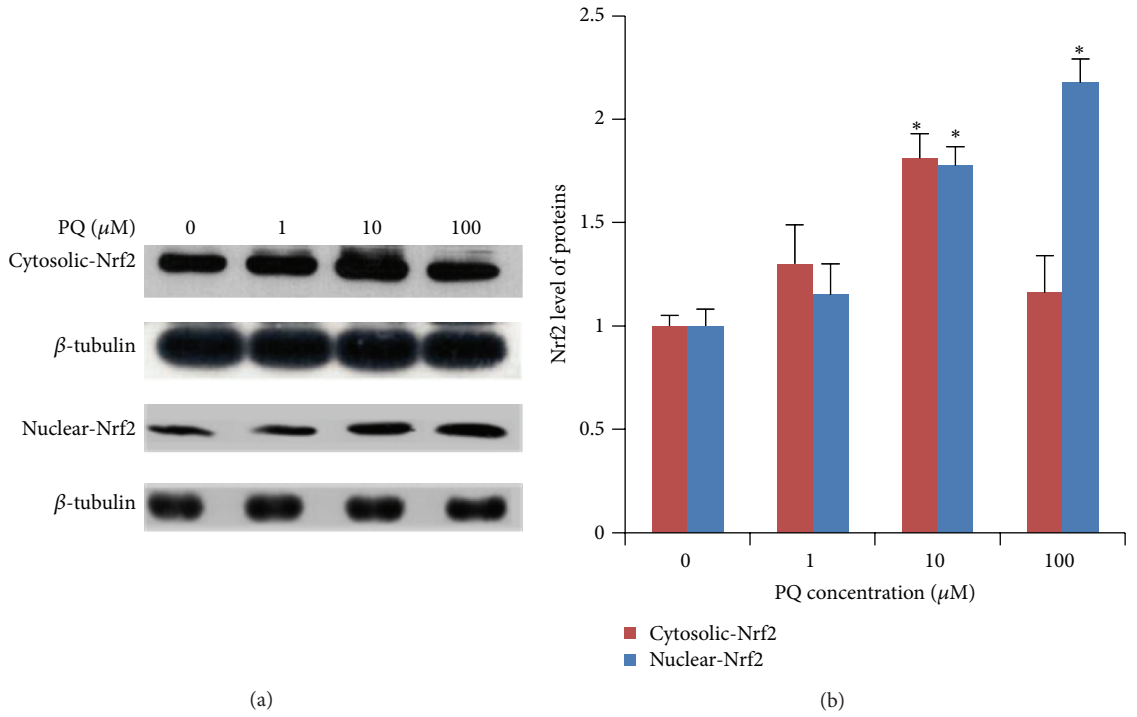

Figure 3: The expression of cytoplasmic and nuclear Nrf2 proteins in hNPCs after exposure to different concentrations of PQ. (a) Electrophoretic band of cytoplasmic and nuclear Nrf2 proteins by western blot. (b) Quantification of cytoplasmic and nuclear Nrf2 proteins expression. Results are expressed as means ± S.D. ($n = 3$). ∗ and ∗∗ mean $p < 0.05$ and $p < 0.01$ when compared with the corresponding control group (0 μM).

3.4. Effect of PQ on Apoptotic Cell Death Signaling Pathways of hNPCs. Oxidative stress had been shown to activate caspase-dependent apoptotic cell death signaling pathways [32]. Cyc combined with Apaf-1 and subsequently activated caspase-9 to initiate downstream effector caspases to cause the cell apoptosis [33, 34]. Herein, we examined the protein expressions of Cyc and caspase-9. Figure 6 showed that Cyc and caspase-9 protein expressions were both significantly increased in 10 μM PQ treatment group compared with the control ($p < 0.05$).

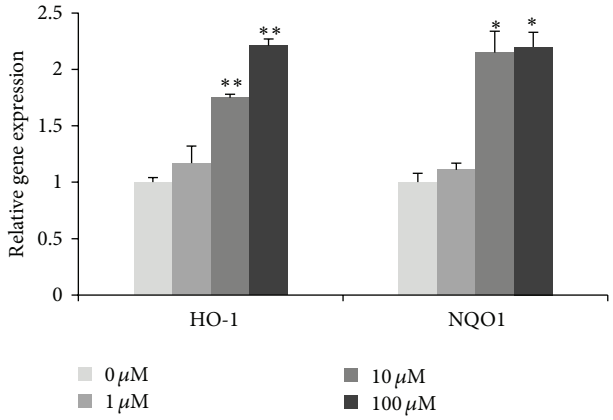

Figure 4: The gene expression of HO-1 and NQO1 in hNPCs after exposure to different concentrations of PQ. Results are expressed as means ± S.D. ($n = 3$). $*$ and $**$ mean $p < 0.05$ and $p < 0.01$ when compared with the corresponding control group (0 μM).

4. Discussion

In the present study, we demonstrate that PQ can directly produce toxicity to hNPCs by inducing ROS generation and decreasing SOD and CAT activity which resulted in redox imbalance and oxidative damage. In particular, we found that PQ induced oxidative stress can activate the Nrf2-Keap1/ARE signaling pathway to initiate the downstream antioxidant responsive elements including HO-1 and NQO1 mRNAs expression to prevent the oxidative damage. Additionally, we observed that PQ can activate PKC and CKII which were involved in the phosphorylation of Nrf2, revealing that PKC and CKII may play an indirect part in antioxidative stress.

As one of the most widely used herbicides in the world, PQ can induce damage to various organs or cells [35–37]. To the nervous system, because of the structural similarity to the parkinsonism-inducing neurotoxic agent 1-methyl-4-phenyl-1, 2, 3, 6-tetrahydropyridine (MPTP), PQ is considered to be a possible environmental risk factor for neurodegenerative disorders like Parkinson's disease (PD) [38, 39]. In addition, the developing brain is much more susceptible to be injured than the adult's brain [21, 22]. Therefore, PQ developmental neurotoxicity deserves more attention. It was reported that PQ could inhibit the proliferation and disrupt the differentiation of neural precursor cells in vitro studies [40]. Also, in our previous study, we found the concentration of PQ reducing the hNPCs viability (100 μM) [9] was lower than other cell types [41, 42], suggesting the sensitivity of hNPCs to PQ induced toxicity. Based on the effect of PQ on hNPCs viability, in this study, we chose 0, 1, 10, and 100 μM as the exposure concentrations.

Because of its extensive effects on cell proliferation, differentiation, apoptosis, and signal transduction, ROS plays an important role in neurotoxicity. Several studies have suggested that PQ could cause dopaminergic neurons and hippocampal neurons damage via generating ROS to cause oxidative damage to brain mitochondria [15, 43]. Our previous study had also shown that PQ exposure could cause a dose-dependent increase in ROS production and significant increases were observed when PQ doses were increased to 10 μM [9]. Besides, LDH which is released when the membrane damaged is considered a kind of sensitive markers of membrane breakage. Similarly, our study showed that PQ increased the LDH and MDA levels. These results suggest that PQ induced the production of lipid peroxidation and oxidative damage in hNCPs.

As a sensitive receptor for oxidative stress, Nrf2/Keap1 signaling pathway played a crucial role in preventing cells from apoptosis, stress, inflammation, and tumor [20]. It was the most important intrinsic antioxidative stress pathway yet discovered [44, 45]. When the Nrf2/Keap1 signaling pathway was activated, Nrf2 was uncoupled from inhibitor protein-Keap1 and accessed to nucleus to bind with ARE, leading to the transcription of the downstream target antioxidative genes, and sequentially improved cell's antioxidative stress ability [46, 47]. Similarly, in our study, 10 μM PQ induced oxidative stress can significantly activate the Nrf2 pathway to prevent the oxidative stress via increasing the level of both cytoplasmic and nuclear Nrf2 protein and the Nrf2 downstream antioxidative genes, HO-1 and NQO1, which meant the activation of Nrf2/Keap1 signaling pathway to increase nuclear antioxidative genes expression to prevent 10 μM PQ caused oxidative stress.

In other way, normal cells can eliminate the redundant ROS through antioxidant enzyme including SOD and CAT to prevent the oxidative damage. But severe exposure to toxicant could increase the oxidation but decrease the antioxidation to damage the oxidative balance. Previous studies have showed that SOD and CAT in dopaminergic neurons were all decreased after PQ exposure [41, 48]. Similarly, our study showed that higher level of PQ (100 μM) can significantly inhibit antioxidant enzymes SOD and CAT activity, which meant the imbalance of oxidation and the severity of 100 μM PQ induced oxidative damage. Enhanced nuclear Nrf2 expression was further augmented by PQ treatment to further activate downstream antioxidative genes HO-1 and NQO1 expressions to defend the oxidative damage. The level of cytoplasmic Nrf2 fell back at 100 μM. Similarly, a previous study also has discovered that higher concentration of PQ exposure (0.5 mmol/L) could inhibit neuroblastoma Nrf2 protein level [49].

In addition, some protein kinases like PKC and CKII could also induce the Nrf2 protein phosphorylation to influence its activity [31, 50]. In our study, the intracellular PKC and CKII protein levels were elevated with the increasing of PQ concentration even at 1 μM, which revealed the correlation between Nrf2 activation and its phosphorylation caused by PKC and CKII.

However, as an important second messenger involved in regulation of cell apoptosis, high level of ROS induced by PQ could inevitably cause mitochondria damage and cell apoptosis [51, 52]. In our study, the mitochondria released Cyc level increased at 10 μM, which resulted in the increase of caspase-9. That was consistent with the cells apoptosis and cells viability alteration discovered in previous study [9], suggesting the obvious cells damage caused by high concentration (100 μM) of PQ.

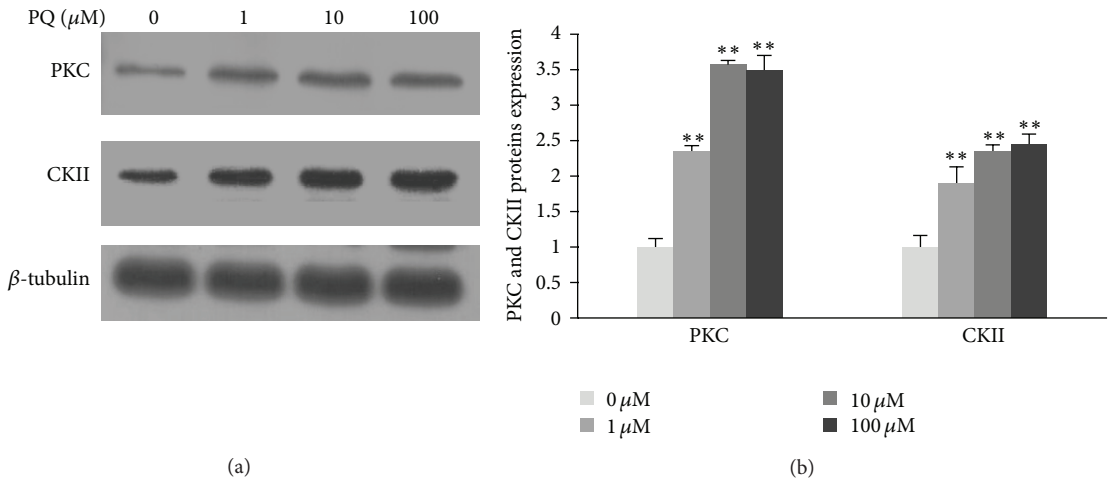

Figure 5: The expression of PKC and CKII proteins in hNPCs after exposure to different concentrations of PQ. (a) Electrophoretic band of PKC and CKII proteins by western blot. (b) Quantification of PKC and CKII proteins expression. Results are expressed as means ± S.D. ($n = 3$). ∗∗ means $p < 0.01$ when compared with the corresponding control group (0 μM).

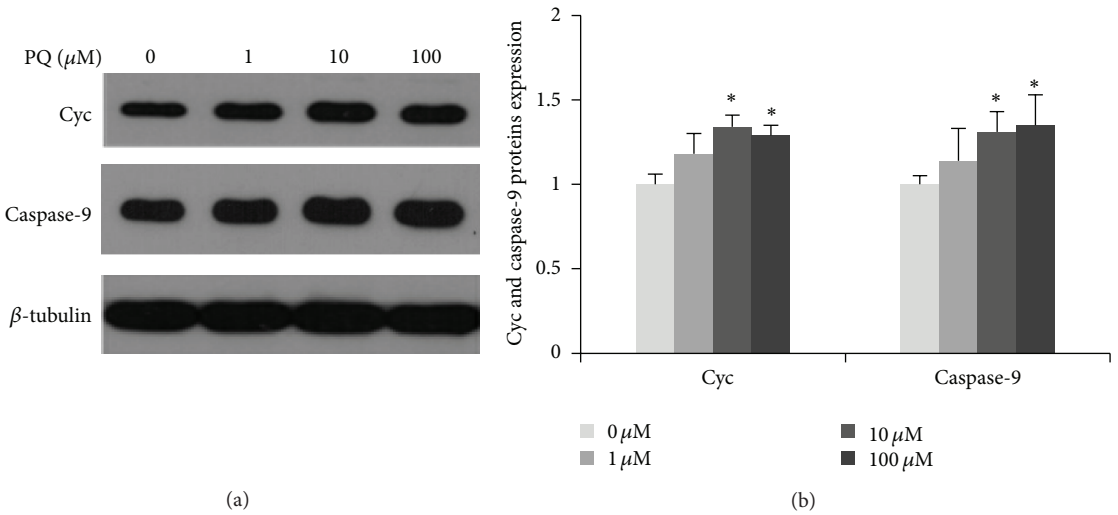

Figure 6: The expression of Cyc and caspase-9 proteins in hNPCs after exposure to different concentrations of PQ. (a) Electrophoretic band of Cyc and caspase-9 proteins by western blot. (b) Quantification of Cyc and caspase-9 proteins expression. Results are expressed as means ± S.D ($n = 3$). ∗ means $p < 0.05$ when compared with the corresponding control group (0 μM).

In general, PQ exposure could significantly induce oxidative stress and cause oxidative imbalance. Low concentration (10 μM) of PQ caused moderate stress could activate Nrf2 pathway to prevent cells from PQ induced oxidative damage; however, the Nrf2 pathway protection was ineffective in high concentration (100 μM) and caused severe stress, which has finally resulted in decrease of cell ability and increase of cell apoptosis [9]. Considering the protection of Nrf2 pathway in PQ induced damage, it may be supposed as a potential and effective therapeutic target for oxidative damage related disease in clinical therapy.

5. Conclusion

We provide important evidence suggesting that PQ has direct toxicity to cause irreversible apoptosis to hNPCs which was associated with the elevated oxidative stress. In addition, PQ induced oxidative stress and redox imbalance could activate the Nrf2/ARE signaling pathway to prevent the oxidative stress via initiating the downstream antioxidant responsive element like HO-1 and NQO1 mRNAs expression. In particular, we also observed that PKC and CKII may be involved in the phosphorylation of Nrf2, revealing that PKC and CKII may play an indirect role in antioxidative stress.

Conflict of Interests

The authors declare that there is no conflict of interests regarding the publication of this paper.

Authors' Contribution

Tingting Dou and Mengling Yan contributed equally to this work.

Acknowledgments

This research was supported by the National Natural Science Funds (NSFC 81472996, and 81072324, China) and Shanghai National Natural Science Funds (10ZR1401700). We thank Dr. Qiangen Wu for helpful comments on this paper.

References

[1] Y.-W. Chen, Y.-T. Yang, D.-Z. Hung, C.-C. Su, and K.-L. Chen, "Paraquat induces lung alveolar epithelial cell apoptosis via Nrf-2-regulated mitochondrial dysfunction and ER stress," *Archives of Toxicology*, vol. 86, no. 10, pp. 1547–1558, 2012.

[2] R. J. Dinis-Oliveira, F. Remião, H. Carmo et al., "Paraquat exposure as an etiological factor of Parkinson's disease," *NeuroToxicology*, vol. 27, no. 6, pp. 1110–1122, 2006.

[3] C.-Y. Lee, C.-H. Lee, C.-C. Shih, and H.-H. Liou, "Paraquat inhibits postsynaptic AMPA receptors on dopaminergic neurons in the substantia nigra pars compacta," *Biochemical Pharmacology*, vol. 76, no. 9, pp. 1155–1164, 2008.

[4] K. Prasad, E. Tarasewicz, J. Mathew et al., "Toxicokinetics and toxicodynamics of paraquat accumulation in mouse brain," *Experimental Neurology*, vol. 215, no. 2, pp. 358–367, 2009.

[5] Registration Eligibility Decision (RED), Office of Prevention, Pesticides and Toxic Substances, United States Environmental Protection Agency, EPA 738-F-96-018: Paraquat dichloride, US EPA, Washington, DC, USA, 1997, http://www.epa.gov/pesticides/reregistration/status.htm.

[6] K. R. Reuhl, "Delayed expression of neurotoxicity: the problem of silent damage," *NeuroToxicology*, vol. 12, no. 3, pp. 341–346, 1991.

[7] B. K. Barlow, D. A. Cory-Slechta, E. K. Richfield, and M. Thiruchelvam, "The gestational environment and Parkinson's disease: evidence for neurodevelopmental origins of a neurodegenerative disorder," *Reproductive Toxicology*, vol. 23, no. 3, pp. 457–470, 2007.

[8] A. M. Tsatsakis, K. Perakis, and E. Koumantakis, "Experience with acute paraquat poisoning in Crete," *Veterinary and Human Toxicology*, vol. 38, no. 2, pp. 113–117, 1996.

[9] X. Chang, W. Lu, T. Dou et al., "Paraquat inhibits cell viability via enhanced oxidative stress and apoptosis in human neural progenitor cells," *Chemico-Biological Interactions*, vol. 206, no. 2, pp. 248–255, 2013.

[10] J. S. Bus, S. D. Aust, and J. E. Gibson, "Superoxide- and singlet oxygen-catalyzed lipid peroxidation as a possible mechanism for paraquat (methyl viologen) toxicity," *Biochemical and Biophysical Research Communications*, vol. 58, no. 3, pp. 749–755, 1974.

[11] J. S. Bus, S. Z. Cagen, M. Olgaard, and J. E. Gibson, "A mechanism of paraquat toxicity in mice and rats," *Toxicology and Applied Pharmacology*, vol. 35, no. 3, pp. 501–513, 1976.

[12] C.-S. Lai and L. H. Piette, "Hydroxyl radical production involved in lipid peroxidation of rat liver microsomes," *Biochemical and Biophysical Research Communications*, vol. 78, no. 1, pp. 51–59, 1977.

[13] D. A. Drechsel and M. Patel, "Chapter 21 paraquat-induced production of reactive oxygen species in brain mitochondria," *Methods in Enzymology*, vol. 456, pp. 381–393, 2009.

[14] A. Zaidi, D. Fernandes, J. L. Bean, and M. L. Michaelis, "Effects of paraquat-induced oxidative stress on the neuronal plasma membrane Ca^{2+}-ATPase," *Free Radical Biology and Medicine*, vol. 47, no. 10, pp. 1507–1514, 2009.

[15] Q. Chen, Y. Niu, R. Zhang et al., "The toxic influence of paraquat on hippocampus of mice: involvement of oxidative stress," *NeuroToxicology*, vol. 31, no. 3, pp. 310–316, 2010.

[16] C. Adrain and S. J. Martin, "The mitochondrial apoptosome: a killer unleashed by the cytochrome seas," *Trends in Biochemical Sciences*, vol. 26, no. 6, pp. 390–397, 2001.

[17] S. Sadasivam, S. Gupta, V. Radha, K. Batta, T. K. Kundu, and G. Swarup, "Caspase-1 activator Ipaf is a p53-inducible gene involved in apoptosis," *Oncogene*, vol. 24, no. 4, pp. 627–636, 2005.

[18] R. Munday and C. M. Munday, "Induction of phase II detoxification enzymes in rats by plant-derived isothiocyanates: comparison of allyl isothiocyanate with sulforaphane and related compounds," *Journal of Agricultural and Food Chemistry*, vol. 52, no. 7, pp. 1867–1871, 2004.

[19] J. A. Rubiolo, G. Mithieux, and F. V. Vega, "Resveratrol protects primary rat hepatocytes against oxidative stress damage: activation of the Nrf2 transcription factor and augmented activities of antioxidant enzymes," *European Journal of Pharmacology*, vol. 591, no. 1–3, pp. 66–72, 2008.

[20] S. K. Kim, J. W. Yang, M. R. Kim et al., "Increased expression of Nrf2/ARE-dependent anti-oxidant proteins in tamoxifen-resistant breast cancer cells," *Free Radical Biology and Medicine*, vol. 45, no. 4, pp. 537–546, 2008.

[21] H.-Y. Cho, A. E. Jedlicka, S. P. M. Reddy et al., "Role of NRF2 in protection against hyperoxic lung injury in mice," *The American Journal of Respiratory Cell and Molecular Biology*, vol. 26, no. 2, pp. 175–182, 2002.

[22] L. Claudio, W. C. Kwa, A. L. Russell, and D. Wallinga, "Testing methods for developmental neurotoxicity of environmental chemicals," *Toxicology and Applied Pharmacology*, vol. 164, no. 1, pp. 1–14, 2000.

[23] H. A. Tilson, "Neurotoxicology risk assessment guidelines: developmental neurotoxicology," *NeuroToxicology*, vol. 21, no. 1-2, pp. 189–194, 2000.

[24] B. A. Reynolds, W. Tetzlaff, and S. Weiss, "A multipotent EGF-responsive striatal embryonic progenitor cell produces neurons and astrocytes," *Journal of Neuroscience*, vol. 12, no. 11, pp. 4565–4574, 1992.

[25] R. Donato, E. A. Miljan, S. J. Hines et al., "Differential development of neuronal physiological responsiveness in two human neural stem cell lines," *BMC Neuroscience*, vol. 8, article 36, 2007.

[26] J.-M. Zhang, H.-C. Wang, H.-X. Wang et al., "Oxidative stress and activities of caspase-8, -9, and -3 are involved in cryopreservation-induced apoptosis in granulosa cells," *European Journal of Obstetrics & Gynecology and Reproductive Biology*, vol. 166, no. 1, pp. 52–55, 2013.

[27] L. Min, S. He, Q. Chen, F. Peng, H. Peng, and M. Xie, "Comparative proteomic analysis of cellular response of human airway epithelial cells (A549) to benzo(a)pyrene," *Toxicology Mechanisms and Methods*, vol. 21, no. 5, pp. 374–382, 2011.

[28] S. M. Hussain and J. M. Frazier, "Cellular toxicity of hydrazine in primary rat hepatocytes," *Toxicological Sciences*, vol. 69, no. 2, pp. 424–432, 2002.

[29] P. Karakashev, L. Petrov, and A. Alexandrova, "Paraquat-induced lipid peroxidation and injury in Ehrlich ascites tumor cells," *Neoplasma*, vol. 47, no. 2, pp. 122–124, 2000.

[30] J. Li, D. Johnson, M. Calkins, L. Wright, C. Svendsen, and J. Johnson, "Stabilization of Nrf2 by tBHQ confers protection against oxidative stress-induced cell death in human neural stem cells," *Toxicological Sciences*, vol. 83, no. 2, pp. 313–328, 2005.

[31] H.-C. Huang, T. Nguyen, and C. B. Pickett, "Phosphorylation of Nrf2 at Ser-40 by protein kinase C regulates antioxidant response element-mediated transcription," *The Journal of Biological Chemistry*, vol. 277, no. 45, pp. 42769–42774, 2002.

[32] B. Peter, M. Wartena, H. H. Kampinga, and A. W. T. Konings, "Role of lipid peroxidation and DNA damage in paraquat toxicity and the interaction of paraquat with ionizing radiation," *Biochemical Pharmacology*, vol. 43, no. 4, pp. 705–715, 1992.

[33] C.-C. Lin, C.-L. Kuo, M.-H. Lee et al., "Wogonin triggers apoptosis in human osteosarcoma U-2 OS cells through the endoplasmic reticulum stress, mitochondrial dysfunction and caspase-3-dependent signaling pathways," *International Journal of Oncology*, vol. 39, no. 1, pp. 217–224, 2011.

[34] Y. Liang and J. P. Sundberg, "SHARPIN regulates mitochondria-dependent apoptosis in keratinocytes," *Journal of Dermatological Science*, vol. 63, no. 3, pp. 148–153, 2011.

[35] M. Tsukamoto, Y. Tampo, M. Sawada, and M. Yonaha, "Paraquat-induced oxidative stress and dysfunction of the glutathione redox cycle in pulmonary microvascular endothelial cells," *Toxicology and Applied Pharmacology*, vol. 178, no. 2, pp. 82–92, 2002.

[36] E. Weidauer, T. Lehmann, A. Rämisch, E. Röhrdanz, and H. Foth, "Response of rat alveolar type II cells and human lung tumor cells towards oxidative stress induced by hydrogen peroxide and paraquat," *Toxicology Letters*, vol. 151, no. 1, pp. 69–78, 2004.

[37] J. Peng, F. F. Stevenson, M. L. Oo, and J. K. Andersen, "Iron-enhanced paraquat-mediated dopaminergic cell death due to increased oxidative stress as a consequence of microglial activation," *Free Radical Biology & Medicine*, vol. 46, no. 2, pp. 312–320, 2009.

[38] C. Hertzmann, M. Wiens, D. Bowering, B. Snow, and D. Calne, "Parkinson's disease: a case-control study of occupational and environmental risk factors," *American Journal of Industrial Medicine*, vol. 17, no. 3, pp. 349–355, 1990.

[39] K. M. Semchuk, E. J. Love, and R. G. Lee, "Parkinson's disease and exposure to agricultural work and pesticide chemicals," *Neurology*, vol. 42, no. 7, pp. 1328–1335, 1992.

[40] H. T. Hogberg, A. Kinsner-Ovaskainen, T. Hartung, S. Coecke, and A. K. Bal-Price, "Gene expression as a sensitive endpoint to evaluate cell differentiation and maturation of the developing central nervous system in primary cultures of rat cerebellar granule cells (CGCs) exposed to pesticides," *Toxicology and Applied Pharmacology*, vol. 235, no. 3, pp. 268–286, 2009.

[41] M. Takizawa, K. Komori, Y. Tampo, and M. Yonaha, "Paraquat-induced oxidative stress and dysfunction of cellular redox systems including antioxidative defense enzymes glutathione peroxidase and thioredoxin reductase," *Toxicology in Vitro*, vol. 21, no. 3, pp. 355–363, 2007.

[42] W. Yang and E. Tiffany-Castiglioni, "The bipyridyl herbicide paraquat produces oxidative stress-mediated toxicity in human neuroblastoma SH-SY5Y cells: relevance to the dopaminergic pathogenesis," *Journal of Toxicology and Environmental Health A*, vol. 68, no. 22, pp. 1939–1961, 2005.

[43] M. G. Purisai, A. L. McCormack, S. Cumine, J. Li, M. Z. Isla, and D. A. Di Monte, "Microglial activation as a priming event leading to paraquat-induced dopaminergic cell degeneration," *Neurobiology of Disease*, vol. 25, no. 2, pp. 392–400, 2007.

[44] G. Y. Wu, Y.-Z. Fang, S. Yang, J. R. Lupton, and N. D. Turner, "Glutathione metabolism and its implications for health," *Journal of Nutrition*, vol. 134, no. 3, pp. 489–492, 2004.

[45] T. Nguyen, P. J. Sherratt, and C. B. Pickett, "Regulatory mechanisms controlling gene expression mediated by the antioxidant response element," *Annual Review of Pharmacology and Toxicology*, vol. 43, pp. 233–260, 2003.

[46] M. McMahon, N. Thomas, K. Itoh, M. Yamamoto, and J. D. Hayes, "Dimerization of substrate adaptors can facilitate cullin-mediated ubiquitylation of proteins by a 'Tethering' mechanism—a two-site interaction model for the Nrf2-Keap1 complex," *Journal of Biological Chemistry*, vol. 281, no. 34, pp. 24756–24768, 2006.

[47] Y. Luo, A. L. Eggler, D. Liu, G. Liu, A. D. Mesecar, and R. B. van Breemen, "Sites of alkylation of human Keap1 by natural Chemoprevention agents," *Journal of the American Society for Mass Spectrometry*, vol. 18, no. 12, pp. 2226–2232, 2007.

[48] J.-P. Ren, Y.-W. Zhao, and X.-J. Sun, "Toxic influence of chronic oral administration of paraquat on nigrostriatal dopaminergic neurons in C57BL/6 mice," *Chinese Medical Journal*, vol. 122, no. 19, pp. 2366–2371, 2009.

[49] W. Yang, E. Tiffany-Castiglioni, M.-Y. Lee, and I.-H. Son, "Paraquat induces cyclooxygenase-2 (COX-2) implicated toxicity in human neuroblastoma SH-SY5Y cells," *Toxicology Letters*, vol. 199, no. 3, pp. 239–246, 2010.

[50] P. L. Apopa, X. He, and Q. Ma, "Phosphorylation of Nrf2 in the transcription activation domain by casein kinase 2 (CK2) is critical for the nuclear translocation and transcription activation function of Nrf2 in IMR-32 neuroblastoma cells," *Journal of Biochemical and Molecular Toxicology*, vol. 22, no. 1, pp. 63–76, 2008.

[51] C.-L. Huang, Y.-C. Lee, Y.-C. Yang, T.-Y. Kuo, and N.-K. Huang, "Minocycline prevents paraquat-induced cell death through attenuating endoplasmic reticulum stress and mitochondrial dysfunction," *Toxicology Letters*, vol. 209, no. 3, pp. 203–210, 2012.

[52] Y.-C. Wang, C.-M. Lee, L.-C. Lee et al., "Mitochondrial dysfunction and oxidative stress contribute to the pathogenesis of spinocerebellar ataxia type 12 (SCA12)," *The Journal of Biological Chemistry*, vol. 286, no. 24, pp. 21742–21754, 2011.

Hindawi Publishing Corporation
Oxidative Medicine and Cellular Longevity
Volume 2016, Article ID 5910695, 11 pages
http://dx.doi.org/10.1155/2016/5910695

Research Article

Redox Stimulation of Human THP-1 Monocytes in Response to Cold Physical Plasma

Sander Bekeschus, Anke Schmidt, Lydia Bethge, Kai Masur, Thomas von Woedtke, Sybille Hasse, and Kristian Wende

Leibniz Institute for Plasma Science and Technology (INP Greifswald), Felix-Hausdorff-Straße 2, 17489 Greifswald, Germany

Correspondence should be addressed to Sander Bekeschus; sander.bekeschus@gmail.com

Received 22 May 2015; Revised 17 July 2015; Accepted 22 July 2015

Academic Editor: Manuela Malatesta

In plasma medicine, cold physical plasma delivers a delicate mixture of reactive components to cells and tissues. Recent studies suggested a beneficial role of cold plasma in wound healing. Yet, the biological processes related to the redox modulation via plasma are not fully understood. We here used the monocytic cell line THP-1 as a model to test their response to cold plasma *in vitro*. Intriguingly, short term plasma treatment stimulated cell growth. Longer exposure only modestly compromised cell viability but apparently supported the growth of cells that were enlarged in size and that showed enhanced metabolic activity. A significantly increased mitochondrial content in plasma treated cells supported this notion. On THP-1 cell proteome level, we identified an increase of protein translation with key regulatory proteins being involved in redox regulation (hypoxia inducible factor 2α), differentiation (retinoic acid signaling and interferon inducible factors), and cell growth (Yin Yang 1). Regulation of inflammation is a key element in many chronic diseases, and we found a significantly increased expression of the anti-inflammatory heme oxygenase 1 (*HMOX1*) and of the neutrophil attractant chemokine interleukin-8 (IL-8). Together, these results foster the view that cold physical plasma modulates the redox balance and inflammatory processes in wound related cells.

1. Introduction

Plasma is generated by substantial energy input to a gas, thereby creating a "fourth state of matter" [1]. Plasma contains active and reactive components of many kinds including electrons, ions, and reactive oxygen and nitrogen species (ROS and RNS) as well as ultraviolet (UV), visible, and infrared radiation [2]. Apart from naturally occurring plasma, for example, lightning, fire, or *Aurelia borealis*, plasma is also created artificially. For plasma jets, such as the one used in the present study (kiNPen), the reactive components of the plasma can be delivered directly and in a controlled manner to cells and tissues without inducing thermal damage [3]. In the device (or kiNPen), the noble gas argon is excited at a central high voltage electrode (AC, several kV, ≈1 MHz). This creates nonequilibrium plasma that contains hot and reactive electrons and relatively cold argon ions in a bulk of nonionized gas atoms that govern the overall temperature [4]. The electrons and argon ions [5] in turn react with ambient oxygen or nitrogen molecules to form ROS/RNS [6]. This may be of therapeutic benefit in pathological skin conditions, as first small-scale clinical studies supported the notion that chronic wounds displayed an improved healing signature after exposure to ROS/RNS generating plasma [7–9].

Cells of the immune system are central players in the regulation of all wound healing phases [10]. During the inflammatory phase, professional phagocytes are attracted via cytokines and reactive molecules from the vasculature to the wound bed where they eradicate invading microorganisms [11]. Among them are monocytes which *in situ* differentiate into macrophages [12]. Macrophages also dominate the center of chronic ulcers and can potently generate reactive species [13]. These cells have key regulatory functions which are reflected by, for example, the phagocytosis of dead cells [14] and debris as well as their release of cytokines [15] and other wound healing-related proteins, such as heme oxygenase 1 (HO-1) [16]. In particular, interleukin-8 (IL-8) is a central molecule in initiating the inflammatory wound

healing phase [17] and its secretion was previously shown to be accented by reactive species, such as hydroxyl radicals [18].

Wound healing is highly redox-controlled [19]. Almost all cells of the wound microenvironment utilize oxygen to generate reactive species, and at low concentration these species seem to be required for proper healing [20]. It is hypothesized that plasma may trigger similar responses in cells. Yet, the mechanisms and biological processes following exposure to plasma are not fully understood [21]. Accordingly, we investigated the neoplastic cell line THP-1 monocytes as a model to study the effects of a plasma-based redox modulation. We identified an increase in free thiol content, cell proliferation, and metabolic activity, arguing for a priming of these cells which was further manifested by significant changes in protein expression as analyzed by mass spectrometry based proteomic tools. We further identified an altered inflammatory signature. Our results implicate a potential significance of redox intonations by plasma that may help to further understand its impending benefit in human skin pathologies.

2. Materials and Methods

2.1. Cell Culture. THP-1 monocytes (ACC 16, DSMZ, Germany) were cultured in RPMI1640 medium (Lonza, Switzerland) containing 10% bovine calf serum (Sigma, USA), 2% glutamine (Pan-Biotech, Germany), and 1% penicillin/streptomycin (Lonza, Switzerland). For total protein expression using stable isotope labeling (SILAC), cells were labeled for at least three passages in complete RPMI containing 10% of dialyzed bovine calf serum with either both isotopically labeled arginine and lysine ($^{13}C_6^{15}N_4$ arginine and $^{13}C_6^{15}N_2$ lysine, Cambridge Isotopes, USA) or regular amino acids.

2.2. Plasma Source and Treatment. The atmospheric pressure argon plasma jet *kiNPen 11* (neoplas tools GmbH, Germany) was used. It was operated with five standard liters per minute (slm) of argon gas (Air Liquide, France) and its flux was controlled using a mass flow controller (MKS instruments, Germany). The jet is equipped with a ceramic capillary (inner radius of 0.8 mm) and an inner pin-type high-frequency electrode (AC ≈ 1 MHz, several kV). Cells were indirectly plasma-treated in experiments where RNA and protein were collected for real-time PCR or mass spectrometry, respectively. Here, 5 mL of cell culture medium in a 60 mm dish was plasma-treated and was subsequently added to 1×10^6 pelleted THP-1 cells. For direct plasma treatment in all other experiments, 5 mL of cell suspension (0.2×10^6/mL of medium) was added to a 60 mm plastic dish (Sarstedt, Germany) and exposed to plasma. In both regimes and using a computer-controlled *xyz*-table (S-400, CNC step, Germany), the jet hovered over the sample in a meandering fashion for the indicated time length. A predetermined amount of destilled water was added after treatment to compensate evaporation. The direct and indirect approaches were previously compared and found to have similar effects. Using the same plasma source, this accounts for toxicity in human PBMC [22] and effects on metabolic activity and proliferation in feline epithelial cells [23]. Analogous results were obtained for other sources using human epithelial cells [24] as well as for inactivating bacteria [25].

2.3. Metabolic Activity Assay. THP-1 monocytes were plasma-treated, aliquoted in 96-well plates (Sarstedt, Germany), and incubated for 72 h at 37°C. Resazurin (Alfa Aesar, USA) was added (final concentration 200 μM), and cells were incubated for 4 h. In active cells, $NADH^+$ is generated during the cellular metabolism which sponsors the transformation of resazurin to its fluorescent product resorfurin [26]. The latter can be detected measuring its fluorescence at 590 nm (excitation wavelength 530 nm) using a microplate reader (M200 pro, Tecan, Austria).

2.4. Flow Cytometry. To assess intracellular redox changes, THP-1 monocytes were stained with 2 μM CM-H_2DCF-DA (Life Technologies, USA) prior to plasma-treatment and subsequent analysis by flow cytometry (Gallios, Beckman-Coulter, USA). Also, cells were plasma-treated, collected at various incubation times, and stained with 10 μM of the ThiolTracker probe (Life Technologies) to assess the intracellular reduced thiol content. Apoptosis was investigated as previously described [27]. Briefly, cells were plasma-treated and after 24 h they were incubated in Annexin V binding buffer containing Annexin V FITC (BioLegend, USA) and 4′,6-diamidin-2-phenylindol (DAPI, Sigma, USA). Alternatively, cells were fixed in ethanol and stained with DAPI to analyze THP-1 cell cycle. To analyze the metabolic activity per cell, resorfurin fluorescence was measured, and DAPI was added prior to cell enumeration using volumetric flow cytometry (Attune, Life Technologies). Viable cell counts were related to total fluorescence obtained by the resazurin-reduction assay. Mean forward and side scatter fluorescence intensity was evaluated as well. To determine mitochondrial content, cells were stained with 0.5 μM MitoTracker red FM (Life Technologies) 72 h after plasma treatment.

2.5. Global Protein Expression. Proteomic analysis was carried out as previously described [28]. Briefly, SILAC-labeled THP-1 cells were exposed to plasma-treated (3 min) medium and cellular protein was collected 24 h later. Proteins were fractionated using SDS gel electrophoresis and in-gel protein digestion was performed. Peptides were analyzed by nano-LC/MS (Proxeon, Denmark), and the eluent was ionized by electrospray ionization and examined using a TripleTOF 5600 (AB Sciex, USA) mass spectrometer. Data were processed using ProteinPilot 4.5 software (AB Sciex) and Ingenuity Pathway Analysis (Qiagen, USA). Between 2200 and 2700 human proteins from about 60,000 peptides were identified out of 240,000 mass spectra. Candidates were selected upon their significant involvement in pathways of metabolisms and/or redox stress as well as on statistical criteria (≥±1.5-fold expression). Additionally, data were analyzed through the use of *Ingenuity Pathway Analysis* (IPA, Qiagen) and free web based applications (*PANTHER* and *Universal Protein Resource*).

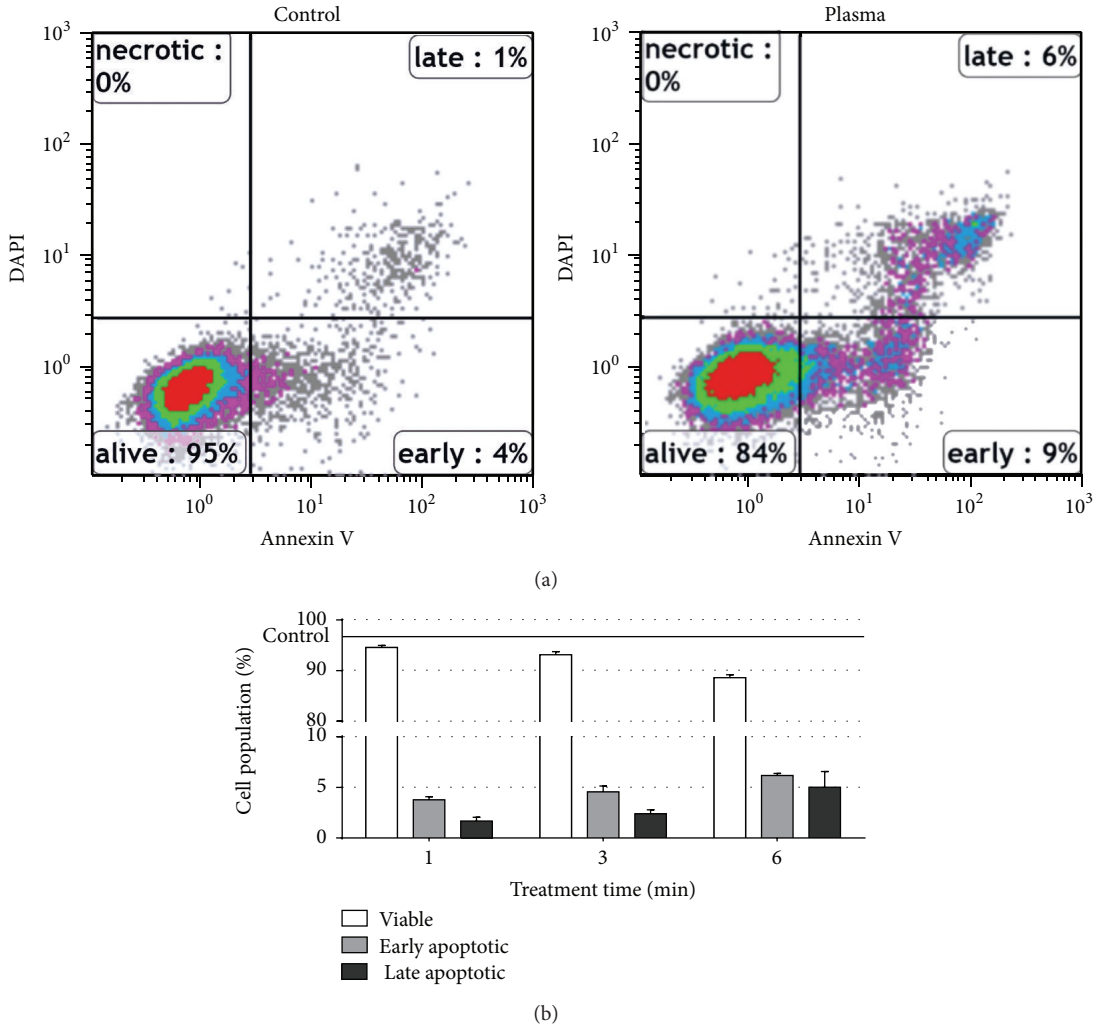

Figure 1: Analysis of THP-1 cell apoptosis. THP-1 monocytes were plasma-treated (6 min). Percentages of viable as well as early and late apoptotic cells were analyzed (a) and quantitated (b) by flow cytometry using Annexin V and DAPI. "Ctrl" represents percent of viable cells in untreated samples; percentages of viable and early and late apoptotic cells add up to 100. Data are shown as one representative (b) or mean + S.E. (b) of five independent experiments.

2.6. Real-Time PCR of IL-8 and HMOX1. THP-1 cells were exposed to plasma-treated medium and incubated for 12 h or 24 h. Cells were harvested and mRNA was isolated (RNA-Mini Kit; Bio&Sell, Germany). Complementary DNA (cDNA) was generated from total RNA using transcriptor first strand cDNA synthesis kit and T4 DNA polymerase for second strand synthesis (both from Roche, Switzerland). For quantitative polymerase chain reaction, the real-time ready catalogue assay kit containing *IL-8* and *HMOX1* primers was utilized, and samples were analyzed using a LightCycler 480 II (all Roche).

2.7. Cytokine Detection. THP-1 cells were incubated for 24 h after plasma treatment. Supernatants were analyzed using an IL-8 (BioLegend) ELISA and a multianalyte inflammatory cytokine ELISA array (Qiagen). Sample values were normalized to control values and displayed as fold change to control.

2.8. Statistics. Experiments were repeated at least three times. Values were displayed as arithmetic mean. For MitoTracker and ThiolTracker fluorescence and for IL-8 and *HMOX1* expression studies, *Student*'s t-test was applied. For comparison in all other experiments, one-way ANOVA with *Dunnett* posttesting was utilized. Significance levels were indicated as follows: $^{*}\alpha = 0.05$, $^{**}\alpha = 0.01$, and $^{***}\alpha = 0.001$.

3. Results and Discussion

3.1. Plasma Altered the Cellular Redox State without Major Apoptosis Induction. In this study, we investigated whether exposure to cold physical plasma affected THP-1 cell viability, metabolic activity, and function. THP-1 cell apoptosis was studied (Figure 1(a)), and viability was compromised only to a minor extent (Figure 1(b)). This is in line with peripheral blood monocyte viability being only marginally affected

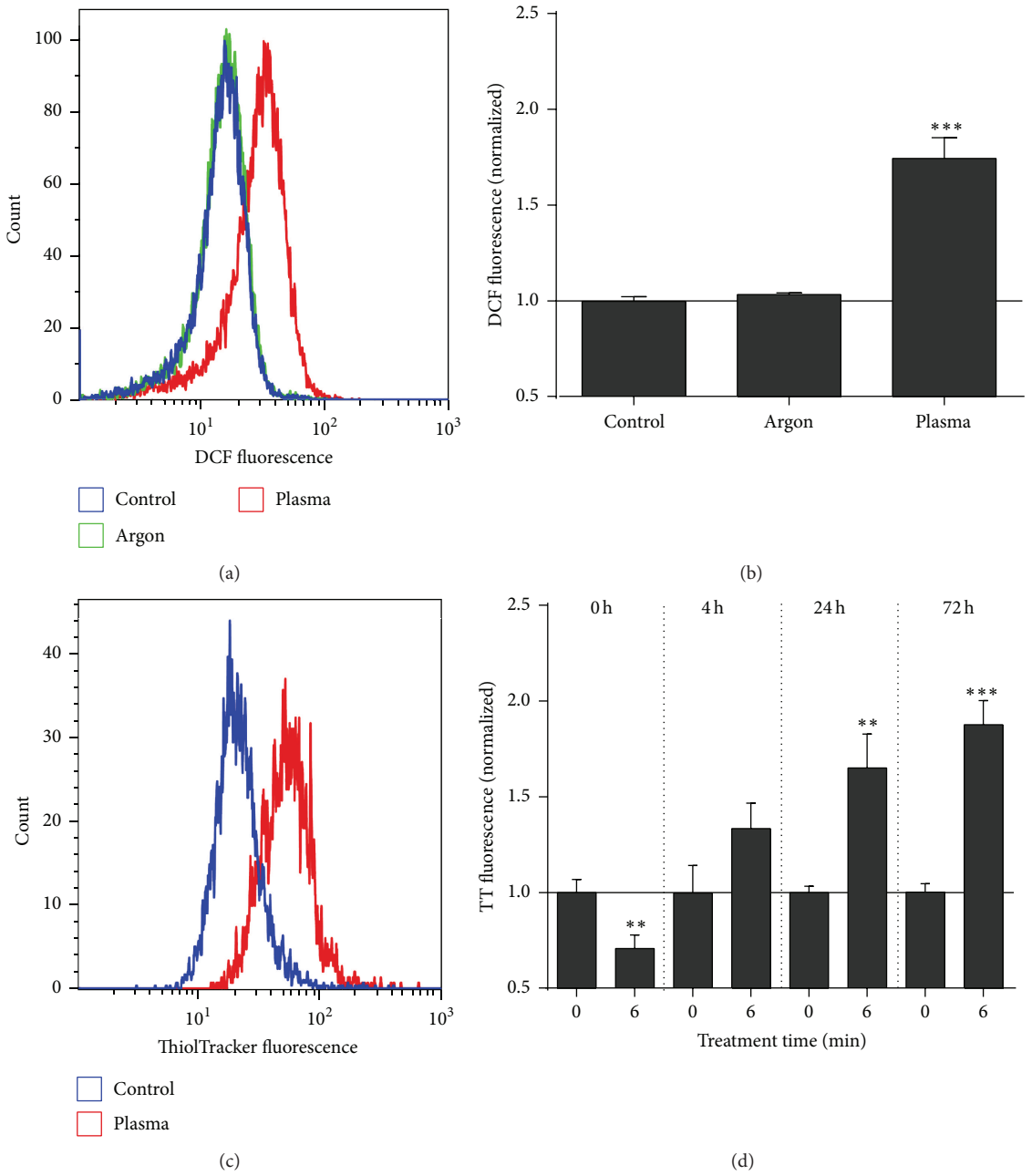

FIGURE 2: Analysis of redox changes in THP-1 cells. THP-1 cells were stained with CM-H_2DCF-DA and plasma-treated (3 min) to evaluate intracellular redox changes by flow cytometry (a, b). THP-1 cells were plasma-treated, and cells were stained at different time point with ThiolTracker dye to examine their total reduced thiol content ((c), shown for 72 h) by flow cytometry (d). Data are shown as one representative (a, c) or mean + S.E. (b, d) of three independent experiments.

by plasma [27]. Yet, plasma did induce changes in the cellular redox state. Immediately following treatment, THP-1 cells showed a significant ($P < 0.001$) increase in DCF fluorescence (Figures 2(a) and 2(b)). Although DCF is regarded as a general redox probe, it is highly sensitive to hydroxyl radicals [29]. These may have been formed in the Fenton reaction of plasma-derived hydrogen peroxide [30] with metals being inevitably present in biological systems [31]. We asked next whether plasma-derived reactive species also affected the cells' antioxidative defense. Here, glutathione is a central molecule which constitutes and regenerates the majority of free thiols in cells to maintain redox homeostasis [32]. The intracellular free thiol content was significantly ($P < 0.01$) decreased immediately following exposure to plasma whereas thiol levels were substantially elevated hours and days after plasma treatment (Figures 2(c) and 2(d)). This argues for a swiftly augmented redox defense in response to plasma with only little induction of apoptosis. This

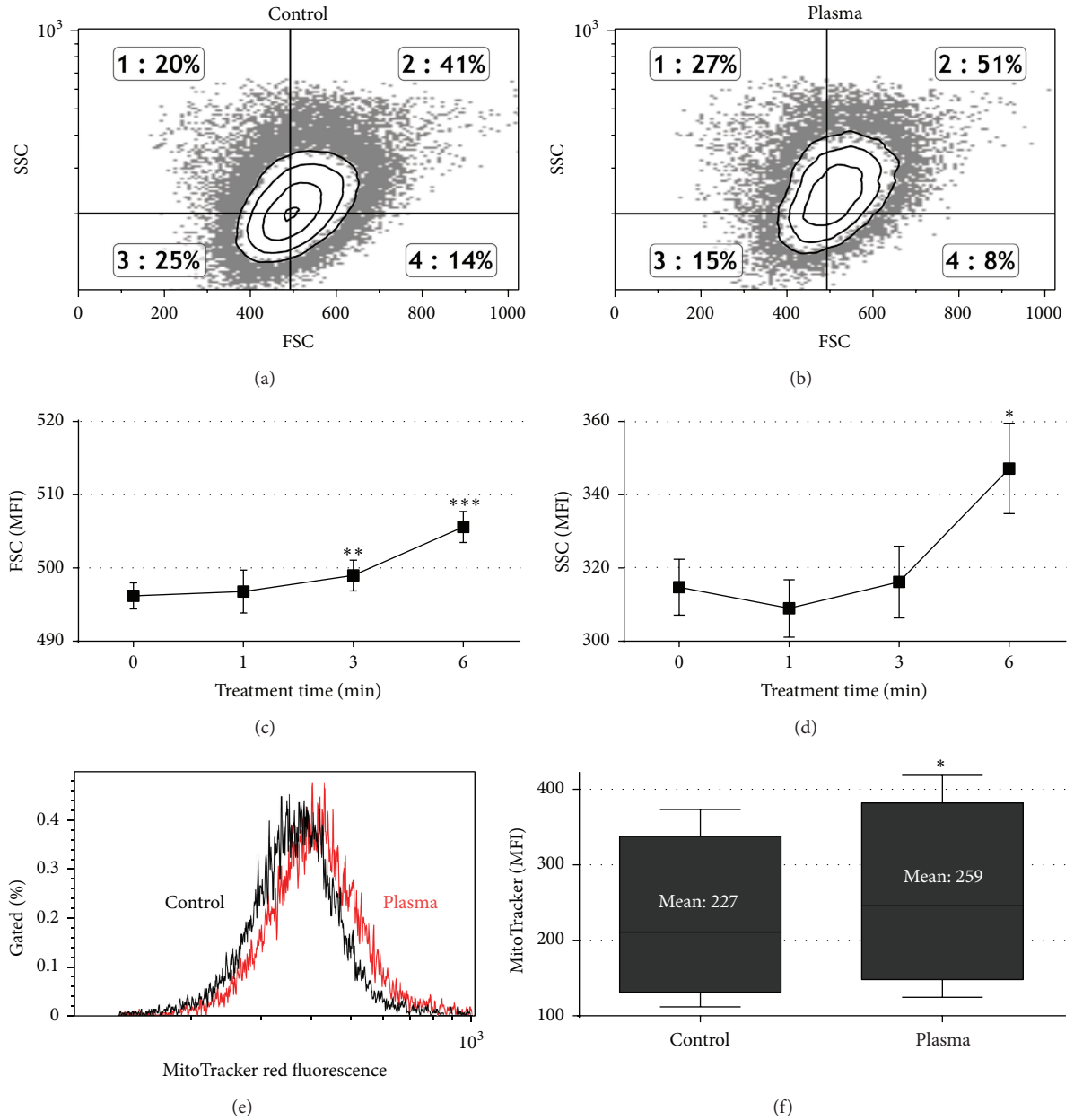

Figure 3: Analysis of THP-1 cell size and mitochondrial content. THP-1 monocytes were plasma-treated. After 72 h, forward (FS) and side scatter (SSC) distribution (a, b) and mean fluorescence intensity (MFI) thereof (c, d) were analyzed in viable cells using flow cytometry. MitoTracker red fluorescence indicative of total mitochondrial content was assessed in viable cells (f) 72 h after plasma treatment. Data are shown as one representative (a, b, e), mean + S.E. (c, d), or boxplot (5–95 percentile, (f)) of three independent experiments.

may be explained by THP-1 cells being derived from an acute monocytic leukemia (AML), and an excessive constitutive ROS production combined with an impaired p38-MAPK and ROS-mediated apoptosis signaling was found in AMLs of oncological patients [33]. Moreover, GSH decrease was also followed by a rebound increase as an adaptive response to oxidative stress in epithelial cells [34], underlining our results, and suggested an adaptation in THP-1 cells following plasma. We subsequently investigated alterations in the cells' morphology and metabolic activity after plasma treatment.

3.2. Plasma Enhanced Cell Size and Stimulated Cellular Proliferation. Compared to control cells (Figure 3(a)), plasma-treated cells (Figure 3(b)) displayed a small but significant enhancement of mean forward scatter (attributed to the cells' size, Figure 3(c)) and side scatter (attributed to the cells' granularity and membrane irregularity, Figure 3(d)). This correlated with mitochondrial content (Figure 3(e)) that was significantly increased in plasma-treated cells as well (Figure 3(f)), possibly pointing to an altered metabolic activity. Indeed, we found a significant elevation ($P < 0.003$)

of cellular respiration for short exposure to plasma (1 min). By contrast, total metabolic activity was significantly ($P < 0.001$) decreased after extended (6 min) plasma treatment (Figure 4(a)). The same cells that were subjected to the assessment of metabolic activity were subsequently analyzed by volumetric flow cytometry and viable cells were counted. Again, we found a significant ($P < 0.001$) increase in cell numbers for short exposure times and a significant decrease ($P < 0.001$) for longer exposure times to plasma (Figure 4(b)). Based on these data, we calculated the metabolic activity on a per-cell basis by combination of the total fluorescence divided by the total number of viable cells (Figure 4(c)). For short exposure times there was no difference compared to untreated controls. On the contrary, the per-cell metabolic activity was significantly ($P < 0.001$) enhanced in cells that were exposed to plasma for 6 min. Supplementation of fresh media during the incubation time yielded similar results and hence the elevated metabolism was not a consequence of nutrient limitation in control cells (data not shown). The decrease in total cell numbers (Figure 4(b)) was reflected by a significant ($P < 0.001$) G2 arrest (Figures 4(d) and 4(e)) 24 h but not 72 h (data not shown) after plasma treatment.

These results suggest that exposure to plasma may have stimulated THP-1 cells, eventually leading to enhanced proliferation for short exposure times. Reactive species delivered to the cells via the plasma altered the intracellular redox state and consequently stimulated growth. This may be reflected by the finding of others who suggested a role of redox changes in, for example, thioredoxin or Id3 in growth stimulation [35, 36]. It was reported that redox modifications in THP-1 monocytes lead to macrophage differentiation [37] which may account for the increase observed in cell size (Figure 3(c)) and metabolic activity (Figure 4(c)). Indeed, THP-1 cell activations via, for example, mitogens increase cell size as well [38]. Yet, mitogen-activated and THP-1 cell-derived macrophages display a distinct surface marker signature (e.g., elevated expression of CD33, CD45, CD49b, CD49d, CD81, and CD141) which was not present on plasma-treated THP-1 cells (data not shown). This argues against a role of plasma in induction of THP-1 cell differentiation. Oxidative stress was also shown to support an accumulation of THP-1 cells in the G2 phase of the cell cycle [39] which supports our findings (Figure 4(e)) and may explain the lower proliferation found after prolonged exposure to plasma (Figure 3(b)). A linkage between the enhanced metabolic activity and the elevated mitochondrial content (Figure 3(f)) is unlikely due to the monocytes' glycolytic nature [40]. It was suggested that monocytes utilize mitochondria to generate ROS for signaling purposes and not mainly for ATP generation [41]. This would imply a combined extrinsic (plasma) and intrinsic (mitochondria) ROS generation, possibly affecting redox signaling and/or other biological responses observed in this study. Finally, growth promotion of plasma-treated cells may be a consequence of elevated GSH levels (Figure 2(d)) protecting from ROS generated during proliferation [42].

3.3. Global Protein Expression Screening. Next, proteome analysis was carried out to further elucidate the THP-1 cell protein response to plasma. In plasma-treated THP-1 monocytes, total protein expression was increased by 1.05-fold, paralleling the observed increase in cell size (Figure 3). An increase of protein translation was also suggested by the finding that the dominant pathways regulated after plasma involved ribosomal protein translation (eIF2 signaling and eIF4/p706K signaling) [43]. Simultaneously, cellular protein degradation was elevated, indicated by an increased expression of several key members of the ubiquitin/proteasome pathway, such as SUGT1 and STUB1 (Table 1) [44, 45].

Table 1: Differential expression of proteins complexed in metabolic and redox processes after plasma treatment. Fold regulation of relevant candidate protein expression identified from global proteomic profiling of THP-1 cells and 24 h after exposure to plasma-treated medium. Data are presented as mean and range of three independent experiments.

Short name/ID	Fold change	Pathway/task
EPAS1 (Q99814)	+4.0 ± 0.7	Transcription factor
YY1 (P25490)	+3.0 ± 0.3	Cell cycle control
CRABP1 (P29762)	+1.9 ± 0.2	Retinoic acid signaling
SUGT1 (Q9Y2Z0)	+1.9 ± 0.3	Protein ubiquitination
STUB1 (Q9UNE7)	+1.7 ± 0.2	Protein ubiquitination
SOD2 (P04179)	−1.5 ± 0.1	Redox balancer
IRF8 (Q02556)	−1.6 ± 0.2	Interferon signaling

These observations point to an anticipated protein stress response triggered by plasma and subsequent changes in the THP-1 monocyte redox state. This notion is further supported by the finding that the endothelial PAS domain-containing protein 1 (EPAS1, also known as hypoxia inducible factor-2α) was highly regulated after plasma (Table 1). Like HO-1, EPAS1 is central in the maintenance of redox homeostasis and is moreover linked to superoxide dismutase (SOD) activity [46]. After plasma treatment, we found a decrease in mitochondrial-resident SOD (SOD2, Table 1). Although SOD2 is a protector against oxidative stress, previous work had found downregulation during the physiological wound healing process in rats [47]. Along with our findings, decreased levels were also reported in response to sublethal oxidative stress in neuronal cells [48]. In oxidatively challenged rats, Yin Yang 1 (YY1), a zinc finger transcription factor, was strongly increased [49] which correlates with our results (Table 1). YY1 is central in cell cycle progression and resistance to apoptotic stimuli [50] and its upregulation in macrophages is associated with an increased expression of cyclooxygenase 2 (COX2) [51]. COX2 is a hallmark of tissue injury and inflammation. Thus, the increase of YY1 expression after plasma may represent the perception of a danger stimulus by THP-1 cells. This may be reflected by changes in the inflammatory signature (Figure 5) and the decrease of interferon regulatory factor 8 expression (IRF8, Table 1) which may indicate the effort to control interleukin production and overshooting cell activation [52, 53]. YY1 also controls respiratory chain expression and mitochondrial activity [54, 55] and may have a role in the modulation of the metabolic activity observed (Figure 4(c)).

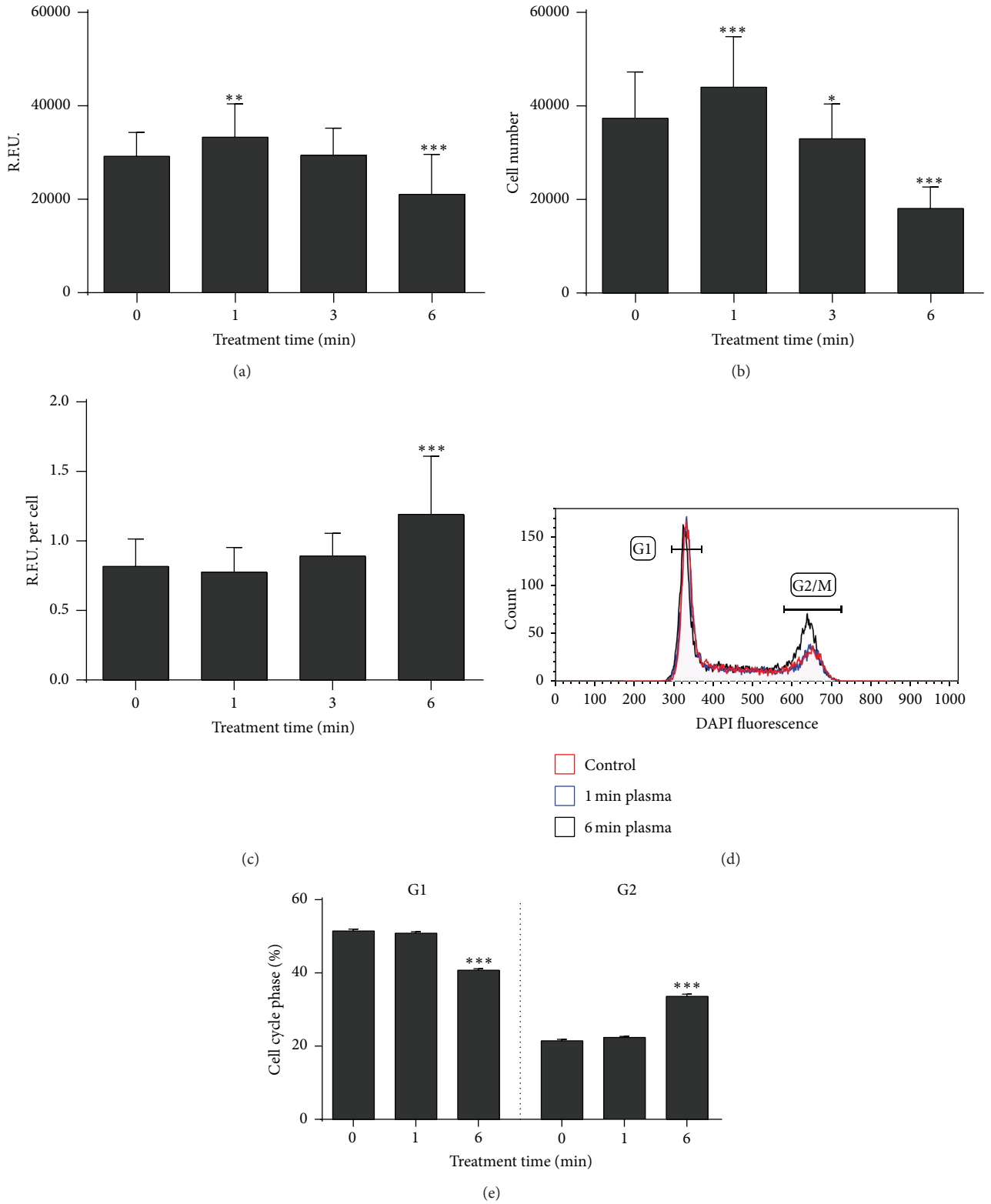

Figure 4: Analysis of total THP-1 cell metabolism and number. THP-1 monocytes were plasma-treated, and after 72 h the total metabolic activity was assessed in a microplate reader using the resazurin assay (a). Viable cell numbers were determined of the same samples (b), and the metabolic activity per cell was calculated (c). Twenty-four hours after plasma treatment, cells were subjected to cell cycle analysis (d) and quantitatively compared to each other (e). Data are shown as one representative (d) or mean + S.E. (a, b, c, and e) of three independent experiments.

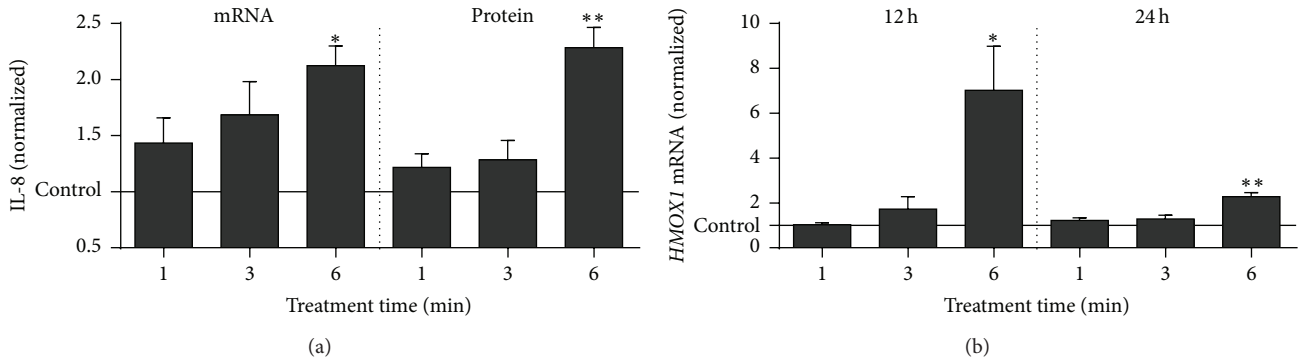

Figure 5: Analysis of THP-1 cell IL-8 and *HMOX1* expression. THP-1 monocytes were plasma-treated, and after 24 h *IL-8* expression and its secretion were analyzed by real-time PCR and ELISA, respectively. Expression of *HMOX1* was examined 12 h and 24 h after treatment using real-time PCR (b). Data are presented as mean + S.E. of three independent experiments.

However, in contrast to human keratinocytes [56], oxidative stress response like nuclear factor erythroid 2-related factor (Nrf2) regulated response was not observed as indicated by unchanged NAD(P)H dehydrogenase (quinone) 1 (NQO1) or carbonyl reductase (NADPH) 1 (CBR1) expression (data not shown). Instead, retinoic acid (RA) signaling was activated as shown by cellular retinoic acid binding protein 1 (CRABP1) expression (Table 1). Corroborating our findings, RA signaling in monocytes has been associated with a slowdown of cell cycle progression and a stimulation of cell differentiation [57, 58]. Additionally, RA signaling plays a role in the oxidative stress response and CRABP1 expression may reflect a reaction towards the reduced SOD2 levels [59].

We identified YY1 to be strongly controlled by plasma. In the human T cell line Jurkat, the IFN-γ cytokine promoter is under control of YY1 [60]. Malondialdehyde-induced ROS stress was found to highly upregulate YY1 expression in Jurkat cells which was subsequently associated with a marked increase of *IL-8* mRNA and its release [61]. Strikingly, YY1 is positively regulated by products of HO-1, such as carbon monoxide [62], and *HMOX1* upregulation was previously found in plasma-treated keratinocytes [56]. Both molecules are associated with inflammation and we asked next whether their expression was affected following exposure to plasma.

3.4. Plasma Treatment Induced Expression of IL-8 and HMOX1. In the inflammatory phase of wound healing, the main function of the proinflammatory chemokine IL-8 (CXCL8) is the attraction of phagocytes from the blood to the site of injury [63]. Exposure of THP-1 monocytes to plasma led to the presence of higher copy numbers of *IL-8* mRNA (Figure 5(a)). This correlated with an increase in secretion of IL-8 (Figure 5(b)) while no release or no change in the release of other inflammation-associated molecules (IL-1β, IL-6, IL-10, IL-17A, IL-22, GM-CSF, INFγ, TNFα, and TGFβ) could be observed (data not shown). IL-8 is also secreted by primary monocytes and macrophages but is not associated with autocrine effects on these cells [64], making a contribution of this molecule to other results of this study unlikely. Substantiating our results, antioxidants were found to decrease steady state ROS and IL-8 levels [65] while increased ROS trigger IL-8 expression in primary monocytes/macrophages [66].

Next to IL-8, *HMOX1* was significantly upregulated after exposure to plasma (Figure 5(b)). The myeloid cell-specific enzyme HO-1 protects against the cytotoxicity of oxidative stress and mediates immunomodulatory and anti-inflammatory properties [67] via the oxidation of free heme under generation of the products carbon monoxide, biliverdin, and iron [68]. It is upregulated during oxidative stress [69] and hypothesized to be central in the protection and homeostatic reestablishment in numerous pathological conditions [70]. Ferritin, a scavenger of free iron, is coinduced with *HMOX1* [71], which may provide a beneficial side effect via, for example, reduced hydroxyl radical generation through the Fenton reaction. Importantly, HO-1 expression was shown to increase the number of mitochondria and total metabolic activity in cardiac cells [72] which corroborates our findings in THP-1 monocytes (Figures 3(f) and 4(c)).

3.5. Study Limitations. Following exposure to cold physical plasma, the widely recognized cell line THP-1 monocytes were used in this study to investigate their biological responses. This includes the identification of their proteomic profile using SILAC mass spectrometry which requires proliferating cells. Yet, owing to the altered ROS-signaling in THP-1 cells [33], the findings identified in this work may not fully represent the redox response in other cell types following exposure to plasma. Moreover, studying the neoplastic THP-1 cells may provide an only imperfect model to mimic responses of wound-resident monocytes/macrophages to plasma. This especially accounts for the changes observed in metabolic activity and cell proliferation as macrophages at the wound site derive from monocyte differentiation rather than cell division [73].

4. Summary

Via generation of ROS/RNS, treatment with cold physical plasma may be beneficial in redox-related diseases, such as impaired wound healing. Using THP-1 monocytes as a model, we investigated the oxidative challenge provided by the plasma to these cells. Although plasma induced changes in the intracellular redox status, it only modestly compromised their viability. Short plasma treatment stimulated THP-1

monocyte growth while longer exposure increased cell size, mitochondrial content, and metabolic activity. Global protein expression analysis revealed an increase in protein synthesis, degradation, and folding processes indicative of both plasma-mediated protein stress response and changes in protein expression pattern. A moderate oxidative stress response was detected, yet not via Nrf2 signaling. Changes in RA signaling, YY1, and IRF8 expression suggested the activation of cell differentiation events. At long exposure times, plasma upregulated the expression of IL-8 (but not other inflammatory cytokines) and *HMOX1* which are both involved in inflammatory processes, such as wounds. Altogether, THP-1 monocytes mounted a distinct response to plasma which was manifested by alterations of their metabolic activity and inflammatory potential. Our results exemplify the delicate balance of cellular redox control and suggest a role of low-dose redox modulation in wound-related cells which is aimed at being triggered by cold plasma in redox-based diseases.

Abbreviations

IL-8:	Interleukin-8
HMOX1, HO-1:	Heme oxygenase 1
YY1:	Yin Yang 1
SOD:	Superoxide dismutase.

Conflict of Interests

The authors declare that no conflict of interests exists.

Acknowledgments

The authors acknowledge the support of Lena Bundscherer who generated the *HMOX1* and *IL-8* expression data. This work was funded by the German Federal Ministry of Education and Research (Grant no. 03Z2DN11) and by Ministry of Education, Science and Culture of the State of Mecklenburg-Western Pomerania and European Union, European Social Fund (Grants nos. AU 11 038 and ESF/IV-BM-B35-0010/13).

References

[1] D. B. Graves, "The emerging role of reactive oxygen and nitrogen species in redox biology and some implications for plasma applications to medicine and biology," *Journal of Physics D: Applied Physics*, vol. 45, no. 26, Article ID 263001, 2012.

[2] K. D. Weltmann, E. Kinde, T. von Woedtke, M. Hähnel, M. Stieber, and R. Brandenburg, "Atmospheric pressure plasma sources—prospective tools for plasma medicine," *Pure and Applied Chemistry*, vol. 82, no. 6, pp. 1223–1237, 2010.

[3] K.-D. Weltmann, M. Polak, K. Masur, T. von Woedtke, J. Winter, and S. Reuter, "Plasma processes and plasma sources in medicine," *Contributions to Plasma Physics*, vol. 52, no. 7, pp. 644–654, 2012.

[4] K.-D. Weltmann, E. Kindel, R. Brandenburg et al., "Atmospheric pressure plasma jet for medical therapy: plasma parameters and risk estimation," *Contributions to Plasma Physics*, vol. 49, no. 9, pp. 631–640, 2009.

[5] S. Bekeschus, S. Iseni, S. Reuter, K. Masur, and K.-D. Weltmann, "Nitrogen shielding of an argon plasma jet and its effects on human immune cells," *IEEE Transactions on Plasma Science*, vol. 43, no. 3, pp. 776–781, 2015.

[6] A. Schmidt-Bleker, J. Winter, S. Iseni, M. Dünnbier, K.-D. Weltmann, and S. Reuter, "Reactive species output of a plasma jet with a shielding gas device—combination of FTIR absorption spectroscopy and gas phase modelling," *Journal of Physics D: Applied Physics*, vol. 47, no. 14, Article ID 145201, 2014.

[7] S. Vandersee, H. Richter, J. Lademann et al., "Laser scanning microscopy as a means to assess the augmentation of tissue repair by exposition of wounds to tissue tolerable plasma," *Laser Physics Letters*, vol. 11, no. 11, Article ID 115701, 2014.

[8] G. Isbary, W. Stolz, T. Shimizu et al., "Cold atmospheric argon plasma treatment may accelerate wound healing in chronic wounds: results of an open retrospective randomized controlled study *in vivo*," *Clinical Plasma Medicine*, vol. 1, no. 2, pp. 25–30, 2013.

[9] F. Brehmer, H. A. Haenssle, G. Daeschlein et al., "Alleviation of chronic venous leg ulcers with a hand–held dielectric barrier discharge plasma generator (PlasmaDerm VU–2010): results of a monocentric, two–armed, open, prospective, randomized and controlled trial (NCT01415622)," *Journal of the European Academy of Dermatology and Venereology*, vol. 29, no. 1, pp. 148–155, 2015.

[10] J. E. Park and A. Barbul, "Understanding the role of immune regulation in wound healing," *The American Journal of Surgery*, vol. 187, no. 5, pp. 11S–16S, 2004.

[11] I. V. Klyubin, K. M. Kirpichnikova, and I. A. Gamaley, "Hydrogen peroxide-induced chemotaxis of mouse peritoneal neutrophils," *European Journal of Cell Biology*, vol. 70, no. 4, pp. 347–351, 1996.

[12] M. P. Rodero and K. Khosrotehrani, "Skin wound healing modulation by macrophages," *International Journal of Clinical and Experimental Pathology*, vol. 3, no. 7, pp. 643–653, 2010.

[13] K. Rosner, C. Ross, T. Karlsmark, A. A. Petersen, F. Gottrup, and G. L. Vejlsgaard, "Immunohistochemical characterization of the cutaneous cellular infiltrate in different areas of chronic leg ulcers," *APMIS*, vol. 103, no. 4, pp. 293–299, 1995.

[14] B. M. Delavary, W. M. van der Veer, M. van Egmond, F. B. Niessen, and R. H. J. Beelen, "Macrophages in skin injury and repair," *Immunobiology*, vol. 216, no. 7, pp. 753–762, 2011.

[15] S. Barrientos, O. Stojadinovic, M. S. Golinko, H. Brem, and M. Tomic-Canic, "Growth factors and cytokines in wound healing," *Wound Repair and Regeneration*, vol. 16, no. 5, pp. 585–601, 2008.

[16] M. Exner, E. Minar, O. Wagner, and M. Schillinger, "The role of heme oxygenase-1 promoter polymorphisms in human disease," *Free Radical Biology & Medicine*, vol. 37, no. 8, pp. 1097–1104, 2004.

[17] E. Engelhardt, A. Toksoy, M. Goebeler, S. Debus, E.-B. Bröcker, and R. Gillitzer, "Chemokines IL-8, GROα, MCP-1, IP-10, and mig are sequentially and differentially expressed during phase-specific infiltration of leukocyte subsets in human wound healing," *The American Journal of Pathology*, vol. 153, no. 6, pp. 1849–1860, 1998.

[18] K. Turpaev, D. Litvinov, and J. Justesen, "Redox modulation of NO-dependent induction of interleukin 8 gene in monocytic U937 cells," *Cytokine*, vol. 23, no. 1-2, pp. 15–22, 2003.

[19] C. K. Sen, "Wound healing essentials: let there be oxygen," *Wound Repair and Regeneration*, vol. 17, no. 1, pp. 1–18, 2009.

[20] C. K. Sen, "The general case for redox control of wound repair," *Wound Repair and Regeneration*, vol. 11, no. 6, pp. 431–438, 2003.

[21] D. B. Graves, "Oxy-nitroso shielding burst model of cold atmospheric plasma therapeutics," *Clinical Plasma Medicine*, vol. 2, no. 2, pp. 38–49, 2014.

[22] S. Bekeschus, K. Masur, J. Kolata et al., "Human mononuclear cell survival and proliferation is modulated by cold atmospheric plasma jet," *Plasma Processes and Polymers*, vol. 10, no. 8, pp. 706–713, 2013.

[23] K. Wende, P. Williams, J. Dalluge et al., "Identification of the biologically active liquid chemistry induced by a nonthermal atmospheric pressure plasma jet," *Biointerphases*, vol. 10, no. 2, 2015.

[24] S. Kalghatgi, C. M. Kelly, E. Cerchar et al., "Effects of non-thermal plasma on mammalian cells," *PLoS ONE*, vol. 6, no. 1, Article ID e16270, 2011.

[25] P. Lukes, E. Dolezalova, I. Sisrova, and M. Clupek, "Aqueous-phase chemistry and bactericidal effects from an air discharge plasma in contact with water: evidence for the formation of peroxynitrite through a pseudo-second-order post-discharge reaction of H_2O_2 and HNO_2," *Plasma Sources Science and Technology*, vol. 23, no. 1, Article ID 015019, 2014.

[26] K. Wende, S. Reuter, T. von Woedtke, K.-D. Weltmann, and K. Masur, "Redox-based assay for assessment of biological impact of plasma treatment," *Plasma Processes and Polymers*, vol. 11, no. 7, pp. 655–663, 2014.

[27] S. Bekeschus, J. Kolata, A. Müller et al., "Differential viability of eight human blood mononuclear cell subpopulations after plasma treatment," *Plasma Medicine*, vol. 3, no. 1-2, pp. 1–13, 2013.

[28] K. Wende, A. Barton, S. Bekeschus et al., "Proteomic tools to characterize non-thermal plasma effects in eukaryotic cells," *Plasma Medicine*, vol. 3, no. 1-2, pp. 81–95, 2013.

[29] K.-I. Setsukinai, Y. Urano, K. Kakinuma, H. J. Majima, and T. Nagano, "Development of novel fluorescence probes that can reliably detect reactive oxygen species and distinguish specific species," *Journal of Biological Chemistry*, vol. 278, no. 5, pp. 3170–3175, 2003.

[30] S. Bekeschus, J. Kolata, C. Winterbourn et al., "Hydrogen peroxide: a central player in physical plasma-induced oxidative stress in human blood cells," *Free Radical Research*, vol. 48, no. 5, pp. 542–549, 2014.

[31] B. Halliwell and J. M. C. Gutteridge, "Biologically relevant metal ion-dependent hydroxyl radical generation. An update," *FEBS Letters*, vol. 307, no. 1, pp. 108–112, 1992.

[32] M. B. Hampton and S. Orrenius, "Redox regulation of apoptotic cell death in the immune system," *Toxicology Letters*, vol. 102-103, pp. 355–358, 1998.

[33] P. S. Hole, J. Zabkiewicz, C. Munje et al., "Overproduction of NOX-derived ROS in AML promotes proliferation and is associated with defective oxidative stress signaling," *Blood*, vol. 122, no. 19, pp. 3322–3330, 2013.

[34] A. Morales, C. García-Ruiz, M. Miranda et al., "Tumor necrosis factor increases hepatocellular glutathione by transcriptional regulation of the heavy subunit chain of γ-glutamylcysteine synthetase," *The Journal of Biological Chemistry*, vol. 272, no. 48, pp. 30371–30379, 1997.

[35] J. R. Gasdaska, M. Berggren, and G. Powis, "Cell growth stimulation by the redox protein thioredoxin occurs by a novel helper mechanism," *Cell Growth and Differentiation*, vol. 6, no. 12, pp. 1643–1650, 1995.

[36] C. Mueller, S. Baudler, H. Welzel, M. Böhm, and G. Nickenig, "Identification of a novel redox-sensitive gene, Id3, which mediates Angiotensin II-induced cell growth," *Circulation*, vol. 105, no. 20, pp. 2423–2428, 2002.

[37] G.-S. Seo, S.-H. Lee, S.-C. Choi et al., "Iron chelator induces THP-1 cell differentiation potentially by modulating intracellular glutathione levels," *Free Radical Biology & Medicine*, vol. 40, no. 9, pp. 1502–1512, 2006.

[38] T. E. DeCoursey and V. V. Cherny, "II. Voltage-activated proton currents in human THP-1 monocytes," *The Journal of Membrane Biology*, vol. 152, no. 2, pp. 131–140, 1996.

[39] A. Eckhardt, N. Gerstmayr, K.-A. Hiller et al., "TEGDMA-induced oxidative DNA damage and activation of ATM and MAP kinases," *Biomaterials*, vol. 30, no. 11, pp. 2006–2014, 2009.

[40] P. A. Kramer, S. Ravi, B. Chacko, M. S. Johnson, and V. M. Darley-Usmar, "A review of the mitochondrial and glycolytic metabolism in human platelets and leukocytes: implications for their use as bioenergetic biomarkers," *Redox Biology*, vol. 2, no. 1, pp. 206–210, 2014.

[41] S. Moncada and J. D. Erusalimsky, "Does nitric oxide modulate mitochondrial energy generation and apoptosis?" *Nature Reviews Molecular Cell Biology*, vol. 3, no. 3, pp. 214–220, 2002.

[42] E. H. Sarsour, A. L. Kalen, and P. C. Goswami, "Manganese superoxide dismutase regulates a redox cycle within the cell cycle," *Antioxidants & Redox Signaling*, vol. 20, no. 10, pp. 1618–1627, 2014.

[43] C. F. Calkhoven, C. Müller, and A. Leutz, "Translational control of gene expression and disease," *Trends in Molecular Medicine*, vol. 8, no. 12, pp. 577–583, 2002.

[44] M. Hochstrasser, "Ubiquitin-dependent protein degradation," *Annual Review of Genetics*, vol. 30, no. 1, pp. 405–439, 1996.

[45] D. L. Swaney, P. Beltrao, L. Starita et al., "Global analysis of phosphorylation and ubiquitylation cross-talk in protein degradation," *Nature Methods*, vol. 10, no. 7, pp. 676–682, 2013.

[46] M. Scortegagna, K. Ding, Y. Oktay et al., "Multiple organ pathology, metabolic abnormalities and impaired homeostasis of reactive oxygen species in *Epas1*$^{-/-}$ mice," *Nature Genetics*, vol. 35, no. 4, pp. 331–340, 2003.

[47] A. Shukla, A. M. Rasik, and G. K. Patnaik, "Depletion of reduced glutathione, ascorbic acid, vitamin E and antioxidant defence enzymes in a healing cutaneous wound," *Free Radical Research*, vol. 26, no. 2, pp. 93–101, 1997.

[48] W.-S. Choi, S.-Y. Yoon, T. H. Oh, E.-J. Choi, K. L. O'Malley, and Y. J. Oh, "Two distinct mechanisms are involved in 6-hydroxydopamine- and MPP^+-induced dopaminergic neuronal cell death: role of caspases, ROS, and JNK," *Journal of Neuroscience Research*, vol. 57, no. 1, pp. 86–94, 1999.

[49] S. Srivastava, B. Chandrasekar, Y. Gu et al., "Downregulation of CuZn-superoxide dismutase contributes to beta-adrenergic receptor-mediated oxidative stress in the heart," *Cardiovascular Research*, vol. 74, no. 3, pp. 445–455, 2007.

[50] S. Gordon, G. Akopyan, H. Garban, and B. Bonavida, "Transcription factor YY1: structure, function, and therapeutic implications in cancer biology," *Oncogene*, vol. 25, no. 8, pp. 1125–1142, 2006.

[51] M. Joo, J. G. Wright, N. H. Ning et al., "Yin Yang 1 enhances cyclooxygenase-2 gene expression in macrophages," *The American Journal of Physiology—Lung Cellular and Molecular Physiology*, vol. 292, no. 5, pp. L1219–L1226, 2007.

[52] T. Tamura, H. Yanai, D. Savitsky, and T. Taniguchi, "The IRF family transcription factors in immunity and oncogenesis," *Annual Review of Immunology*, vol. 26, pp. 535–584, 2008.

[53] A. D. Friedman, "Transcriptional control of granulocyte and monocyte development," *Oncogene*, vol. 26, no. 47, pp. 6816–6828, 2007.

[54] R. C. Scarpulla, "Nuclear control of respiratory chain expression by nuclear respiratory factors and PGC-1-related coactivator," *Annals of the New York Academy of Sciences*, vol. 1147, pp. 321–334, 2008.

[55] R. C. Scarpulla, R. B. Vega, and D. P. Kelly, "Transcriptional integration of mitochondrial biogenesis," *Trends in Endocrinology & Metabolism*, vol. 23, no. 9, pp. 459–466, 2012.

[56] A. Schmidt, S. Dietrich, A. Steuer et al., "Non-thermal plasma activates human keratinocytes by stimulation of antioxidant and phase II pathways," *The Journal of Biological Chemistry*, vol. 290, no. 11, pp. 6731–6750, 2015.

[57] Q. Chen and A. C. Ross, "Retinoic acid regulates cell cycle progression and cell differentiation in human monocytic THP-1 cells," *Experimental Cell Research*, vol. 297, no. 1, pp. 68–81, 2004.

[58] S. Han and N. Sidell, "Peroxisome-proliferator-activated-receptor gamma (PPARγ) independent induction of CD36 in THP-1 monocytes by retinoic acid," *Immunology*, vol. 106, no. 1, pp. 53–59, 2002.

[59] B. Ahlemeyer, E. Bauerbach, M. Plath et al., "Retinoic acid reduces apoptosis and oxidative stress by preservation of SOD protein level," *Free Radical Biology & Medicine*, vol. 30, no. 10, pp. 1067–1077, 2001.

[60] J. Ye, P. Ghosh, M. Cippitelli et al., "Characterization of a silencer regulatory element in the human interferon-gamma promoter," *The Journal of Biological Chemistry*, vol. 269, no. 41, pp. 25728–25734, 1994.

[61] S. Raghavan, G. Subramaniyam, and N. Shanmugam, "Proinflammatory effects of malondialdehyde in lymphocytes," *Journal of Leukocyte Biology*, vol. 92, no. 5, pp. 1055–1067, 2012.

[62] K. Beck, B. J. Wu, J. Ni et al., "Interplay between heme oxygenase-1 and the multifunctional transcription factor Yin Yang 1 in the inhibition of intimal hyperplasia," *Circulation Research*, vol. 107, no. 12, pp. 1490–1497, 2010.

[63] T. Matsumoto, K. Yokoi, N. Mukaida et al., "Pivotal role of interleukin-8 in the acute respiratory distress syndrome and cerebral reperfusion injury," *Journal of Leukocyte Biology*, vol. 62, no. 5, pp. 581–587, 1997.

[64] B. A. Premack and T. J. Schall, "Chemokine receptors: gateways to inflammation and infection," *Nature Medicine*, vol. 2, no. 11, pp. 1174–1178, 1996.

[65] S. K. Jain, P. Manna, D. Micinski et al., "In African American type 2 diabetic patients, is vitamin d deficiency associated with lower blood levels of hydrogen sulfide and cyclic adenosine monophosphate, and elevated oxidative stress?" *Antioxidants & Redox Signaling*, vol. 18, no. 10, pp. 1154–1158, 2013.

[66] A. Luís, J. D. Martins, A. Silva, I. Ferreira, M. T. Cruz, and B. M. Neves, "Oxidative stress-dependent activation of the eIF2α–ATFr unfolded protein response branch by skin sensitizer 1-fluoro-2,4-dinitrobenzene modulates dendritic-like cell maturation and inflammatory status in a biphasic manner," *Free Radical Biology and Medicine*, vol. 77, pp. 217–229, 2014.

[67] A. Paine, B. Eiz-Vesper, R. Blasczyk, and S. Immenschuh, "Signaling to heme oxygenase-1 and its anti-inflammatory therapeutic potential," *Biochemical Pharmacology*, vol. 80, no. 12, pp. 1895–1903, 2010.

[68] K. D. Poss and S. Tonegawa, "Heme oxygenase 1 is required for mammalian iron reutilization," *Proceedings of the National Academy of Sciences of the United States of America*, vol. 94, no. 20, pp. 10919–10924, 1997.

[69] C.-Y. Lin, W.-C. Hsiao, C.-J. Huang, C.-F. Kao, and G.-S. W. Hsu, "Heme oxygenase-1 induction by the ROS-JNK pathway plays a role in aluminum-induced anemia," *Journal of Inorganic Biochemistry*, vol. 128, pp. 221–228, 2013.

[70] F. A. D. T. G. Wagener, C. E. Carels, and D. M. S. Lundvig, "Targeting the redox balance in inflammatory skin conditions," *International Journal of Molecular Sciences*, vol. 14, no. 5, pp. 9126–9167, 2013.

[71] M. P. Soares and F. H. Bach, "Heme oxygenase-1: from biology to therapeutic potential," *Trends in Molecular Medicine*, vol. 15, no. 2, pp. 50–58, 2009.

[72] C. A. Piantadosi, M. S. Carraway, A. Babiker, and H. B. Suliman, "Heme oxygenase-1 regulates cardiac mitochondrial biogenesis via nrf2-mediated transcriptional control of nuclear respiratory factor-1," *Circulation Research*, vol. 103, no. 11, pp. 1232–1240, 2008.

[73] S. Gordon and P. R. Taylor, "Monocyte and macrophage heterogeneity," *Nature Reviews Immunology*, vol. 5, no. 12, pp. 953–964, 2005.

Hindawi Publishing Corporation
Oxidative Medicine and Cellular Longevity
Volume 2016, Article ID 9636937, 17 pages
http://dx.doi.org/10.1155/2016/9636937

Research Article

Intermittent Hypoxia Affects the Spontaneous Differentiation *In Vitro* of Human Neutrophils into Long-Lived Giant Phagocytes

Larissa Dyugovskaya, Slava Berger, Andrey Polyakov, Peretz Lavie, and Lena Lavie

The Lloyd Rigler Sleep Apnea Research Laboratory, Unit of Anatomy and Cell Biology, The Ruth and Bruce Rappaport Faculty of Medicine, Technion-Israel Institute of Technology, 31096 Haifa, Israel

Correspondence should be addressed to Lena Lavie; lenal@tx.technion.ac.il

Received 20 May 2015; Accepted 1 July 2015

Academic Editor: Stefania Meschini

Previously we identified, for the first time, a new small-size subset of neutrophil-derived giant phagocytes (Gϕ) which spontaneously develop *in vitro* without additional growth factors or cytokines. Gϕ are $CD66b^+/CD63^+/MPO^+/LC3B^+$ and are characterized by extended lifespan, large phagolysosomes, active phagocytosis, and reactive oxygen species (ROS) production, and autophagy largely controls their formation. Hypoxia, and particularly hypoxia/reoxygenation, is a prominent feature of many pathological processes. Herein we investigated Gϕ formation by applying various hypoxic conditions. Chronic intermittent hypoxia (IH) (29 cycles/day for 5 days) completely abolished Gϕ formation, while acute IH had dose-dependent effects. Exposure to 24 h (56 IH cycles) decreased their size, yield, phagocytic ability, autophagy, mitophagy, and gp91-*phox*/p22-*phox* expression, whereas under 24 h sustained hypoxia (SH) the size and expression of LC3B and gp91-*phox*/p22-*phox* resembled Gϕ formed in normoxia. Diphenyl iodide (DPI), a NADPH oxidase inhibitor, as well as the PI3K/Akt and autophagy inhibitor LY294002 abolished Gϕ formation at all oxygen conditions. However, the potent antioxidant, N-acetylcysteine (NAC) abrogated the effects of IH by inducing large $CD66b^+/LC3B^+$ Gϕ and increased both NADPH oxidase expression and phagocytosis. These findings suggest that NADPH oxidase, autophagy, and the PI3K/Akt pathway are involved in Gϕ development.

1. Introduction

Neutrophils, the first line of defense against invading pathogens and harmful particles, are known as professional phagocytes. Yet, increased neutrophil survival within tissues or in the circulation can promote persistent inflammation resulting in tissue injury and dysfunction [1]. During the last decade it has become increasingly evident that neutrophil activities go far beyond pathogen clearance while new unanticipated functions were recognized [2]. Moreover, concepts such as "neutrophil plasticity" and "neutrophil heterogeneity" have emerged [3], implying that there are conditions under which neutrophils may differentiate into discrete subsets with increased longevity and with new phenotypes and functions [2]. Thus, by exposing neutrophils to GM-CSF/IL-4/TNF-α, long-lived neutrophil subsets with efficient phagocytosis, increased production of reactive oxygen (ROS), IL-1, and IL-8 developed [4]. Also transforming or reprogramming into other cell types, like macrophages or dendritic cells (DCs), was demonstrated [5, 6]. Murine neutrophils cultured with GM-CSF, or upon recruitment to inflammatory or infectious sites, are differentiated into a hybrid population with prolonged life span, exhibiting dual features and functionality of neutrophils and DCs [7–9]. Notably, the existence of long-lived neutrophil subsets is suggested through their ability to modulate their survival response by both intrinsic host-derived and extrinsic factors, such as G-CSF, GM-CSF, IFN-γ, TNF-α, and/or pathogen-derived products, nucleic acids, or hypoxic environmental conditions [10]. Specifically, inflammatory sites tend to become depleted of oxygen. Thus, the concept of "inflammatory hypoxia," in which inflammation and hypoxia are inseparably linked, was proposed [11, 12].

Both sustained and intermittent hypoxia (SH and IH) were shown to profoundly inhibit neutrophil apoptosis resulting in increased neutrophil survival and activation [13, 14]. Moreover, prolonged neutrophil survival was also evident in patients with obstructive sleep apnea (OSA), a morbidity associated with nightly IH resulting in intermittent blood hypoxemia resembling ischemia/reperfusion (I/R) and associated with increased ROS production, oxidative stress, and systemic inflammation [15, 16].

To adapt to hypoxia, cells undergo a metabolic shift by increasing the cellular dependency on anaerobic metabolism and activate autophagy for degrading damaged or unnecessary proteins and organelles. In neutrophils, autophagy plays a cell death role in inflammatory/infectious conditions and in tumors which are characterized by hypoxia. Of note, autophagy is vital in sensing oxidative stress and removing oxidatively damaged cellular components and is activated by stress or triggered by cytoplasmic overload of these proteins or organelles. It may also play a role in neutrophil differentiation [17] and has been shown to control the generation of neutrophils in the bone marrow [18]. Additionally, a specific mitochondrial autophagy—mitophagy—has been demonstrated as a selective mechanism to remove dysfunctional or damaged mitochondria [19]. One of the key proteins of autophagy activation and a prominent autophagosome marker is LC3B. Generation of autophagosome structures requires conversion of the cytosolic LC3BI to the lipidated LC3BII and its translocation to autophagosomes [20]. Autophagy is negatively regulated by mTOR while it requires phosphatidylinositol 3-kinase (PI3K) for inducing the autophagic machinery [20] and for generating NADPH oxidase-dependent ROS [21]. Autophagy is also enhanced in cardiac I/R injury but acts as a double-edged sword in I/R related pathological processes [22]. Hence, besides its detrimental effects, autophagy can protect cardiac myocytes against I/R injury [23]. However, the interplay between ROS, autophagy, and cell survival is complex, cell specific, and not entirely understood [24]. All in all, these findings suggest that ROS might be involved in autophagic processes in conditions associated with IH.

In a previous study we have shown, for the first time, that freshly isolated purified PMN from healthy subjects maintained in prolonged culture conditions without additional growth factors or cytokines give rise to a small subpopulation of Gϕ within 5–7 days [25]. These Gϕ are characterized by unique morphology, phenotype, and functions. They are vastly enlarged due to autophagocytosis of dead neutrophil remnants, are vacuolated, and contain phagolysosomes. They express a marker of specific neutrophil granules CD66b, a marker of azurophilic granules CD63, CD15, CD11b, and MPO, the gp91-*phox* subunit of NADPH, and autophagy markers (LC3B). Functionally, they actively take up particles as latex and opsonized zymosan and generate ROS in response to these particulate stimuli and to PMA. Interestingly, unlike fresh PMN, Gϕ which also intensively expressed CD68 scavenger receptor took up oxidized LDL (oxLDL) and generated ROS in response to stimulation with oxLDL. Additionally, specific autophagy inhibitors as 3-methyladenine (3-MA) or bafilomycin (BafA1) abolished Gϕ development, demonstrating the importance of autophagy to Gϕ development [25]. However, the exact factors which determine Gϕ formation remain to be unveiled.

To further elucidate the conditions and mechanisms involved in Gϕ formation, we sought to investigate the effects of various hypoxic treatments on Gϕ development. To gain further insights into Gϕ development in hypoxic conditions, PMN were also treated with various pharmacologic inhibitors for ROS generation and signalling pathways.

2. Materials and Methods

2.1. Isolation and Culture of Polymorphonuclear Cells (PMN) and the Development of Giant Phagocytes (Gϕ) in Culture. Blood samples were obtained from 28 (26 males/2 females) healthy nonsmoker volunteers with a mean age of 28.0 ± 6.6 years and BMI of 24.9 ± 3.9 Kg/m^2. Sleep studies were performed on all subjects using the WatchPAT-200 device [26], to rule out occult sleep disordered breathing. All subjects had less than 5 oxygen desaturation (ODI) breathing events per hour which is considered a normal value. The protocol was approved by the local Human Rights Committee according to the Declaration of Helsinki, and all participants signed an informed consent form. Some of the subjects were tested from two to six times. PMN were isolated using two-step density gradients of equal volumes of Ficoll-Histopaque-1077 and Ficoll-Histopaque-1.119 (Sigma-Aldrich, Israel) according to manufacturer's instructions, followed by lysis of red blood cells with 0.2% sodium chloride for 30 sec on ice. PMN were cultured in RPMI-1640 medium supplemented with 10% heat inactivated FCS (Biological Industries, Beit HaEmek, Israel). Half of the growth medium was carefully replaced every 3 days. After 5–7 days, Gϕ were evident in culture. Depending on the donor, from each 10^6 neutrophils plated, 100–200 Gϕ developed. As a control, in some experiments, the culture medium was supplemented with 30 ng/mL granulocyte macrophage-stimulating factor (GM-CSF) and 30 ng/mL IL-4 (R&D Systems, Minneapolis, MN). GM-CSF/IL-4 was added at each medium change. The LPS content in FCS was lower than 1.0 ng/mL and the addition of 1–10 ng/mL LPS to the culture medium did not affect Gϕ formation [25].

Of note, to validate the neutrophilic origin of Gϕ, in earlier experiments we also prepared a FACS-purified population of CD15/CD11b/CD63/CD66b neutrophils. Their development in culture was similar to that obtained from PMN isolated by Ficoll only. Moreover, by coculturing PMN with autologous monocytes, Gϕ did not develop. Thus, excluding the possibility that Gϕ arise from contaminating cells or cells other than mature PMN, we should also note that since the yield of Gϕ formed from neutrophils in culture is low (0.01–0.02% of cultured PMN in normoxia), biochemical and molecular measures are hard to implement [25]. Therefore in this study the analyses rely mostly on a follow-up by confocal microscopy.

2.2. In Vitro Intermittent (IH) and Sustained Hypoxia (SH) Protocol. Purified PMN (0.6 mL per well; 3×10^6 cells/mL)

were plated into 24-well plates after which they were exposed to normoxia, SH, or IH in custom-designed incubation chambers attached to an external O_2-CO_2-N_2 computer-driven controller using BioSpherix-OxyCycler-C42 system (Redfield, NY, USA). This system enables creating periodic changes in external O_2 concentrations that control air gas levels in each chamber individually as previously described [13]. Oxygen levels in the medium were determined by a fiber-optic dissolved oxygen electrode (BioSpherix, Redfield, NY, USA). The actual lowest % of O_2 in the medium dropped to 5% during the hypoxic period for about 1.5 min, and this level of hypoxia was achieved after 15 min of incubation. In the reoxygenation period, O_2 levels reached normoxic levels (20%) after 10 min of incubation. Carbon dioxide was held constant (5%) at all treatments. For modeling chronic IH, the purified PMN were exposed for 5 consecutive days to 29 IH cycles/day (approximately 12 h/day). Acute IH was induced by exposing PMN to 10 cycles (250 min), 29 cycles (12 h), or 56 cycles (approximately 24 h), each in the first day in culture. SH was employed for comparable times at 5% actual oxygen in the medium for the entire periods (250 min, 12 h, and 24 h). Thereafter, the hypoxia treated cells were transferred to normoxia for additional six days, after which various measures were performed. Control cells were maintained in normoxia for the entire period.

2.3. Confocal Laser Scanning Microscopy. Cytospins prepared from 7-day Gϕ were fixed with 4% paraformaldehyde and washed with PBS. For intracellular staining, cells were permeabilized with 0.5% Triton X-100 (Sigma-Aldrich, Israel) in PBS, at room temperature for 10 min. After blocking with 10% normal goat serum in RPMI-1640, cells were incubated overnight at 4°C using the following primary Abs (dilution 1 : 100) or the corresponding isotype controls: mouse monoclonal anti-CD66b Abs (80H3, AbD Serotec, Oxford, UK) and anti-cytochrome b-245 light chain (p22-*phox* identification, Clone 44.1, BioLegend, San Diego, CA), rabbit polyclonal anti-neutrophil elastase (NE) (Calbiochem, San Diego, CA), anti-LC3B Abs (Sigma, Israel), and anti-Nox2/gp91-*phox* Abs (ab131083, Abcam, UK). Isotype controls included purified mouse IgG1 (clone MG1-45) and IgG2 (clone MOPC-173, BioLegend, San Diego, CA) and rabbit IgG (Santa Cruz Biotechnologies, Santa Cruz, CA). Then, the cells were washed and incubated with 1/400 secondary antibodies CF 488A or CF 647 goat anti-rabbit IgG and/or CF 647 goat anti-mouse IgG (Biotium, Hayward, CA). After washing, slides were mounted with mounting medium containing 4′,6-diamidino-2-phenylindole (DAPI) for nuclear staining (Vectashield H-1000, Vector Lab. Inc., Burlingame, CA). Slides were analyzed by a confocal laser scanning system (LSM 700) using Nikon E600 (Japan) fluorescence microscope and Plan Apo X40 immersion oil objective. Cells' area and fluorescent intensities (FI) were integrated with Image J 1.49k Software (Wayne Rasband, NIH, USA). Data are presented as FI = Raw integrated density (sum of pixel values)/Area of cells.

2.4. Fluorescence Labeling of Cells. The fluorescence membrane stains PKH-26 (red) and PKH-67 (green) (Sigma-Aldrich) were used to label freshly isolated neutrophils according to manufacturer's instructions. The labeling vehicle provided by the kits (Diluent C) is an aqueous solution designed to maintain cell viability. Cells were washed in serum-free medium; the pellets were resuspended in 0.5 mL of PKH-26 or PKH-67 (1 : 500 in Diluent C) and incubated for 5 min at room temperature. Labeling was stopped by adding 0.5 mL FCS. Then, cells were washed three times with complete medium and cocultured.

2.5. Phagocytosis. The phagocytic activity of Gϕ was determined on day 7 using fluorescent latex beads of 1.0 μm in diameter (phagocytosis is considered when the particles internalized are about 0.75 μm or larger). Briefly, Gϕ were incubated for 2 h with carboxylate-modified fluorescent yellow-green latex beads (Polyscience, Warrington, PA) at a cell : bead ratio of 1 : 500 (because of the large Gϕ cell size). Cytospins were prepared and fixed as described above and analyzed by confocal microscopy. Three types of controls were performed to ensure intracellular localization of the beads. (1) Control Gϕ were kept on ice for 15 min and cytospins were prepared immediately or 2 h after adding the latex beads. (2) To inhibit phagocytosis, Gϕ were preincubated with 10 μM cytochalasin B (Sigma-Aldrich, Israel) for 30 min prior to adding the latex beads, and cytospins were prepared 2 h after incubation with latex. (3) To ensure intracellular localization rather than adhesion, the intracellular localization of latex beads was confirmed in Gϕ by 3D images (*xy*, *xz*, and *yz* cross sections) using 3D reconstructing software IMARIS *z*-stack analysis (Bitplane AG, Switzerland), and only latex beads in the plane of the nucleus were considered positive for phagocytosis.

2.6. Lysosomal and Mitochondrial Distribution. LysoTracker (Invitrogen, Molecular Probes, Eugene, Oregon, USA) was used to detect acidified endosomes. Viable Gϕ were incubated with 50 nM of LysoTracker for 90 min at 37°C in the dark. To identify mitochondria, viable cells were stained for 30 min at 37°C in the dark with 100 nM MitoTracker Orange CMTM-Ros (Invitrogen, Molecular Probes, Eugene, Oregon, USA). To further detect mitophagy, fixed cytospins were stained with LC3B, as described above.

Colocalization was quantified by ZEN 2010 (version 6.0) Carl Zeiss MicroImaging GmbH, Germany using Manders Overlap Coefficient (MOC) [27]. Only cells with MOC > 0.6 were considered as cells with significant colocalization.

2.7. Treatments of Neutrophils with Inhibitors. Freshly isolated PMN were exposed for 24 h to IH, SH, or normoxia with or without various inhibitors. Each inhibitor was added 10 min prior to the various oxygen treatments and remained throughout the treatments. The following inhibitors were used: a NADPH oxidase inhibitor, 10 μM diphenyl iodide (DPI); a ROS scavenger, 20 μM N-acetylcysteine (NAC) (all purchased from Sigma-Aldrich, St. Louis, MO, USA); and PI3K inhibitor LY-294002, 20 μM (L-1023, A.G. Scientific, San Diego, CA, USA) which is indicated to act at this concentration as a PI3K inhibitor not affecting TLR signaling

cascade. Equal volumes of DMSO were used as a negative control.

2.8. NBT Test. Intracellular ROS was determined in 7-day Gϕ by NBT test. NBT (Sigma-Aldrich) was dissolved in RPMI 1640 without phenol red (0.2%). Cells were incubated without or with 100 nM PMA at 37°C for 15 min, then kept at room temperature for 10 min, and assessed by light microscopy. In some experiments also DPI was added to Gϕ, 2 h prior to PMA stimulation. Cytoplasmic clumps of formazan deposits in Gϕ were considered positive for ROS.

2.9. Cell Viability by WST-1 Assay. Cell viability was monitored in the various oxygen and inhibitor treatments by using a commercial reagent WST-1 (Roche Diagnostics GmbH, Mannheim, Germany), according to manufacturer's instructions [28]. Briefly, purified PMN were exposed for 24 h duration to normoxia, SH or IH with or without various inhibitors (see above). Then cells were seeded at a concentration of 5×10^4 cells/well in 100 μL culture medium (tissue culture grade, 96 wells, flat bottom) and were incubated with the WST-1 reagents (10 μL/well) for 1 h. The formazan dye formed was determined with ELISA reader at 450/650 nM. The measured absorbance directly correlates to the number of viable cells.

2.10. SDS-PAGE and Western Blot Analysis. Cells were washed twice and extracts were prepared in lysis buffer containing 50 mM Tris-HCl (pH 7.4), 150 mM NaCl, and 1% NP-40 supplemented with a mixture of protease inhibitors (Roche Applied Science). Protein concentration was determined using the Bradford reagent (Bio-Rad), and 30 μg of protein was loaded onto SDS-PAGE under reducing conditions. After electrophoresis, proteins were transferred to polyvinylidene difluoride (PVDF) membrane (Bio-Rad) and probed with rabbit polyclonal antibody to LC3B (Sigma, Saint Louis, USA), followed by horseradish peroxidase-conjugated secondary antibody (Jackson ImmunoResearch Laboratories, Inc., West Grove, PA) and an enhanced chemiluminescent substrate (Beit HaEmek, Israel). Densitometric analysis was performed using TotalLab TL100 v.2006c software (Nonlinear Dynamics Ltd., Newcastle Upon Tyne, UK). Data were normalized over β-actin and the ratio of LC3BII/LC3BI was also calculated.

2.11. Statistical Analysis. Data are expressed as mean ± SD for each experimental group. A two-tailed Student's t-test with Bonferroni correction was used for multiple comparisons. Therefore, only values of $p < 0.008$ were considered significant. The NCSS 2004 statistical package (Kaysville, Utah) was used.

3. Results and Discussion

3.1. Development of Gϕ in Normoxia. Previously we have shown that, under normoxic conditions, a new neutrophil-derived subpopulation of cells characterized by neutrophilic markers CD15/CD11b/CD63/CD66b, as well as a unique morphology and functions, spontaneously develop into Gϕ under prolonged culture conditions [25]. Accordingly, in this study, Gϕ which developed in normoxic conditions had the same characteristics of Gϕ as previously shown ($CD66b^+$, $LC3B^+$, *gp91-phox* expression, large phagolysosomes, and phagocytosis). These Gϕ avidly phagocytosed neutrophil remnants, including granules and microparticles, suggesting that this active phagocytosis of neutrophil remnants may induce activation of some neutrophil subsets or precursors resulting in their transformation into Gϕ [25]. Thus, we treated PMN with cytochalasin B, which inhibits phagocytosis by inhibiting the polymerization of actin and prevents phagosome closure. As illustrated in Figure 1(a), cytochalasin B abolished the formation of Gϕ, indicating the importance of autophagocytosis to their development.

In addition, for comparison, we also followed PMN cultures supplemented with GM-CSF/IL-4. These cells were shown to develop into various cell types after 7–14 days in culture as previously described [9, 29]. Unlike Gϕ, the cells which developed in GM-CSF/IL-4 supplemented medium were mostly smaller in size, showed widespread cytoplasmic projections (Figure 1(b)), and were negative or had a low CD66b expression (data not shown). Morphologically, they resembled DC-like cells as reported by Oehler et al. [29] or the murine neutrophil-DC "hybrid" population demonstrated by Matsushima et al. [9]. Figure 1(c) illustrates the size differences between Gϕ and the cells which developed in GM-CSF/IL-4 supplemented medium. We divided freshly isolated PMN into two, and half of PMN were labeled with PKH-26 (red) dye and cultured in cytokine-free medium for 7 days, while the other half of PMN were labeled with PKH-67 (green) dye and cultured in GM-CSF/IL-4 supplemented medium for 7 days. Then, both cell types were mixed in a 1 : 1 ratio and cocultured for 2 h and cytospins were prepared. Notably, Gϕ formation is dependent on the local cytokine milieu, and culturing neutrophils with GM-CSF/IL-4 did not induce Gϕ formation but rather a different long-lived subpopulation. Since cells obtained in GM-CSF/IL-4 supplemented cultures did not resemble Gϕ, we did not follow their phenotypic and functional characteristics.

3.2. Development of Gϕ under Hypoxic Conditions. Hypoxic environments are common in inflammatory and other pathological conditions. Neutrophils adapt to such hypoxic-pathological environments for the resolution of inflammation by relying on their unique molecular features such as preferential glycolysis as an ATP source over the mitochondria and a potent NADPH oxidase-dependent machinery producing massive amounts of ROS [30]. Thus, freshly isolated purified PMN from healthy subjects were exposed to various acute and chronic hypoxic conditions and compared to normoxia, as indicated in Materials and Methods. A typical profile of 10 IH cycles is presented in Figure 2(a). In the chronic IH protocol PMN were exposed to 29 cycles (12 h) of IH/day for five consecutive days. PMN were also maintained in SH (12 h/day for 5 days) and normoxia for the same period of time. As shown in Figure 2(b), treatment with chronic IH completely abolished Gϕ formation, but their development was evident in SH and in normoxic cultures. Thus, in the

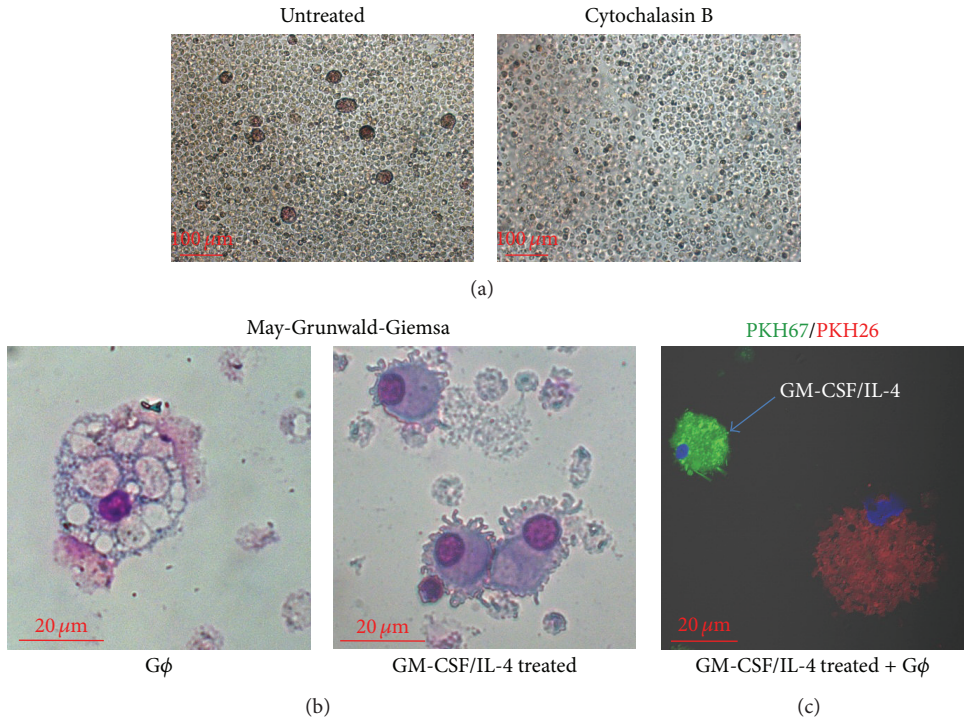

Figure 1: Effects of cytochalasin B and GM-CSF/IL-4 on giant phagocyte (Gϕ) formation. (a) Freshly isolated PMN were incubated at time 0 without or with 10 μM cytochalasin B and followed for 7 days in culture. Bright-field microscopy of 7-day living cultures. (b) Representative photomicrographs of May-Grünwald-Giemsa-stained cytospin preparations of PMN cultured without (Gϕ) or with GM-CSF/IL-4 for 7 days. Samples were analyzed with a bright-field microscopy. Magnification, ×40. Cells developed in cultures with medium supplemented with GM-CSF/IL-4 show widespread cytoplasmic projections. Representative data out of 3 independent experiments. (c) PKH-26 (red) dye labeled PMN were cultured in cytokine-free medium for 7 days and PKH-67 (green) dye labeled PMN were cultured in medium supplemented with GM-CSF/IL-4 for 7 days. Then the developed cells were mixed in a ratio of 1 : 1 and cocultured for 2 h. Cytospins were fixed and analyzed by confocal microscopy.

following experiments we focused on acute IH treatments for Gϕ development.

In the acute IH protocol, purified PMN were exposed to 10 cycles (250 min), 29 cycles (approximately 12 h), or 56 cycles (approximately 24 h) of IH, each on the first day in culture. In parallel cells were also exposed to corresponding times of SH (250 min, 12 h, and 24 h). Subsequently, PMN were cultured during the following 6 days at normoxic conditions. Control cells were maintained in normoxia for the entire durations.

Exposing PMN to 10 cycles of IH (250 min) had no effect on Gϕ development (Figure 2(c)). However, exposing PMN to 29 cycles of IH slightly decreased the quantity and size of the developed Gϕ. By exposure to 56 cycles of IH, Gϕ size was further decreased by about 30% ($p < 0.005$ (Table 1)) and the yield was only 20–25% of that obtained in controls. In SH, cell yield and size were unaffected (Table 1), although some variation in Gϕ cell size was noted after 24 h of SH. Confocal microscopy revealed that most of the SH-treated Gϕ had a normoxic appearance but some were smaller or slightly bigger than the control cells (Figures 2(b) and 2(c)). Moreover, two of the subjects were studied twice one month apart with similar results in both experiments. Jointly, these findings raise the possibility that, at sites of "inflammatory hypoxia," neutrophils may adapt to SH and transform into Gϕ able of removing dead cells and/or cell debris, possibly when the macrophage/DCs system is insufficient. The autophagocytosis of apoptotic PMN remnants by the developing Gϕ, which we have previously demonstrated, is in accord with this possibility [25]. However, in IH which is a signature feature of I/R injury in a great number of pathologies and induces activation of various leukocytes [13, 15, 16], exposure of PMN to prolonged acute IH in the first day in culture might have switched the cells' program towards inhibiting Gϕ formation.

Since acute exposure to 56 IH cycles (24 h IH) had the strongest effect on Gϕ formation, it was chosen to further investigate Gϕ phenotype and functions. As shown in Figure 3(a), Gϕ formed at all oxygen treatments were CD66b positive. The developed Gϕ were also neutrophil elastase (NE) positive, indicating that Gϕ express this important neutrophil specific protein after differentiation. However, the expression of NE was significantly lower in IH-treated Gϕ compared to Gϕ formed in normoxia or SH. Although in SH-treated Gϕ NE levels were also attenuated, they did not significantly differ from controls (Table 1, Figure 3(b)). By staining Gϕ with LysoTracker (Figure 3(d)), a stain commonly used as a lysosomal marker exhibiting a proportional fluorescence to the volume of lysosome-related organelles

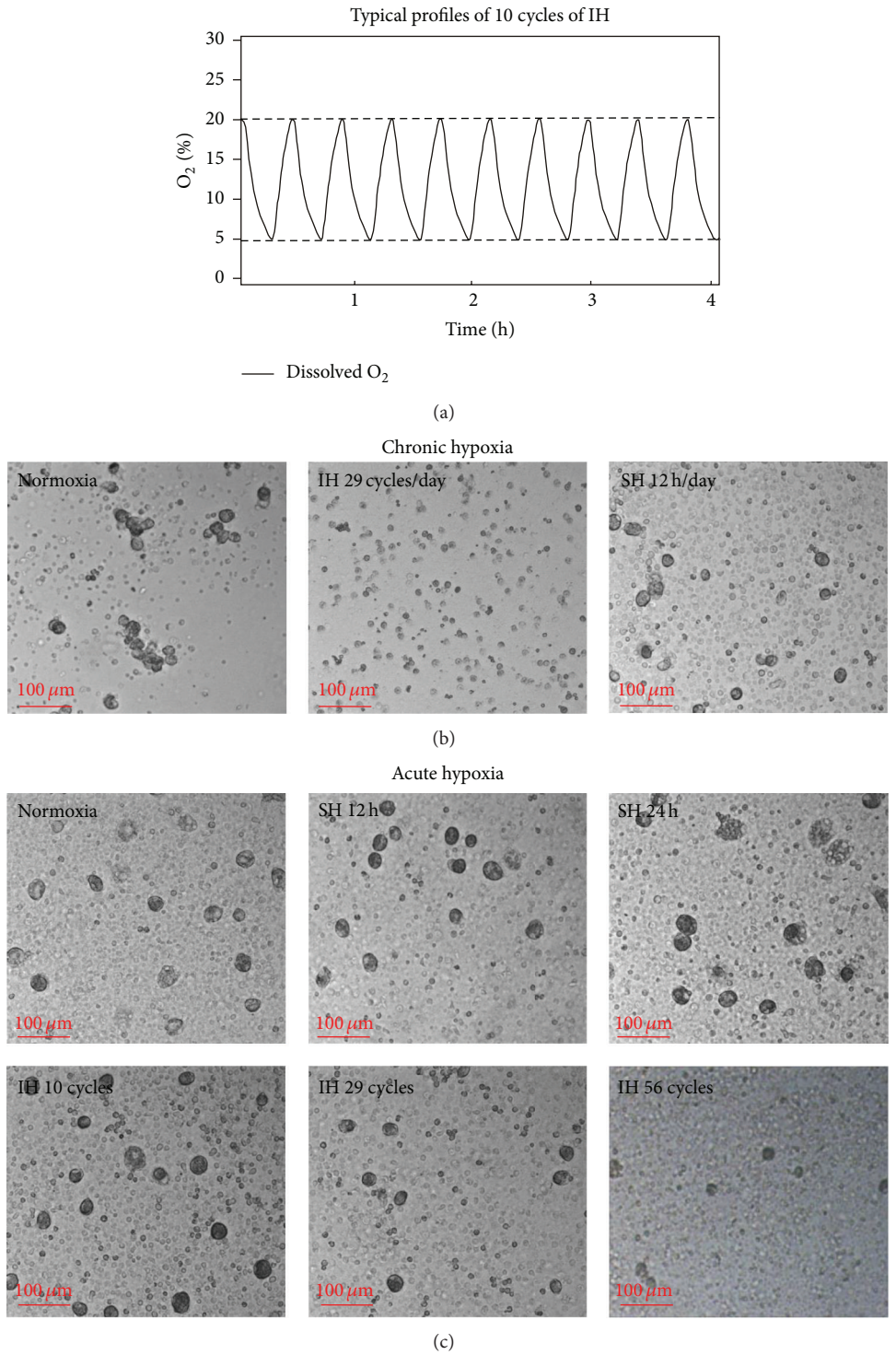

Figure 2: Effects of chronic and acute hypoxia on the development of giant phagocytes (Gϕ). (a) A typical profile of 10 intermittent hypoxia (IH) cycles. During IH actual % O_2 in the medium (solid line) decreased to 5% oxygen concentration during the hypoxia. In the reoxygenation period O_2 levels reached 20% oxygen. (b) For chronic hypoxia treatments, PMN were exposed to 29 cycles (approximately 12 h) of IH/day for 5 days or to a comparable time of sustained hypoxia (SH)/day. Controls were maintained at normoxia for the entire period. (c) For acute hypoxia treatments, PMN were exposed to 10 IH cycles (250 min), 29 IH cycles (approximately 12 h), or 56 IH cycles (approximately 24 h), each in the first day in culture. SH was employed for comparable times at 5% actual oxygen in the medium for the entire period (12 h and 24 h) and control cells were maintained at normoxia. Thereafter, the hypoxia treated cells were transferred to normoxia for additional six days. Light microscopy of living culture. Representative data out of 3 independent experiments. In (b) and (c) is bright-field microscopy of living cells.

Table 1: Effects of hypoxia on giant phagocytes (Gϕ) area and markers.

Measures	N	IH	SH
Area of cells (μm^2) ($n = 9$)	1486 ± 129	1051 ± 101†,††	1527 ± 158
Neutrophil elastase			
relative % ($n = 3$)*	100 ± 36.4	16.7 ± 3.8†,††	58.1 ± 23.6
FI$^{\#}$	35,888 ± 13,326	4,847 ± 1,003	19,383 ± 7,304
LysoTracker			
relative % ($n = 3$)*	100 ± 47.1	31.7 ± 9.1†,††	116.7 ± 51.7
FI$^{\#}$	17,501 ± 10,900	3,023 ± 1,748	21,633 ± 12,869
MitoTracker			
relative % ($n = 3$)*	100 ± 40	59.7 ± 25.6†,††	98.2 ± 43.4
FI$^{\#}$	11,582 ± 4,183	6,284 ± 2,759	11,459 ± 6,063
LC3B			
relative % ($n = 5$)*	100 ± 33.8	59.2 ± 20.8†,††	81.8 ± 27.7
FI$^{\#}$	34,246 ± 10,319	15,912 ± 6,962	27,078 ± 9,928
gp91-*phox*			
relative % ($n = 5$)*	100 ± 46.2	28.4 ± 15.4†,††	65.1 ± 30.9
FI$^{\#}$	19,886 ± 8,975	5,506 ± 2,459	13,072 ± 6,844
p22-*phox*			
relative % ($n = 3$)*	100 ± 41.5	45.0 ± 18.4†,††	165.3 ± 54.9†††
FI$^{\#}$	18,384 ± 9,569	5,772 ± 2,962	34,938 ± 11,756

Freshly isolated PMN were exposed for 24 h to intermittent hypoxia (IH), sustained hypoxia (SH), or normoxia (N). Then, cells were cultured at normoxia for additional six days. Area of cells and fluorescence intensity (FI), defined as Raw integrated density (sum of pixel values)/Area of cells, was integrated with Image J 1.49k Software as indicated in Materials and Methods.

*FI at normoxia was considered as 100% and the effects of IH and SH were calculated as relative % of normoxia for each of the indicated number of experiments.

$^{\#}$FI representative data of one independent experiment. In each experiment at least 10 cells were counted at each condition.

†Significance IH versus N, $p < 0.005$.

††Significance IH versus SH, $p < 0.005$.

†††Significance SH versus N, $p < 0.01$.

in a cell [31], a different lysosomal morphology was noted between the various acute oxygen treatments. Unlike the large phagolysosomes formed in normoxia- or SH-treated Gϕ, the phagolysosomes of IH-treated Gϕ were small, and only small spots of lysosome-like structures were stained by LysoTracker. Also the intensity of LysoTracker staining was significantly lower by nearly 70% in these IH-treated Gϕ (Table 1), indicating lysosomal dysfunction.

All in all, Gϕ development under SH treatments basically resembled the development of normoxia-treated Gϕ, mainly with regard to size, CD66b, and LysoTracker expression. Yet other measures as NE varied. However, under IH, Gϕ development was significantly attenuated in a severity-dependent manner.

3.3. Effects of Hypoxia on Autophagy. Autophagy represents an adaptive response to various stresses such as starvation, hypoxia, and excessive ROS by regulating cell death/survival, phagocytosis of dead cells, and contributing to neutrophil differentiation [17]. We have previously shown that, under normoxia, autophagy is a constitutive trait of Gϕ by demonstrating the presence of LC3B-II as vesicular puncta associated with autophagosomes and that treatment with specific autophagy inhibitors abolished Gϕ formation [25]. Herein we further confirmed the expression LC3B-II in Gϕ at the protein level as illustrated in Figure 4(a). Densitometric analysis of LC3BII normalized over β-actin and normalizing by LC3BII/LC3BI ratio revealed a high LC3BII expression in Gϕ compared to fresh PMN, clearly indicating active autophagy in Gϕ. Examples of Gϕ stained for LC3B at the various oxygen treatments are depicted in Figure 4(b). Unlike the case in normoxia, LC3B expression was significantly lowered by about 40% in 24 h IH-treated Gϕ (Table 1). Additionally, also in SH-treated Gϕ LC3B levels were attenuated; however, they did not significantly differ from controls ($p = 0.1$) (Table 1). These findings clearly suggest that autophagy might be decreased in Gϕ to various degrees depending on the type of the hypoxia inflicted.

Mitochondrial autophagy (mitophagy) mediates the selective elimination of dysfunctional or unwanted mitochondria [32]. Therefore, the effects of 24 h IH on mitophagy were investigated by double labeling for the autophagosomal compartment LC3B (green) and the mitochondria with MitoTracker (red). Two types of Gϕ were noted (Figure 4(c)). In normoxia, Gϕ expressing LC3B positive structures containing mitochondria (mitophagy) were the predominant Gϕ type (57.4 ± 7.2% expressed mitophagy, $n = 4$). These appeared as yellow spots with significant colocalization

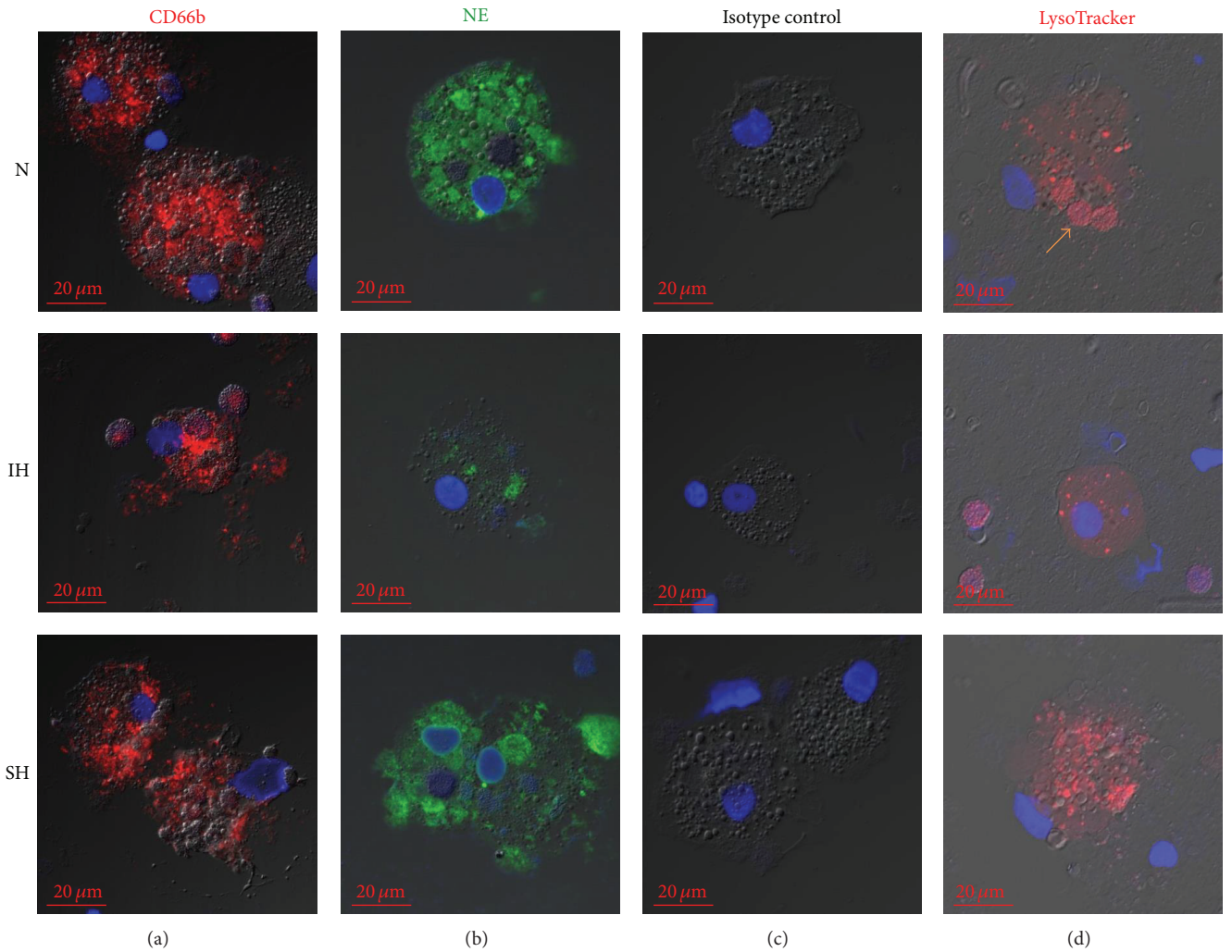

Figure 3: Effects of acute hypoxia on the development of giant phagocytes (Gϕ). Freshly isolated PMN were exposed for 24 h to intermittent hypoxia (IH, 56 cycles), sustained hypoxia (SH), or normoxia (N) and then cultured at normoxia for additional six days. Cytospins were prepared and analyzed by confocal microscopy (see Materials and Methods). Nuclei were stained with DAPI (blue). (a) Fixed cytospins were stained with anti-CD66b Abs and (b) neutrophil elastase (NE). (c) Isotype controls: fixed cytospins were stained with mouse IgG2 followed by 1/400 CF 647 goat anti-mouse IgG (red) staining. (d) Viable cells were stained with LysoTracker before fixation (see Materials and Methods). Arrow indicates large phagolysosomes. Representative data out of 3 independent experiments.

of LC3B and MitoTracker (MOC > 0.6). In SH, 34.8 ± 2.8% expressed mitophagy, but the morphology was mixed (Figure 4(c), inserts in normoxia and SH). However, in the 24 h IH-treated cells, the predominant type had mitochondria without LC3B (only 3–6% of Gϕ expressed mitophagy). Thus, in IH, mitochondria and LC3B were mostly not colocalized (Figure 4(c) red dots, arrow). Also, the intensity of MitoTracker expression in 24 h IH-treated Gϕ was 59.7 ± 25.6% of that expressed in normoxic-Gϕ, indicating the loss of membrane potential (Table 1). These findings indicate that, in the IH-treated Gϕ, mitochondria are dysfunctional and display an abnormal mitophagy.

3.4. Effects of Hypoxia on the Cellular Localization of gp91-phox and p22-phox and Its Involvement in Gϕ Development. NADPH oxidase-derived ROS are a key signal for autophagy through LC3 recruitment to phagosomes [33]. In resting inflammatory cells NADPH oxidase is predominantly inactive and its components are separately distributed between the cytosol and the membranes. However, upon stimulation, its subunits (gp91-*phox*, p22-*phox*, p-47-*phox*, p67-*phox*, p40-*phox*, and Rac2) are assembled as the functional NADPH oxidase at the phagosomes and/or the plasma membrane [34–37]. We therefore determined the expression of two of its critical subunits, namely, gp91-*phox* and p22-*phox*. The intracellular localization of gp91-*phox* (green) and p22-*phox* (red) was determined by double immunofluorescence staining, as depicted in Figure 5. The gp91-*phox* subunit was highly expressed in normoxic-Gϕ and as expected was localized in the plasma and phagolysosome membranes as previously shown [25]. In 24 h SH-treated Gϕ the gp91-*phox* expression was on average lower than that of normoxia.

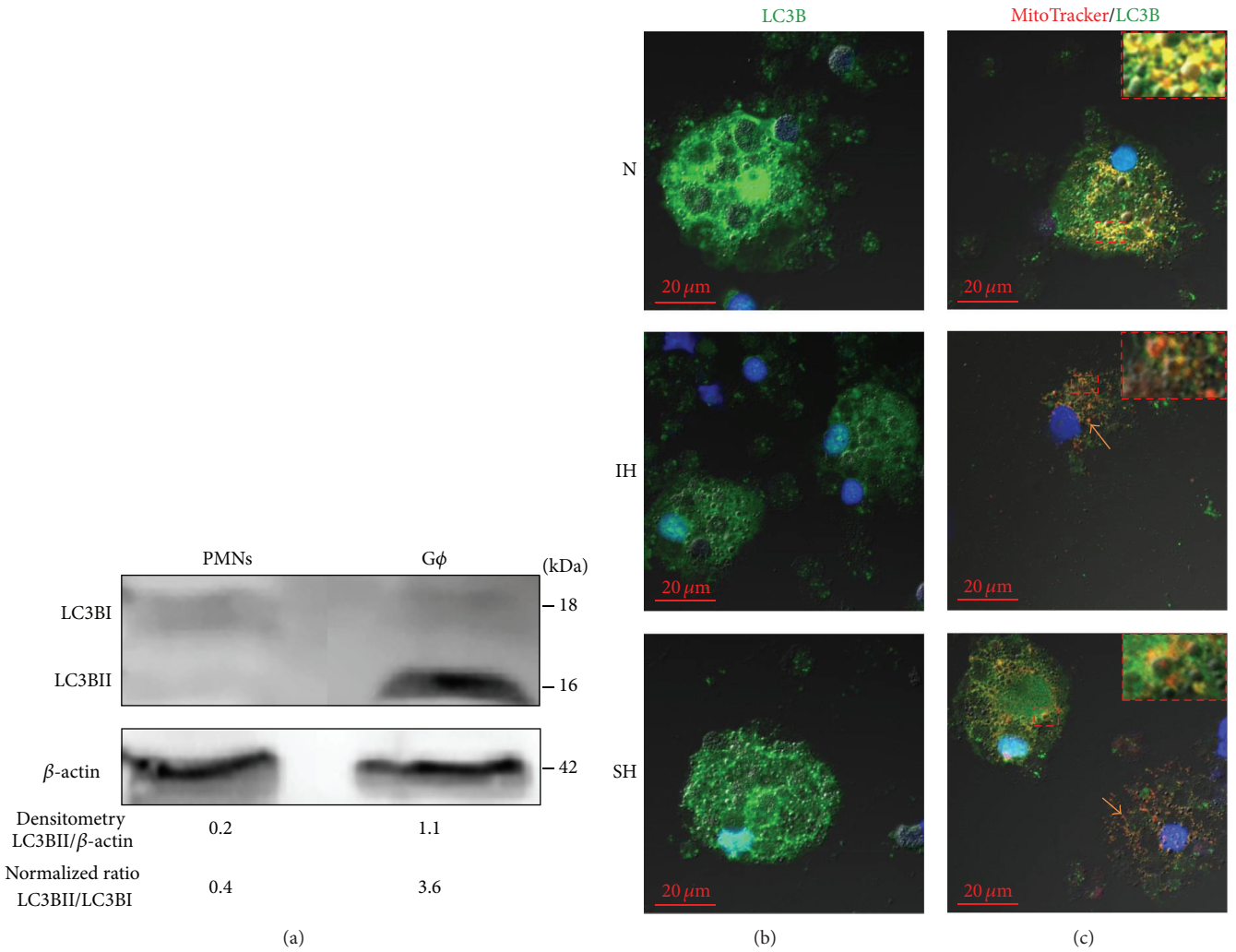

Figure 4: Effects of acute hypoxia on LC3B expression in giant phagocytes (Gϕ). Freshly isolated PMN were exposed for 24 h to intermittent hypoxia (IH, 56 cycles), sustained hypoxia (SH), or normoxia (N) and then cultured at normoxia for additional six days. (a) A representative western blot for LC3BI and LC3BII expression in freshly isolated PMN and normoxic-Gϕ. Densitometric analysis of LC3BII normalized over β-actin and normalizing by LC3BII/LC3BI ratio are presented. (b) Fixed cytospins were stained with LC3B (see Materials and Methods). Nuclei were stained with DAPI (blue). (c) Viable cells were labeled with MitoTracker Orange CMTMRos following fixation and LC3B staining. Mitophagy (LC3B positive structures containing mitochondria) appears as yellow spots (inserts in N and SH) with significant colocalization (MOC > 0.6) of LC3B/MitoTracker. Mitochondria without LC3B (red dots, arrows) were mainly noted in IH-Gϕ but also in SH-Gϕ. Representative data out of 4 independent experiments.

However, in 24 h IH-treated Gϕ, the expression of gp91-*phox* was significantly lowered to 28.4 ± 15.4 of normoxic-Gϕ ($n = 5$). Typical examples of gp91-*phox* fluorescence intensity of expression at different oxygen conditions are depicted in Table 1.

The p22-*phox* subunit was also mainly localized in the plasma membranes and phagolysosomes in normoxic and in 24 h SH-treated Gϕ. However, while, in 24 h IH-treated Gϕ, the intensity of the p22-*phox* subunit expression was lowered to 45% of normoxic-Gϕ, in 24 h SH-treated Gϕ its intensity of expression was significantly increased to 165% compared to normoxic-Gϕ ($p < 0.01$). Typical examples of p22-*phox* fluorescence intensity of expression at different oxygen conditions are depicted in Table 1. Colocalization of gp91-*phox* with p22-*phox* was evident in the cell membranes of normoxic- and 24 h SH-treated Gϕ (Figure 5). However, in 24 h IH-treated Gϕ these subunits were rarely colocalized but rather were located separately. The inability of NADPH oxidase to undergo assembly in response to IH may indicate that the enzyme is not activated in IH-treated Gϕ and thus its signaling properties might be altered. This is clearly evidenced by the lower NBT dye reduced into formazan in IH-treated Gϕ that were stimulated by PMA to produce ROS, compared to normoxia- and SH-treated Gϕ (Figure 6(a)). Moreover, inhibiting NADPH oxidase with DPI, prior to PMA stimulation, confirms the data regarding NADPH oxidase distribution and colocalization in the various oxygen treatments (in Figure 8(b)) but also indicates that NADPH

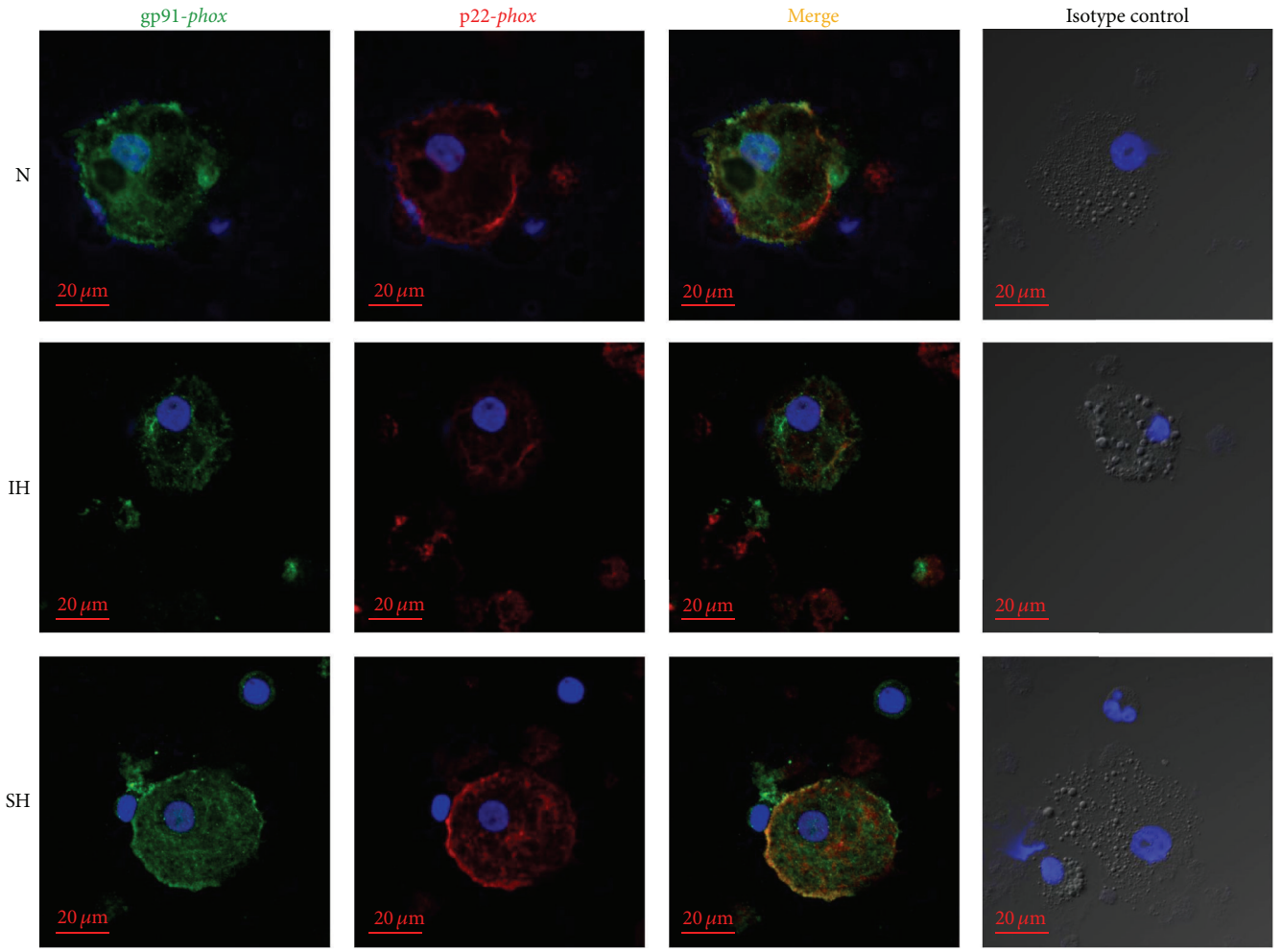

Figure 5: Effects of hypoxia on gp91-*phox* and p22-*phox* expression in giant phagocytes (Gϕ). Freshly isolated PMN were exposed for 24 h to intermittent hypoxia (IH, 56 cycles), sustained hypoxia (SH), or normoxia (N) and then cultured at normoxia for additional six days. For double immunofluorescence staining fixed cytospins were stained with rabbit anti-gp91-*phox* and mouse anti-p22-*phox* primary Abs (1/100) or the corresponding isotype controls (rabbit IgG and mouse IgG2) followed by 1/400 CF 488A goat anti-rabbit IgG (green) and CF 647 goat anti-mouse IgG (red) staining. Nuclei were stained with DAPI (blue). Representative data out of 3 independent experiments.

oxidase is a ROS contributor in normoxia and SH and less so in IH, thus, likely maintaining its signaling properties in normoxia and SH, but not in IH.

To explore the potential involvement of NADPH oxidase in Gϕ development, 10 μM DPI was added to fresh PMN cultures 10 min prior to the exposure to the various 24 h oxygen treatments. After 7 d in culture the development of Gϕ was completely abolished at all oxygen conditions (Figure 6(b)), but it did not affect cell viability after 24 h in culture as determined with WST-1 test (Figure 6(c)). Although DPI is an inhibitor of flavin containing enzymes and mitochondria, it was shown to be less potent for mitochondrial oxidative phosphorylation and other flavin enzymes than for NADPH oxidase. Moreover, mitochondria are scarce in neutrophils. Therefore the effects of DPI are mostly attributed to inhibition of NADPH oxidase [38].

Jointly, the lower expression and assembly of NADPH oxidase as well as its lower production of ROS in IH-treated Gϕ and its inhibition by DPI at all oxygen conditions which prevented Gϕ formation may suggest that NADPH oxidase-dependent ROS production contributes to Gϕ formation, likely through signaling pathways that regulate autophagy. Possibly, decreased NADPH oxidase expression in IH-treated cells might prevent LC3B recruitment or alter NADPH-dependent ROS signaling pathways such as PI3K [39] and therefore mitigate the autophagy-depend Gϕ development.

3.5. Effects of PI3K Inhibitor on Gϕ Development. The PI3K specific inhibitor LY-294002 was added at 20 μM to PMN cultures 10 min prior to the exposure to the various 24 h oxygen treatments (this concentration does not inhibit the TLR signaling cascade). Equal volumes of DMSO were added as a negative control. Inhibiting the PI3K kinase pathway with LY-294002 abolished Gϕ formation at all oxygen conditions studied (data not shown). Also, inhibition of class III PI3K by 3-methyladenine (3-MA), a commonly used autophagy inhibitor, was previously shown to inhibit Gϕ formation [25].

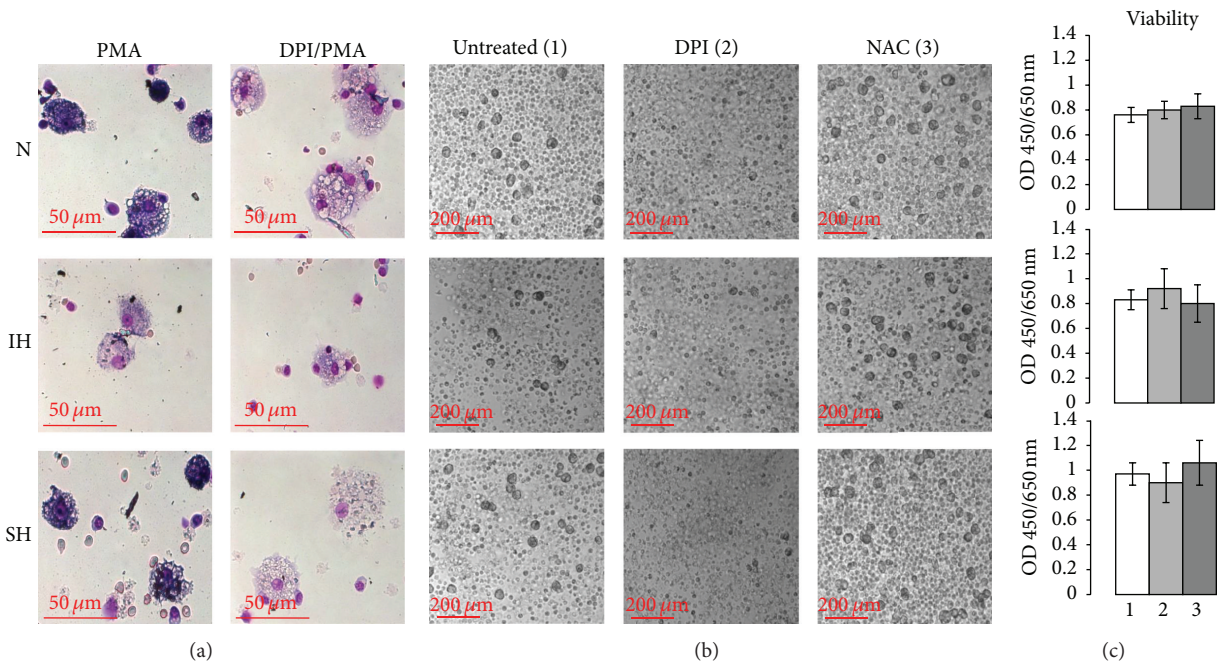

Figure 6: PMA-dependent ROS production, and the effects of diphenyl iodide (DPI) (10 μM) and N-acetylcysteine (NAC) (20 μM) on viability and development of giant phagocytes (Gϕ). PMN were cultured during 24 h in normoxia (N), intermittent hypoxia (IH) (56 cycles), or sustained hypoxia (SH) without or with inhibitors and then cultured at normoxia for additional six days. (a) Intracellular ROS production was detected in PMA-activated Gϕ by NBT test (see Materials and Methods). DPI was added to Gϕ 2 h prior to PMA stimulation. Bright-field microscopy of Giemsa-stained cultures in the various oxygen treatments. (b) DPI or NAC were added to PMN cultures 10 min prior to exposing to N, IH, and SH. Then PMN were cultured during the next 6 days at normoxia. Equal volumes of DMSO were added as a negative control. Bright-field microscopy of living cultures in the various treatments. (c) PMN viability was detected immediately after 24 h of the hypoxic treatments in untreated (1), DPI treated (2), or NAC-treated cells (3) using WST-1 assay. The measured absorbance (OD) directly correlates to the number of viable cells in each treatment.

Jointly, these findings support the involvement of PI3K pathway in the formation of Gϕ.

The PI3K/Akt signaling pathway is essential for several neutrophil functions, including migration, degranulation, and superoxide production by controlling NADPH oxidase activation [40–42]. Akt phosphorylates p47*phox*, facilitating its membrane translocation and activation [41]. Akt is also a well-established inhibitor of apoptosis and inhibiting Akt promotes apoptosis [43]. Thus, it is likely that PI3K/Akt may act as an indispensable pathway for Gϕ formation via controlling NADPH oxidase activation.

3.6. Effects of NAC on Gϕ Development. To further probe the potential involvement of ROS in Gϕ development, the potent antioxidant and glutathione precursor—NAC—was used [44]. NAC (20 μM) was added to PMN cultures 10 min prior to the exposure to 24 h of normoxia, SH, or IH. Viability of the cells in the presence of NAC, measured after 24 h, was unaffected at all three oxygen conditions (Figure 6(c)). Treatment with NAC did not affect Gϕ development in normoxia or in SH. However, it had a robust impact on IH-treated PMN cultures exposed to 56 cycles. After 7 days in culture morphology and functions were altered; the Gϕ size and LC3B expression were significantly increased and resembled normoxia-treated cells (Figures 7(a)–7(c)). Treatment with NAC also increased CD66b expression and phagolysosome size (Figure 8(a)). Additionally, the expression of gp91-*phox* and p22-*phox* subunits and their redistribution in cell membranes, as well as around phagosomes in these 24 h IH-treated Gϕ, resembled those maintained in normoxia (Figure 8(b)). Thus, treatment with NAC abolished the effects of IH and partially restored the normoxic phenotype. Treatment with NAC twice weekly was also shown to promote hematopoietic differentiation of induced pluripotent stem cells (iPSCs) in long-term culture by mitigating oxidative stress [45]. Accordingly, in our study, treatment with NAC increased Gϕ size and punctuation of LC3B in the IH-treated Gϕ already after 2 days in culture (data not shown). It is thus suggested that the presence of NAC can restore the cellular ROS balance by replenishing the intracellular glutathione levels during IH and therefore facilitate the development of Gϕ with similar characteristics to those obtained in normoxia with regard to size, LC3B, and NADPH oxidase expression.

3.7. Effects of Hypoxia and NAC on the Phagocytic Activity of Gϕ. Gϕ were shown to internalize carboxylate-modified fluorescent yellow-green latex beads (1 μm) more avidly than freshly isolated neutrophils. Yet, the IH-treated Gϕ (12 h, 29 cycles) exhibited a lower phagocytic activity ($p = 0.015$) compared to normoxic-Gϕ (Figure 9(a)), which was further attenuated in 24 h IH-treated Gϕ to about 50% of the ability of normoxic-Gϕ ($p = 0.001$) (Figures 9(a) and 9(b)). Treatment

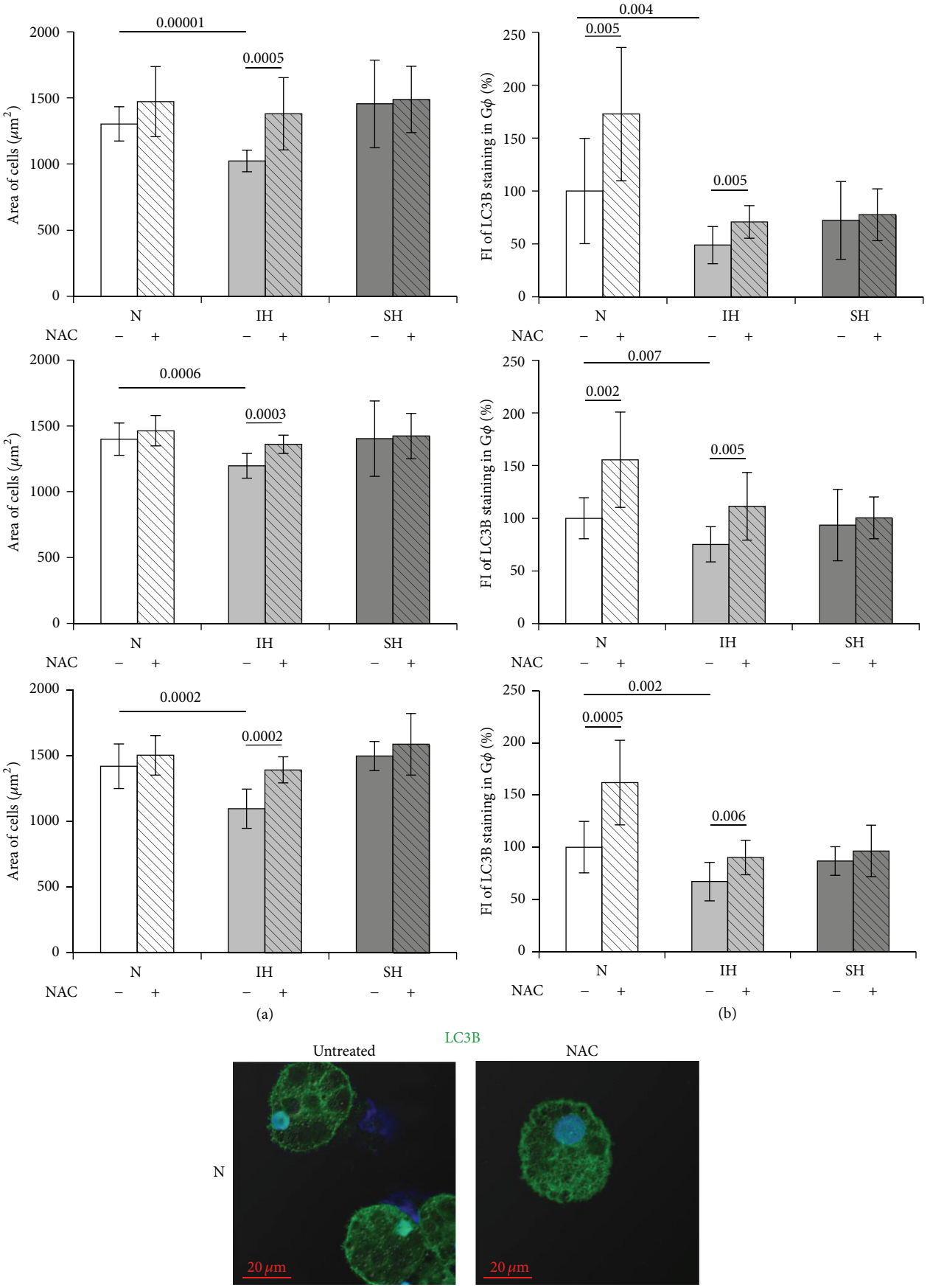

Figure 7: Continued.

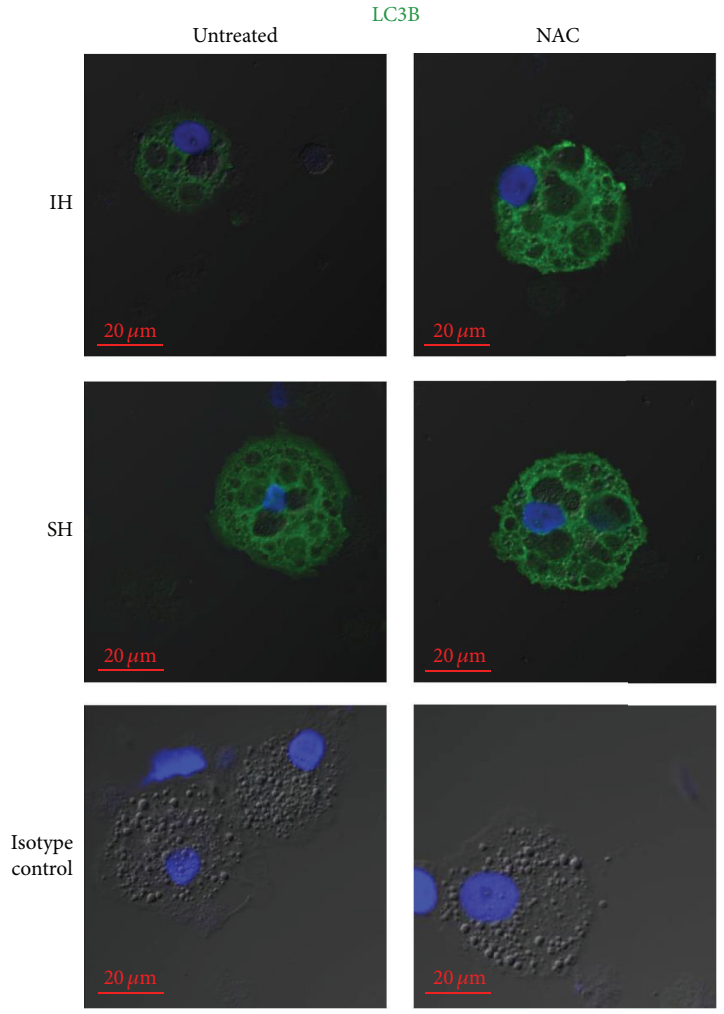

(c)

Figure 7: Effects of N-acetylcysteine (NAC) on giant phagocytes (Gϕ) size and LC3B expression. Freshly isolated PMN were exposed for 24 h to intermittent hypoxia (IH, 56 cycles), sustained hypoxia (SH), or normoxia (N) and then cultured at normoxia for additional six days. NAC (20 μM) was added to PMN cultures 10 min prior to exposing to N, IH, or SH. Equal volumes of DMSO were added as a negative control. Fixed cytospins were stained with rabbit anti-LC3B primary Abs (diluted 1/100) or corresponding isotype controls (rabbit IgG) followed by 1/400 CF 488A anti-rabbit IgG staining (green). Nuclei were stained with DAPI (blue). (a) Area of cells (μm^2) in three independent experiments. (b) Fluorescence intensity (FI) of LC3B expression, integrated with Image J Software (see Materials and Methods), in three independent experiments. (c) Representative photomicrographs of Gϕ which developed after exposure to N, IH, or SH without (untreated) or with NAC. Isotype controls: untreated or NAC-treated normoxic-Gϕ.

with NAC significantly increased this ability of normoxic-Gϕ, as well as that of the IH-treated Gϕ compared to the corresponding NAC-untreated Gϕ, whereas, in 24 h SH, NAC treatment had no effect on the phagocytosis compared to untreated Gϕ (Figures 9(a) and 9(b)). To exclude possible cytospinning-dependent false-positive latex internalization, we used as negative controls Gϕ that were kept on ice and cytospins were prepared immediately or 2 h after adding latex beads. Also, uptake of the beads was blocked by inhibiting actin (cytochalasin B, 10 μM). Additionally, the intracellular localization of latex beads was also validated in Gϕ by 3D *z*-stack images as illustrated in Figure 9(c).

Enhanced phagocytosis in NAC-treated neutrophils was previously shown in a number of studies. While treatment *in vitro* of human neutrophils with NAC enhanced their phagocytic ability [46], also oral administration of NAC *in vivo* to healthy individuals increased this ability [47]. Similarly, the phagocytosis of neutrophils was augmented in NAC-treated patients in the intensive care unit [48]. Thus, treatment with NAC restored the phagocytic activity of the developed Gϕ under IH similarly to increasing their size, the expression of LC3B, and that of NADPH oxidase subunits gp91-*phox* and p22-*phox*. This may indicate that phagocytosis is one of the mechanisms contributing to the formation of Gϕ,

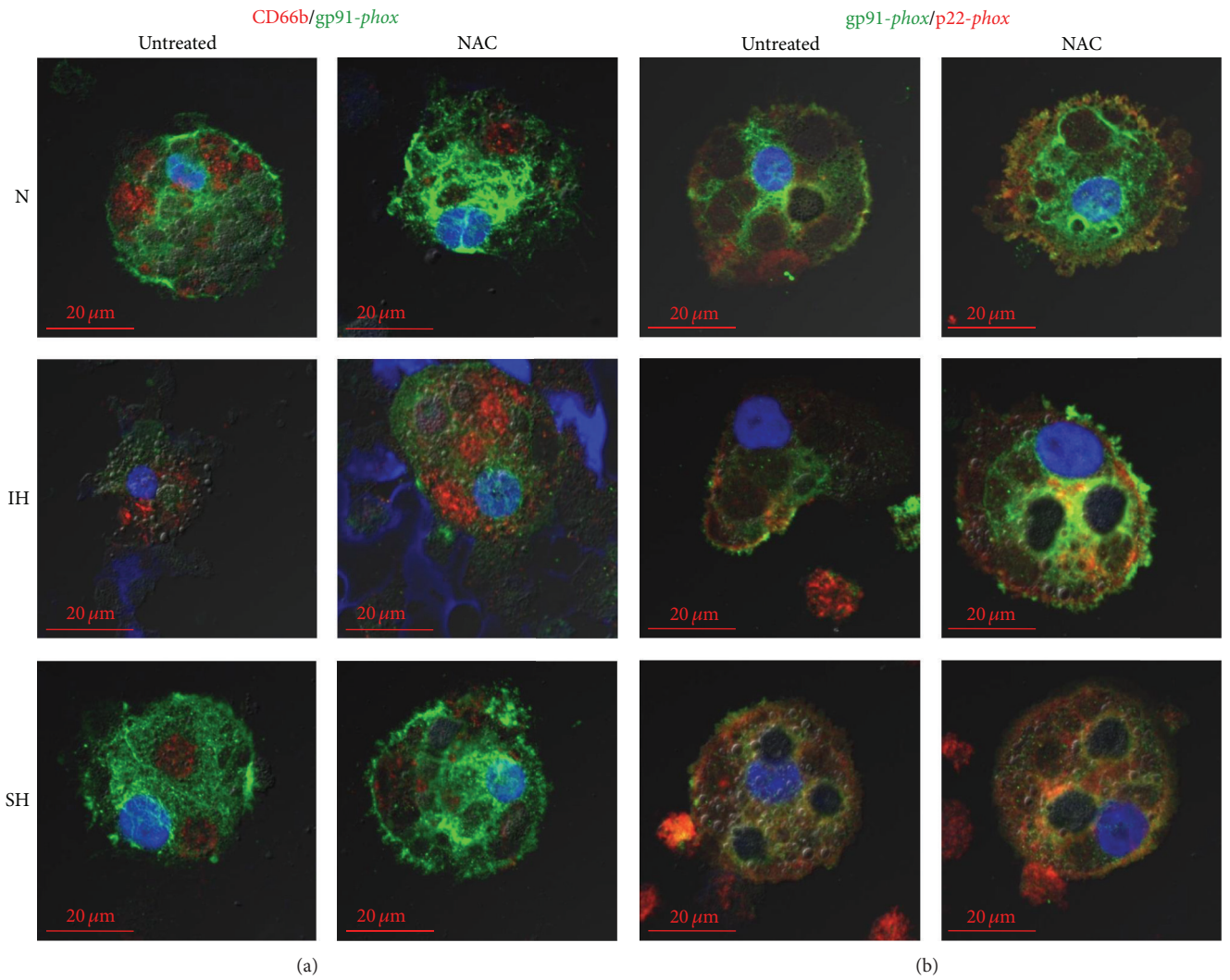

Figure 8: Expression of NADPH oxidase subunits in giant phagocytes (Gϕ) and the effects of NAC on their expression. Freshly isolated PMN were exposed for 24 h to intermittent hypoxia (IH, 56 cycles), sustained hypoxia (SH), or normoxia (N) and then cultured at normoxia for additional six days. NAC (20 μM) was added to PMN cultures 10 min prior to exposing to N, IH, or SH. Equal volumes of DMSO were added as a negative control. Cytospins were prepared and analyzed by confocal microscopy (see Materials and Methods). The developed Gϕ were stained by double immunofluorescence: (a) for CD66b (red) and gp91-*phox* (green) in untreated and NAC-treated Gϕ and (b) for gp91-*phox* (green) and p22-*phox* (red) in untreated and NAC-treated Gϕ. Nuclei were stained with DAPI. Representative photomicrographs out of 3 independent experiments.

as already indicated by restoring the formation of Gϕ under IH in the presence of NAC.

The importance of NAC in restoring, at least partially, Gϕ phenotype and functions in IH-treated cells may have clinical relevance to conditions associated with cyclic-intermittent hypoxia. NAC that is best known for treating glutathione deficiency [44] was also shown to exert protective effects in various systems including neuroprotection in ischemic stroke [49]. Treatment with NAC was also shown to affect the IH associated with OSA [16]. For instance, in animal models mimicking OSA treated with NAC, oxidative stress and liver inflammation were attenuated [50], pancreatic β cells were protected from apoptosis [51], pharyngeal muscle dilator performance was also improved [52], and diaphragm muscle dysfunction was prevented [53]. In addition, oral administration of NAC to patients with OSA improved sleep efficiency, shortened the duration of apneas, decreased lipid peroxidation, and increased total reduced glutathione [54]. Taken together, these findings demonstrate the protective effects exerted by the antioxidant NAC against IH-induced oxidative stress, inflammation, and overall improving OSA associated consequences.

4. Conclusions

Previously we have described for the first time a new subpopulation of giant phagocytes (Gϕ) derived from neutrophils maintained in prolonged culture conditions [25]. Exposing PMN to acute intermittent hypoxia (IH), common in inflammatory conditions, cancer, and sleep apnea, hampered Gϕ

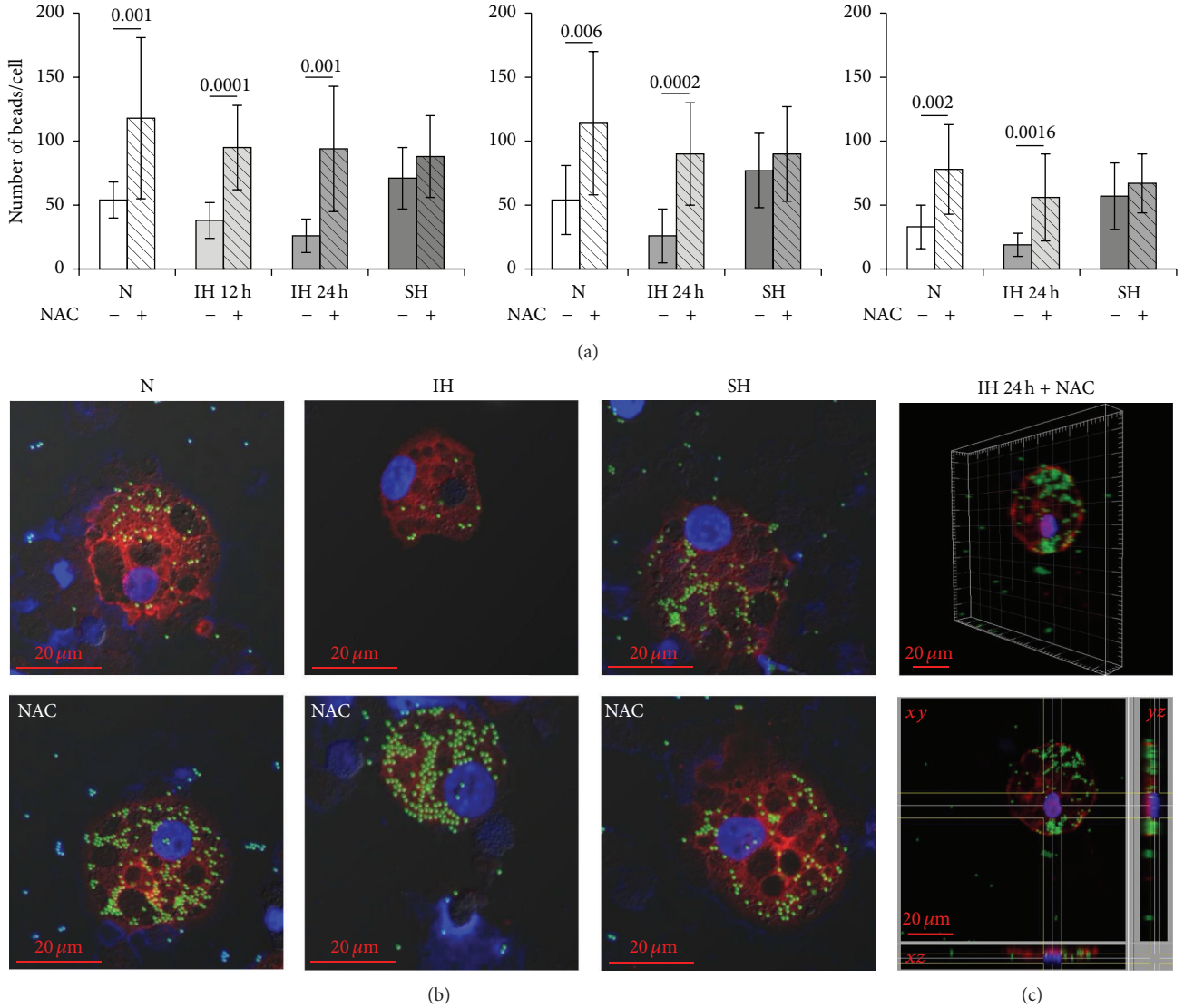

Figure 9: Phagocytic activity of giant phagocytes (Gϕ) and the effects of NAC on Gϕ phagocytosis. Freshly isolated PMN were exposed for 12 h (29 cycles) or 24 h (56 cycles) to intermittent hypoxia (IH), 24 h sustained hypoxia (SH), or normoxia (N) and then cultured at normoxia for additional six days. NAC (20 μM) was added to PMN cultures 10 min prior to exposing to N, IH, or SH. The developed Gϕ (7 d culture) were incubated for 2 h with carboxylate-modified fluorescent yellow-green latex beads. Cytospins were prepared, fixed, stained with LC3B (red), and analyzed by confocal microscopy (see Materials and Methods). Nuclei were stained with DAPI. (a) The average number of beads/cell in Gϕ developed after exposure to N, IH, or SH without or with NAC in three independent experiments. In each experiment at least 10 cells were counted in each condition. (b) Representative photomicrographs of phagocytosis by Gϕ developed after exposure to N, IH, or SH without (upper panel) or with (lower panel) NAC. (c) A representative analysis of intracellular latex beads localization using 3D reconstructing software IMARIS z-stack for 24 h IH-treated Gϕ in the presence of NAC. Upper panel in (c) represents an image of the Gϕ. Lower panel in (c) represents cross sections (xy, xz, and yz) for localization of the latex beads.

development in a dose-dependent manner whereas sustained hypoxia had no (or minimal) effect on their development. Intermittent hypoxia reduced Gϕ size, autophagy, neutrophil elastase and NADPH oxidase expression, and their phagocytic activity. Inhibiting NADPH oxidase or the PI3K/Akt signaling pathway completely abolished Gϕ development at all oxygen conditions investigated, indicating their importance for this process. Conversely, the antioxidant N-acetylcysteine (NAC) abrogated the IH-associated effects and partially restored a control like phenotype and functions.

The physiological/pathophysiological significance of Gϕ development *in vivo* is yet unknown. However, our earlier findings indicate their potential involvement in atherogenic processes by demonstrating their ability to internalize oxidized LDL (oxLDL) and to generate ROS in response to oxLDL uptake, unlike fresh neutrophils [25]. In accord with this line we have recently identified the presence of Gϕ in carotid plaques from patients undergoing elective endarterectomy. Thus, a better understanding of Gϕ formation may provide insights into basic neutrophil biology in

inflammatory and atherogenic conditions or in the resolution of neutrophilic inflammation. Moreover, the a priori low yield of Gϕ may indicate that they have a unique function and may represent a subgroup of progenitor cells. However, their identification and roles *in vivo* warrant intensive investigation.

Conflict of Interests

The authors declare that there is no conflict of interests regarding the publication of this paper.

Authors' Contribution

Larissa Dyugovskaya and Slava Berger contributed equally to this work.

Acknowledgments

The authors thank Ms. Eva Leder for her invaluable technical support, Dr. Edith Suss-Toby for her invaluable help with the confocal microscopy, and Victoria Cohen-Kaplan for her technical support with western blotting. The support of the Lloyd E. Rigler-Lawrence E. Deutsch Foundation to this study (Lena Lavie and Peretz Lavie) is gratefully acknowledged. The support of the Ministry of Immigration Absorption and the Committee for Planning and Budgeting of the Council for Higher Education under the framework of the KAMEA Program (Larissa Dyugovskaya and Andrey Polyakov) is gratefully acknowledged.

References

[1] T. N. Mayadas, X. Cullere, and C. A. Lowell, "The multifaceted functions of neutrophils," *Annual Review of Pathology: Mechanisms of Disease*, vol. 9, pp. 181–218, 2014.

[2] P. Scapini and M. A. Cassatella, "Social networking of human neutrophils within the immune system," *Blood*, vol. 124, no. 5, pp. 710–719, 2014.

[3] B. Amulic, C. Cazalet, G. L. Hayes, K. D. Metzler, and A. Zychlinsky, "Neutrophil function: from mechanisms to disease," *Annual Review of Immunology*, vol. 30, pp. 459–489, 2012.

[4] A. Chakravarti, D. Rusu, N. Flamand, P. Borgeat, and P. E. Poubelle, "Reprogramming of a subpopulation of human blood neutrophils by prolonged exposure to cytokines," *Laboratory Investigation*, vol. 89, no. 10, pp. 1084–1099, 2009.

[5] H. Araki, N. Katayama, Y. Yamashita et al., "Reprogramming of human postmitotic neutrophils into macrophages by growth factors," *Blood*, vol. 103, no. 8, pp. 2973–2980, 2004.

[6] A. S. Cowburn, A. M. Condliffe, N. Farahi, C. Summers, and E. R. Chilvers, "Advances in neutrophil biology: clinical implications," *Chest*, vol. 134, no. 3, pp. 606–612, 2008.

[7] S. Geng, H. Matsushima, T. Okamoto, Y. Yao, R. Lu, and A. Takashima, "Reciprocal regulation of development of neutrophil-dendritic cell hybrids in mice by IL-4 and interferon-gamma," *PLoS ONE*, vol. 8, no. 11, Article ID e82929, 2013.

[8] S. Geng, H. Matsushima, T. Okamoto et al., "Emergence, origin, and function of neutrophil-dendritic cell hybrids in experimentally induced inflammatory lesions in mice," *Blood*, vol. 121, no. 10, pp. 1690–1700, 2013.

[9] H. Matsushima, S. Geng, R. Lu et al., "Neutrophil differentiation into a unique hybrid population exhibiting dual phenotype and functionality of neutrophils and dendritic cells," *Blood*, vol. 121, no. 10, pp. 1677–1689, 2013.

[10] V. Witko-Sarsat, M. Pederzoli-Ribeil, E. Hirsch, V. Witko-Sarsat, and M. A. Cassatella, "Regulating neutrophil apoptosis: new players enter the game," *Trends in Immunology*, vol. 32, no. 3, pp. 117–124, 2011.

[11] S. P. Colgan and C. T. Taylor, "Hypoxia: an alarm signal during intestinal inflammation," *Nature Reviews—Gastroenterology & Hepatology*, vol. 7, no. 5, pp. 281–287, 2010.

[12] E. L. Campbell, W. J. Bruyninckx, C. J. Kelly et al., "Transmigrating neutrophils shape the mucosal microenvironment through localized oxygen depletion to influence resolution of inflammation," *Immunity*, vol. 40, no. 1, pp. 66–77, 2014.

[13] L. Dyugovskaya, A. Polyakov, V. Cohen-Kaplan, P. Lavie, and L. Lavie, "Bax/Mcl-1 balance affects neutrophil survival in intermittent hypoxia and obstructive sleep apnea: effects of p38MAPK and ERK1/2 signaling," *Journal of Translational Medicine*, vol. 10, no. 1, article 211, 2012.

[14] S. R. Walmsley, C. Print, N. Farahi et al., "Hypoxia-induced neutrophil survival is mediated by HIF-1α-dependent NF-κB activity," *The Journal of Experimental Medicine*, vol. 201, no. 1, pp. 105–115, 2005.

[15] L. Dyugovskaya, A. Polyakov, P. Lavie, and L. Lavie, "Delayed neutrophil apoptosis in patients with sleep apnea," *American Journal of Respiratory and Critical Care Medicine*, vol. 177, no. 5, pp. 544–554, 2008.

[16] L. Lavie, "Oxidative stress in obstructive sleep apnea and intermittent hypoxia—revisited—the bad ugly and good: implications to the heart and brain," *Sleep Medicine Reviews*, vol. 20, pp. 27–45, 2015.

[17] C. C. Mihalache and H.-U. Simon, "Autophagy regulation in macrophages and neutrophils," *Experimental Cell Research*, vol. 318, no. 11, pp. 1187–1192, 2012.

[18] S. Rožman, S. Yousefi, K. Oberson, T. Kaufmann, C. Benarafa, and H. U. Simon, "The generation of neutrophils in the bone marrow is controlled by autophagy," *Cell Death & Differentiation*, vol. 22, no. 3, pp. 445–456, 2015.

[19] M. V. Jain, A. M. Paczulla, T. Klonisch et al., "Interconnections between apoptotic, autophagic and necrotic pathways: implications for cancer therapy development," *Journal of Cellular and Molecular Medicine*, vol. 17, no. 1, pp. 12–29, 2013.

[20] I. Mitroulis, I. Kourtzelis, K. Kambas et al., "Regulation of the autophagic machinery in human neutrophils," *European Journal of Immunology*, vol. 40, no. 5, pp. 1461–1472, 2010.

[21] C. C. Mihalache, S. Yousefi, S. Conus, P. M. Villiger, E. M. Schneider, and H.-U. Simon, "Inflammation-associated autophagy-related programmed necrotic death of human neutrophils characterized by organelle fusion events," *Journal of Immunology*, vol. 186, no. 11, pp. 6532–6542, 2011.

[22] S. Ma, Y. Wang, Y. Chen, and F. Cao, "The role of the autophagy in myocardial ischemia/reperfusion injury," *Biochimica et Biophysica Acta*, vol. 1852, no. 2, pp. 271–276, 2015.

[23] A. Hamacher-Brady, N. R. Brady, and R. A. Gottlieb, "Enhancing macroautophagy protects against ischemia/reperfusion injury in cardiac myocytes," *The Journal of Biological Chemistry*, vol. 281, no. 40, pp. 29776–29787, 2006.

[24] R. Scherz-Shouval and Z. Elazar, "Regulation of autophagy by ROS: physiology and pathology," *Trends in Biochemical Sciences*, vol. 36, no. 1, pp. 30–38, 2011.

[25] L. Dyugovskaya, S. Berger, A. Polyakov, and L. Lavie, "The development of giant phagocytes in long-term neutrophil cultures," *Journal of Leukocyte Biology*, vol. 96, no. 4, pp. 511–521, 2014.

[26] S. Berger, D. Aronson, P. Lavie, and L. Lavie, "Endothelial progenitor cells in acute myocardial infarction and sleep-disordered breathing," *American Journal of Respiratory and Critical Care Medicine*, vol. 187, no. 1, pp. 90–98, 2013.

[27] E. M. M. Manders, F. J. Verbeek, and J. A. Aten, "Measurement of co-localization of objects in dual-colour confocal images," *Journal of Microscopy*, vol. 169, no. 3, pp. 375–382, 1993.

[28] A. K. Gupta, S. Giaglis, P. Hasler, and S. Hahn, "Efficient neutrophil extracellular trap induction requires mobilization of both intracellular and extracellular calcium pools and is modulated by cyclosporine A," *PLoS ONE*, vol. 9, no. 5, Article ID e97088, 2014.

[29] L. Oehler, O. Majdic, W. F. Pickl et al., "Neutrophil granulocyte-committed cells can be driven to acquire dendritic cell characteristics," *Journal of Experimental Medicine*, vol. 187, no. 7, pp. 1019–1028, 1998.

[30] B. Geering and H.-U. Simon, "Peculiarities of cell death mechanisms in neutrophils," *Cell Death and Differentiation*, vol. 18, no. 9, pp. 1457–1469, 2011.

[31] J. L. van der Velden, I. Bertoncello, and J. L. McQualter, "LysoTracker is a marker of differentiated alveolar type II cells," *Respiratory Research*, vol. 14, no. 1, article 123, 2013.

[32] D. Feng, L. Liu, Y. Zhu, and Q. Chen, "Molecular signaling toward mitophagy and its physiological significance," *Experimental Cell Research*, vol. 319, no. 12, pp. 1697–1705, 2013.

[33] J. Huang, V. Canadien, G. Y. Lam et al., "Activation of antibacterial autophagy by NADPH oxidases," *Proceedings of the National Academy of Sciences of the United States of America*, vol. 106, no. 15, pp. 6226–6231, 2009.

[34] Y. Groemping and K. Rittinger, "Activation and assembly of the NADPH oxidase: a structural perspective," *The Biochemical Journal*, vol. 386, part 3, pp. 401–416, 2005.

[35] W. M. Nauseef, "Biological roles for the NOX family NADPH oxidases," *The Journal of Biological Chemistry*, vol. 283, no. 25, pp. 16961–16965, 2008.

[36] Y. Zhu, C. C. Marchal, A.-J. Casbon et al., "Deletion mutagenesis of p22phox subunit of flavocytochrome b558: identification of regions critical for gp91phox maturation and NADPH oxidase activity," *The Journal of Biological Chemistry*, vol. 281, no. 41, pp. 30336–30346, 2006.

[37] M. T. Quinn and K. A. Gauss, "Structure and regulation of the neutrophil respiratory burst oxidase: comparison with nonphagocyte oxidases," *Journal of Leukocyte Biology*, vol. 76, no. 4, pp. 760–781, 2004.

[38] A. C. Bulua, A. Simon, R. Maddipati et al., "Mitochondrial reactive oxygen species promote production of proinflammatory cytokines and are elevated in TNFR1-associated periodic syndrome (TRAPS)," *The Journal of Experimental Medicine*, vol. 208, no. 3, pp. 519–533, 2011.

[39] D. N. Douda, L. Yip, M. A. Khan, H. Grasemann, and N. Palaniyar, "Akt is essential to induce NADPH-dependent NETosis and to switch the neutrophil death to apoptosis," *Blood*, vol. 123, no. 4, pp. 597–600, 2014.

[40] M. O. Hannigan, C. K. Huang, and D. Q. Wu, "Roles of PI3K in neutrophil function," *Current Topics in Microbiology and Immunology*, vol. 282, pp. 165–175, 2004.

[41] J. Chen, H. Tang, N. Hay, J. Xu, and R. D. Ye, "Akt isoforms differentially regulate neutrophil functions," *Blood*, vol. 115, no. 21, pp. 4237–4246, 2010.

[42] P. T. Hawkins, L. R. Stephens, S. Suire, and M. Wilson, "PI3K signaling in neutrophils," *Current Topics in Microbiology and Immunology*, vol. 346, no. 1, pp. 183–202, 2010.

[43] M. J. Rane and J. B. Klein, "Regulation of neutrophil apoptosis by modulation of PKB/Akt activation," *Frontiers in Bioscience*, vol. 14, no. 7, pp. 2400–2412, 2009.

[44] K. R. Atkuri, J. J. Mantovani, L. A. Herzenberg, and L. A. Herzenberg, "N-acetylcysteine—a safe antidote for cysteine/glutathione deficiency," *Current Opinion in Pharmacology*, vol. 7, no. 4, pp. 355–359, 2007.

[45] I. Berniakovich, L. Laricchia-Robbio, and J. C. I. Belmonte, "N-acetylcysteine protects induced pluripotent stem cells from *in vitro* stress: impact on differentiation outcome," *International Journal of Developmental Biology*, vol. 56, no. 9, pp. 729–735, 2012.

[46] L. Ohman, C. Dahlgren, P. Follin, D. Lew, and O. Stendahl, "N-acetylcysteine enhances receptor-mediated phagocytosis by human neutrophils," *Agents and Actions*, vol. 36, no. 3-4, pp. 271–277, 1992.

[47] T. Urban, B. Åkerlund, C. Jarstrand, and B. Lindeke, "Neutrophil function and glutathione-peroxidase (GSH-px) activity in healthy individuals after treatment with N-acetyl-L-cysteine," *Biomedicine & Pharmacotherapy*, vol. 51, no. 9, pp. 388–390, 1997.

[48] A. R. Heller, G. Groth, S. C. Heller et al., "N-acetylcysteine reduces respiratory burst but augments neutrophil phagocytosis in intensive care unit patients," *Critical Care Medicine*, vol. 29, no. 2, pp. 272–276, 2001.

[49] Z. Zhang, J. Yan, S. Taheri, K. J. Liu, and H. Shi, "Hypoxia-inducible factor 1 contributes to N-acetylcysteine's protection in stroke," *Free Radical Biology & Medicine*, vol. 68, pp. 8–21, 2014.

[50] D. P. da Rosa, L. F. Forgiarini, M. B. e Silva et al., "Antioxidants inhibit the inflammatory and apoptotic processes in an intermittent hypoxia model of sleep apnea," *Inflammation Research*, vol. 64, no. 1, pp. 21–29, 2015.

[51] Y. Fang, Q. Zhang, J. Tan, L. Li, X. An, and P. Lei, "Intermittent hypoxia-induced rat pancreatic β-cell apoptosis and protective effects of antioxidant intervention," *Nutrition & Diabetes*, vol. 4, no. 9, p. e131, 2014.

[52] J. R. Skelly, A. Bradford, J. F. X. Jones, and K. D. O'Halloran, "Superoxide scavengers improve rat pharyngeal dilator muscle performance," *American Journal of Respiratory Cell and Molecular Biology*, vol. 42, no. 6, pp. 725–731, 2010.

[53] C. M. Shortt, A. Fredsted, H. B. Chow et al., "Reactive oxygen species mediated diaphragm fatigue in a rat model of chronic intermittent hypoxia," *Experimental Physiology*, vol. 99, no. 4, pp. 688–700, 2014.

[54] K. Sadasivam, K. Patial, V. K. Vijayan, and K. Ravi, "Antioxidant treatment in obstructive sleep apnoea syndrome," *The Indian Journal of Chest Diseases & Allied Sciences*, vol. 53, no. 3, pp. 153–162, 2011.

Hindawi Publishing Corporation
Oxidative Medicine and Cellular Longevity
Volume 2015, Article ID 671839, 9 pages
http://dx.doi.org/10.1155/2015/671839

Research Article

hCLOCK Causes Rho-Kinase-Mediated Endothelial Dysfunction and NF-κB-Mediated Inflammatory Responses

Xiao Tang,[1] Daqiao Guo,[1] Changpo Lin,[1] Zhenyu Shi,[1] Ruizhe Qian,[2] Weiguo Fu,[1] Jianjun Liu,[3] Xu Li,[3] and Longhua Fan[3]

[1]*Institute of Vascular Surgery, Department of Vascular Surgery, Zhongshan Hospital, Fudan University, Shanghai 200032, China*
[2]*Department of Physiology and Pathophysiology, Fudan University Shanghai Medical College, Shanghai 200032, China*
[3]*Department of Vascular Surgery, Qingpu Branch of Zhongshan Hospital, Fudan University, Shanghai 200032, China*

Correspondence should be addressed to Longhua Fan; fanlonghuazs@163.com

Received 16 March 2015; Accepted 21 May 2015

Academic Editor: Manuela Malatesta

Background. The human Circadian Locomotor Output Cycle protein Kaput (CLOCK) gene was originally discovered as a regulator of essential human daily rhythms. This seemingly innocuous gene was then found to be associated with a multitude of human malignancies, via several biochemical pathways. We aimed to further investigate the role of hCLOCK in the hypoxia-oxidative stress response system at the biochemical level. *Methods*. Expression levels of Rho GTPases were measured in normoxic and hypoxic states. The effect of hCLOCK on the hypoxic response was evaluated with the use of a retroviral shRNA vector system, a Rho inhibitor, and a ROS scavenger by analyzing expression levels of hCLOCK, Rho GTPases, and NF-κB pathway effectors. Finally, in vitro ROS production and tube formation in HUVECs were assessed. *Results*. Hypoxia induces ROS production via hCLOCK. hCLOCK activates the RhoA and NF-κB signaling pathways. Conversely, inhibition of hCLOCK deactivates these pathways. Furthermore, inhibition of RhoA or decreased levels of ROS attenuate these pathways, but inhibition of RhoA does not lead to decreased levels of ROS. Overall findings show that hypoxia increases the expression of hCLOCK, which leads to ROS production, which then activates the RhoA and NF-κB pathways. *Conclusion*. Our findings suggest that hypoxic states induce vascular oxidative damage and inflammation via hCLOCK-mediated production of ROS, with subsequent activation of the RhoA and NF-κB pathways.

1. Introduction

The human Circadian Locomotor Output Cycle protein Kaput (CLOCK) gene was originally discovered as a regulator of essential human daily rhythms, as its name implies. The human circadian rhythm encompasses a multitude of physiologic activities, from macroscopic processes such as sleep-wake cycles and core body temperature to molecular mechanisms such as hormone secretion, metabolism, and cell cycle timing [1, 2]. These are all ultimately controlled by a system of feedback loops, with one well-established model describing interactions between the heterodimer transcriptional factors CLOCK and BMAL1, the cryptochromes Cry1 and Cry2, and the period regulator genes Per1, Per2, and Per3 [3]. Of these, CLOCK has been described as the master controller gene. On the other hand, however, some studies have shown that the CLOCK protein is not required for rhythmic gene expression but attributes to robust maximal peak expression levels of rhythmic gene [4–6].

The sphere of influence of CLOCK extends further still, as disruptions in circadian rhythm and defects in circadian rhythm genes are known to be associated with human malignancy. Recent research has described the proneoplastic effects of hCLOCK in brain, breast, colorectal, renal, hepatocellular, and endometrial cancer [7–11]. Despite its seemingly innocent name, hCLOCK operates via multiple pathways related to the regulation of apoptosis, cell proliferation, hormone receptor expression, and hypoxia response.

The hypoxia response in cancer progression has been previously described but has not been studied with particular attention to CLOCK [12]. Broadly speaking, cells respond to hypoxia, pseudohypoxia, or gene mutations by generating reactive oxygen species (ROS) which cause oxidative

damage to DNA. Some of these resultant DNA modifications are involved in the initiation of various cancers [13, 14]. Interestingly, cancer cells themselves must express increased antioxidant protein levels to protect against these same ROS [15]. This introduces a delicate balance between ROS and antioxidant levels that cancer cells need to precisely manage in order to develop and survive. Antineoplastic therapeutic strategies must therefore be tailored accordingly. Additional study of the relationships between hCLOCK and oxidative damage and the inflammatory response is required.

Research over the past decade has discovered new molecular links between the Rho GTPases and the nuclear factor κB (NF-κB) pathway in inflammation [16]. The Rho GTPases are a collection of 20 proteins, most notably RhoA, Rac, and Cdc42, which are widely found within cells and serve to mediate cell spreading, adhesion, and movement. ROCK1 is a major downstream effector of the Rho GTPases, in particular RhoA. These Rho GTPases are regulated by GTPase-activating proteins (GAPs), guanine-nucleotide-exchange factors (GEFs), and guanosine-nucleotide-dissociation inhibitors (GDIs). The NF-κB pathway is a signaling cascade involved in multiple physiologic processes, most notably its close integration with tumor suppressor pathways, its proinflammatory functions, chronic inflammatory, and its role in immune homeostasis [17–20]. Inducers of the NF-κB pathway, such as tumor necrosis factor (TNF), interleukins (IL), and viral and bacterial products such as lipopolysaccharide (LPS), have been shown to induce Toll-like receptor (TLR) signaling and cellular stress, such as DNA damage and hypoxia [19]. Activation of the NF-κB pathway by Rho GTPases was found to increase expression of inflammatory mediators IL-1, collagenase-1 [21], and tumor necrosis factor alpha (TNF-α) [22] and to produce a mutant version of the inflammatory suppressor p120 catenin [23]. Rho GTPases have been shown to inhibit the NF-κB pathways in certain situations as well, when activated by lipopolysaccharide (LPS) and interferon gamma (IFN-γ), disrupting the precise homeostasis of central nervous system inflammation [24].

The intersection between the inflammatory and neoplastic mechanisms of hCLOCK and Rho GTPase/NF-κB therefore carries important potential for application toward future therapeutic strategies. We aimed to further investigate the role of hCLOCK in the hypoxia response and oxidative stress at the biochemical level.

2. Materials and Methods

2.1. Chemicals. A Rho inhibitor allows specific study of this Rho pathway and uncovers alternate pathways of ROS production. A ROS scavenger allows facile manipulation of ROS concentrations. Cell-permeative Rho inhibitor C-3 transferase (CT-04) was purchased from Cytoskeleton (Denver, CO, USA) and dissolved in DMSO to make a 20 μg/mL stock solution. Cells were treated with dilutions of this CT-04 solution for 24 hours prior to analysis. Tiron (4,5-dihydroxy-1,3-benzene disulfonic acid-disodium salt, Sigma, St. Louis, MO, USA), a ROS scavenger, was dissolved in dimethyl sulfoxide (DMSO, final concentration less than 0.1%) to make a 100 mM stock solution. Cells were treated with dilutions of this Tiron solution for 12 hours prior to analysis.

2.2. Cell Culture and Treatment. Human Umbilical Vein Endothelial Cells (HUVECs) were purchased from the American Type Culture Collection (ATCC, Rockville, MD, USA) and maintained in an EGM-2 BulletKit (Lonza, Basel, Switzerland) containing 10% fetal bovine serum, 100 U/mL penicillin, and 100 μg/mL streptomycin.

The Xvivo Closed Incubation System (Xvivo system 300 C, BioSpherix, Lacona, New York, USA) was used in order to accurately maintain different oxygen tensions in different chambers. Cells were grown at 37°C in an atmosphere of 5% CO_2/95% room air. After 24 hours of cultivation in the conventional cell culture, the cells were divided into separate chambers with different oxygen controls for varying periods of time and then harvested for measurement of ROS level and tube formation, as well as Western blotting.

2.3. Preparation of the Retroviral Vector. Retroviruses were used to introduce hCLOCK into the HUVECs and serve as vectors for negative control cells and scrambled control cells.

Stable transfectants overexpressing hCLOCK (GenBank Accession Number: NM_004898) were generated via retroviral transduction using a pGV186 retroviral vector (GeneChem Co., Ltd., Shanghai, China). As a control, a retroviral vector expressing green fluorescent protein alone was also generated.

The short hairpin RNA (shRNA) sequences targeting hCLOCK were constructed using a pGV113 retroviral vector (GeneChem Co., Ltd., Shanghai, China). Scrambled shRNA expressing vectors (SCR) serving as controls were made in a similar fashion.

2.4. Determination of RhoA Activation. RhoA activation was assessed by loading the RhoA protein in cell lysates, using the RhoA Activation Assay Biochem Kit (Cytoskeleton, Denver, CO, USA), based on the method described by Cao et al. [25], whereby cellular GTP-bound RhoA is detected by Western blot after affinity precipitation with a fusion protein containing glutathione-S-transferase (GST) and the Rho-binding domain of Rhotekin (GST-RBD). Briefly, total cellular proteins were extracted and quantitated with a Bradford protein assay (Bio-Rad, Hercules, CA, USA). These proteins were then incubated with 25 μg aliquots of brightly colored glutathione affinity beads coupled to GST-RBD in order to pull down the GTP-bound form of RhoA. RhoA activation was quantitatively analyzed by standard Western blot analysis using anti-RhoA antibody.

2.5. Measurement of Reactive Oxygen Species (ROS) Levels. Reactive oxygen species (ROS) is a term encompassing a variety of reactive molecules and free radicals derived from molecular oxygen. ROS generation in HUVECs was evaluated using the oxidant-sensing 2′,7′-dichlorofluorescein diacetate (DCFH-DA, 5 μM, Invitrogen, Grand Island, NY,

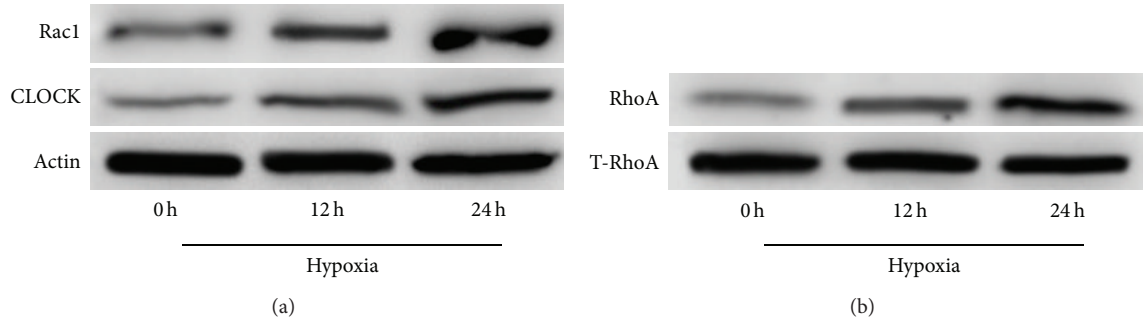

Figure 1: Effect of hypoxia over time on protein expression levels of hCLOCK and RhoA in HUVECs. (a) Western blot analysis was performed to evaluate Rac1 and CLOCK protein expression levels in HUVECs exposed to a hypoxic environment. Expression levels are measured at 0, 12, and 24 hours, normalized to β-actin control. (b) RhoA activation assay and Western blot analysis were performed to measure protein expression levels of activated GTPase-bound RhoA in HUVECs exposed to a hypoxic environment. Expression levels are measured at 0, 12, and 24 hours, normalized to total cellular RhoA.

USA). DCFH-DA is a nonpolar nonfluorescent dye which is converted into the polar, highly fluorescent DCF by cellular esterases in a dose-dependent manner when oxidized by intracellular ROS. The fluorescence intensity of DCFH was measured using a spectrophotometer (Leica, Heidelberg, Germany) at an excitation wavelength of 488 nm and an emission wavelength of 525 nm.

2.6. Tube-Formation Assay. Tube formation in HUVECs is a well-established in vitro assay of angiogenesis reorganization. Compounds inhibiting tube formation could be useful in various inflammatory or neoplastic disease states. Tube formation was assessed in HUVECs among the control normoxic group and the hypoxic scrambled control (SCR) and shCLOCK-transduced groups. HUVECs (2×10^4 per well) were transduced with pGV113-scrambled control (SCR) or pGV113-shRNA-hCLOCK (shCLOCK) and seeded into Matrigel-coated wells of a 24-well plate. Photographs were taken with a Leica DFC290 digital microscope camera (Leica Camera AG, Wetzlar, Germany) 8 hours later.

2.7. Western Blot Analysis. Relative expression levels of hCLOCK, RhoA, Rac1, IL-6, ROCK1, COX2, Phospho-NF-κB p65, and β-actin were measured by Western blotting using standard methods. Anti-Rac1 (ab15880) and anti-hCLOCK (ab98948) antibodies were purchased from Abcam (Cambridge, MA, USA). Anti-IL-6 antibody (21865-1-AP) was purchased from Proteintech (Chicago, IL, USA). Anti-ROCK1 (# 4035), anti-COX2 (# 4842), and anti-Phospho-NF-κB p65 (Ser536, # 3033) antibodies were purchased from Cellsignal (Beverly, MA, USA). Anti-β-actin antibody (sc-47778) was purchased from Santa Cruz Biotechnology (Santa Cruz, CA, USA). Band intensities of RhoA were normalized to the band intensities of the total RhoA. The band intensities of the other proteins were normalized to the band intensity of the cell structural protein β-actin.

2.8. Statistical Analysis. All results reported represent the mean ± SD of at least three experiments performed in triplicate. Statistical comparisons between groups were made using two-tailed t-tests comparing two variables. Differences were considered statistically significant if $p < 0.05$.

3. Results

3.1. Expression Levels of hCLOCK and RhoA Are Increased in a Hypoxic State. We measured the effects of a hypoxic state on expression levels of hCLOCK and the Rho GTPases RhoA and Rac1 in HUVECs via Western blot over a 24-hour period. Relative levels of both Rac1 and hCLOCK were found to increase significantly at both the 12-hour and 24-hour time points in hypoxic environments (Figure 1(a)). Furthermore, levels of RhoA GTPase increased with time exposed to hypoxia as well, when normalized to total RhoA (T-RhoA) (Figure 1(b)). These findings demonstrate that hCLOCK and RhoA are both involved in the hypoxic response and form the fundamental basis of the remainder of this study.

3.2. Hypoxia Induces ROS Production via hCLOCK and Inhibits HUVEC Tube Formation. We then reconfirmed the hypoxia response by quantifying ROS production and HUVEC tube formation. A control HUVEC group in normoxic conditions was transduced with a control retroviral vector as described previously and served as a baseline for comparison of ROS levels. Two hypoxic HUVEC groups were transduced with scrambled (SCR) and hCLOCK knockdown (shCLOCK) retroviral vectors. Relative ROS levels were determined with DCFH analysis (Figure 2(b)). Tube formation was visualized with a digital microscope camera. Efficacy of hCLOCK knockdown via shCLOCK transduction is shown in Figures 2(a) and 2(d). Following transduction with the scrambled retroviral vector (SCR) in a hypoxic environment, DCFH analysis shows a statistically significant increase in relative ROS levels in HUVECs when compared to the normoxic control ($p < 0.01$, Figure 2(b)). Tube formation in this group was significantly decreased ($p < 0.01$, Figure 2(c)). Interestingly though, relative ROS levels of the cells in the hypoxic environment transduced with the hCLOCK knockdown retroviral vector (shCLOCK) resulted in ROS levels significantly less than the SCR group ($p < 0.05$,

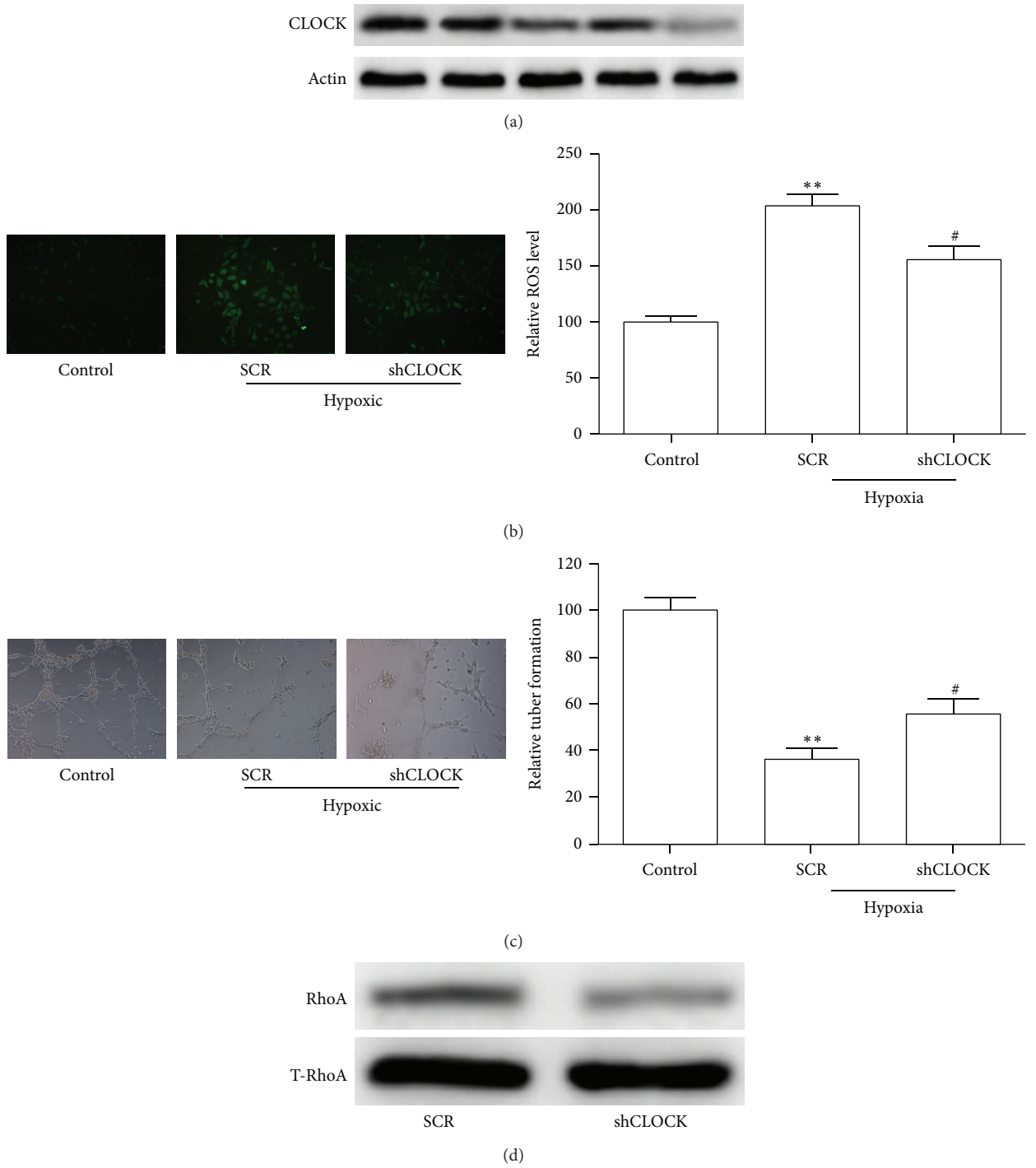

Figure 2: Effect of knockdown of hCLOCK on ROS production, tube formation, and RhoA activity. (a) Western blot analysis was performed to confirm successful knockdown of hCLOCK. (b) Representative images obtained during analysis of fluorescence intensity, comparing ROS levels with and without knockdown of hCLOCK. The control HUVEC group was kept in normoxic conditions and was transduced with a control retroviral vector. The SCR HUVEC group was exposed to hypoxic conditions and was transduced with a scrambled control retroviral vector. The shCLOCK HUVEC group was exposed to hypoxic conditions and transduced with an hCLOCK knockdown retroviral vector. Bar graph shows relative ROS levels normalized to the normoxic control group. $^{**}p < 0.01$ compared to control; $^{\#}p < 0.05$ compared to SCR. (c) Photographs obtained during tube-formation assay comparing tube-formation levels in HUVECs with and without knockdown of hCLOCK. Bar graph quantifies relative tube-formation levels. $^{**}p < 0.01$ compared to control; $^{\#}p < 0.05$ compared to SCR. (d) Western blot analysis showing activated RhoA normalized to total RhoA in HUVECs with and without knockdown of hCLOCK.

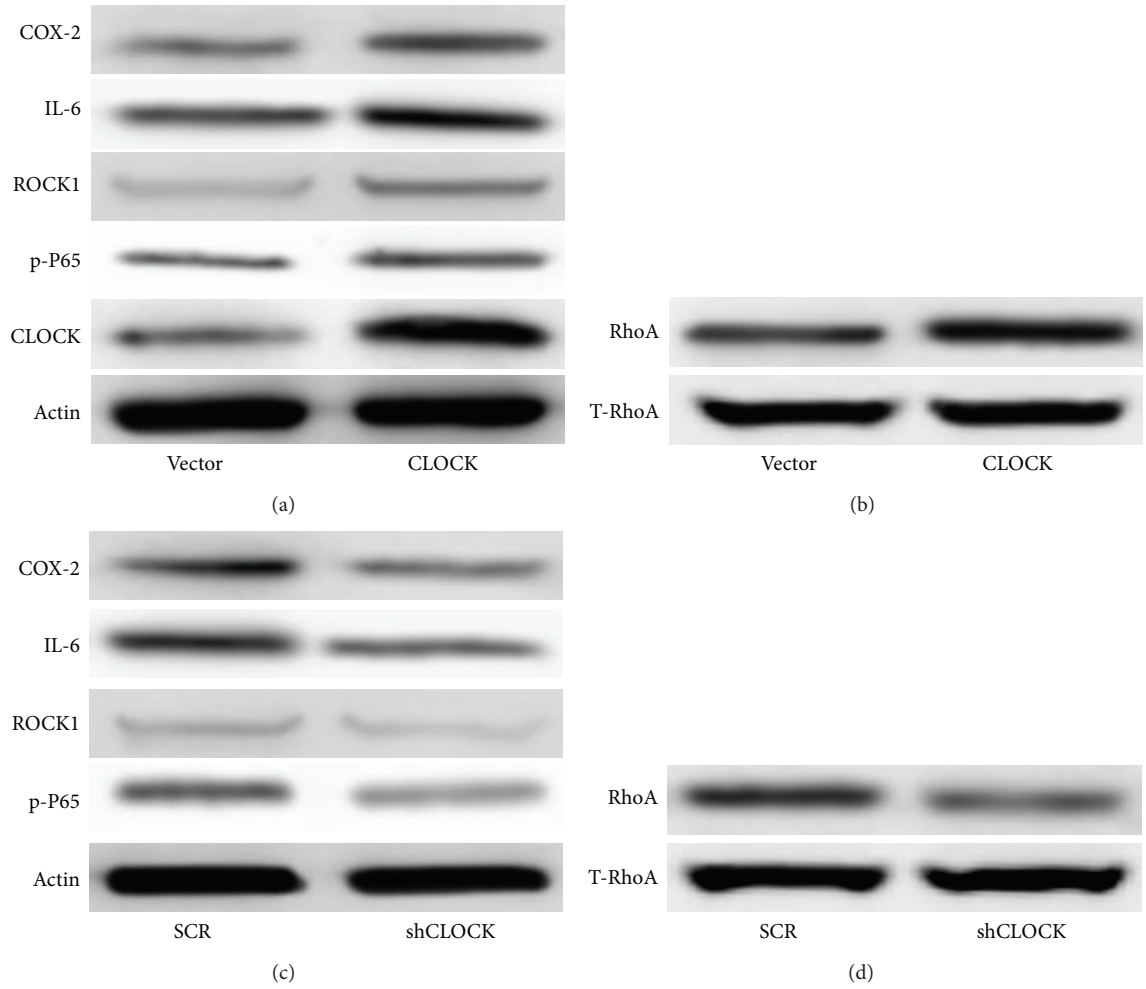

Figure 3: Induction of the RhoA and NF-κB pathways by hCLOCK. (a) Western blot analysis of RhoA pathway effector ROCK1 and NF-κB pathway effectors COX-2, IL-6, and p-P65 in HUVECs transduced with control vector or hCLOCK-overexpressing vector. Expression levels are normalized to β-actin. (b) Western blot analysis showing activated RhoA normalized to total RhoA in HUVECs transduced with control vector or hCLOCK-overexpressing vector. (c) Western blot analysis of the same RhoA and NF-κB pathway effectors in HUVECs transduced with scrambled control vector or shCLOCK vector. (d) Western blot analysis showing activated RhoA normalized to total RhoA in HUVECs transduced with scrambled control vector or shCLOCK vector.

Figure 2(b)), though still higher than control levels. Relative tube formation was significantly higher than the SCR group ($p < 0.05$, Figure 2(c)). These findings directly implicate hCLOCK in the pathway of ROS production as well as the more physiologic measure of tube-formation inhibition.

3.3. hCLOCK Activates the RhoA and NF-κB Signaling Pathways in HUVECs. We performed initial testing of our hypothesis that CLOCK activates the RhoA and NF-κB signaling pathways by overexpressing hCLOCK and observing downstream protein levels. Knowing that hypoxia induces ROS production, we conducted all following experiments under hypoxic conditions. Expression levels of key proteins in the RhoA and NF-κB signaling pathways were measured via Western blot in HUVEC groups which were transduced with either a control retroviral vector or an hCLOCK-overexpressing retroviral vector. Protein expression levels of hCLOCK itself were observed, confirming proper technique. COX-2, IL-6, and p-P65, major effectors in the NF-κB signaling pathway, were significantly upregulated in the HUVEC group transduced with the hCLOCK-overexpressing vector, compared to control (Figure 3(a)). Likewise, ROCK1 and RhoA, key proteins in the RhoA pathway, were significantly upregulated in the cell group transduced with the hCLOCK-overexpressing vector, compared to control (Figures 3(a) and 3(b)). These findings confirm that CLOCK is involved in the RhoA and NF-κB signaling pathways, key pathways in tumorigenesis, and the inflammatory response.

3.4. Inhibition of hCLOCK Deactivates the RhoA and NF-κB Signaling Pathways in HUVECs. We then sought to confirm a direct relationship between hCLOCK and the RhoA and NF-κB signaling pathways. Inhibition of hCLOCK was performed to evaluate this converse association. Expression levels of the same key proteins in these pathways were measured via Western blot following transduction of HUVECs with

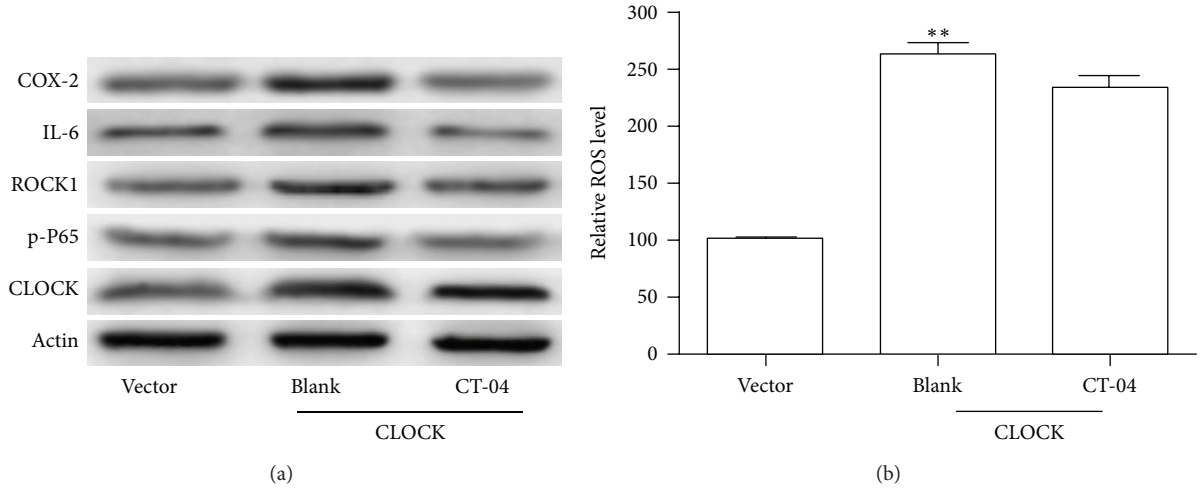

Figure 4: Induction of the NK-κB pathway by RhoA. (a) Western blot analysis of RhoA pathway effector ROCK1 and NF-κB pathway effectors COX-2, IL-6, and p-P65 in HUVECs overexpressing hCLOCK and exposed to 5 μg/mL RhoA inhibitor CT-04 or control solution for 24 hours. Vector control group consists of HUVECs transduced with control retroviral vector exposed to control solution. (b) Bar graph showing relative ROS levels in the same HUVEC groups. $^{**}p < 0.01$ compared to vector control.

the shCLOCK (hCLOCK knockdown) vector. These results were then compared to protein expression levels in HUVECs transduced by a scrambled control retroviral vector.

We found that all of the key effector proteins previously examined, COX-2, IL-6, p-P65, ROCK1, and RhoA, were significantly downregulated by transduction of shCLOCK, compared to control (Figures 3(c) and 3(d)), thus identifying hCLOCK as directly involved in the activation of the RhoA and NF-κB signaling pathways.

3.5. Inhibition of RhoA Attenuates hCLOCK-Induced p-P65, ROCK1, IL-6, and COX-2 Expression but Not ROS Production. We subsequently targeted the RhoA signaling pathway to discern whether downstream effectors were suppressed with inhibition of RhoA itself. We examined HUVECs transduced with the hCLOCK-overexpressing vector, exposed to either cell-permeative Rho inhibitor C-3 transferase (CT-04) or blank solution. The control hCLOCK-overexpressing group expressed higher levels of the RhoA and NF-κB pathway effectors as expected. When the hCLOCK-overexpressing HUVECs were exposed to the Rho inhibitor (CT-04) solution, however, all of the previously overexpressed effector proteins were found to be downregulated (Figure 4(a)). These findings proved that inhibition of hCLOCK attenuates the production of the RhoA and NF-κB pathway effectors COX-2, IL-6, p-P65, and ROCK1. We then sought to examine the effects of hCLOCK on ROS production.

The hCLOCK-overexpressing cell group which was exposed to blank solution produced 2.5-fold more ROS than the control vector group ($p < 0.01$), as expected (Figure 4(b)). Interestingly, however, the hCLOCK-overexpressing cell group exposed to the Rho inhibitor (CT-04) produced a similar amount of ROS compared to the noninhibited group (Figure 4(b)). This interesting result shows that while inhibition of RhoA attenuates the RhoA and NF-κB pathway effectors, it does not in fact suppress the production of ROS. This suggests that ROS may either have a place in the overall signaling pathway upstream of RhoA or have a separate pathway.

3.6. The hCLOCK-Induced RhoA and NF-κB Pathways Are Inhibited in the Presence of a ROS Scavenger. In order to answer the question raised by the previous experiment, we decided to target ROS and reveal its role in the hypoxic response. We used Tiron, a ROS scavenger, to reduce cellular ROS levels and examine the effects on downstream proteins. We conducted this experiment with three groups: (1) HUVECs transduced with control GFP vector and treated with control solution, (2) HUVECs transduced with hCLOCK-overexpressing vector and treated with control solution, and (3) HUVECs transduced with hCLOCK-overexpressing vector and treated with Tiron solution. Similar to the prior experiment, the hCLOCK-overexpressing group treated with control solution expressed increased levels of COX-2, IL-6, p-P65, RhoA, and ROCK1 (Figures 5(a) and 5(b)). When the hCLOCK-overexpressing HUVECs were treated with Tiron solution, however, they expressed decreased protein levels of all of these downstream effectors. Our finding that decreased ROS levels inhibit the RhoA and NF-κB pathways, while inhibition of RhoA inhibits these same pathways without significantly altering ROS levels, further elucidates the hCLOCK-induced hypoxic response pathway. We have determined that hypoxia increases the expression of hCLOCK, which leads to ROS production, which then activates the RhoA and NF-κB pathways (Figure 6).

4. Discussion

We hereby describe the hCLOCK-induced hypoxia response pathway, which leads to a Rho GTPase and NF-κB mediated endothelial inflammatory response. Specifically, this study

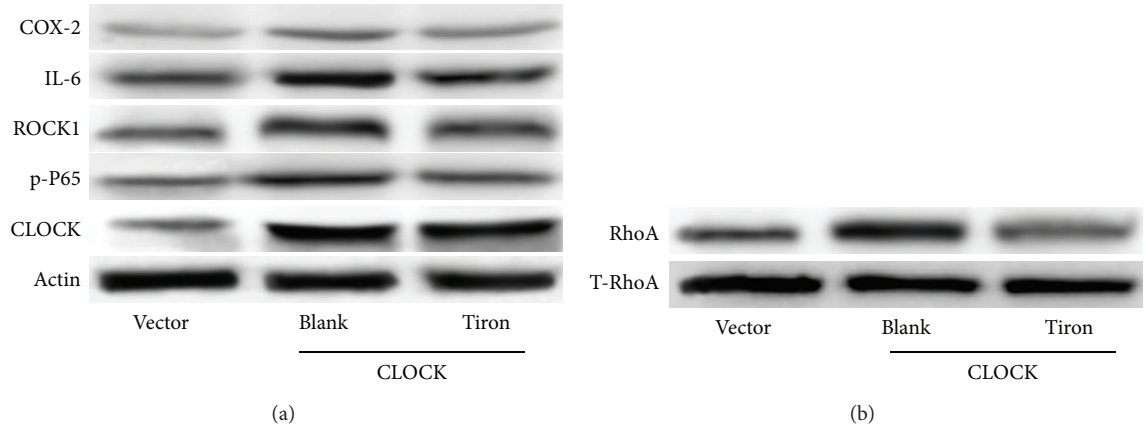

Figure 5: Effect of ROS levels on RhoA and NF-κB pathways. (a) Western blot analysis of RhoA pathway effector ROCK1 and NF-κB pathway effectors COX-2, IL-6, and p-P65 in HUVECs overexpressing hCLOCK and treated with either 10 μM Tiron or control solution for 12 hours. Vector control group consists of HUVECs transduced with control retroviral vector exposed to control solution. (b) Western blot analysis of activated RhoA normalized to total RhoA in HUVECs overexpressing hCLOCK and treated with either 10 μM Tiron or control solution for 12 hours. Vector control group consists of HUVECs transduced with control retroviral vector exposed to control solution.

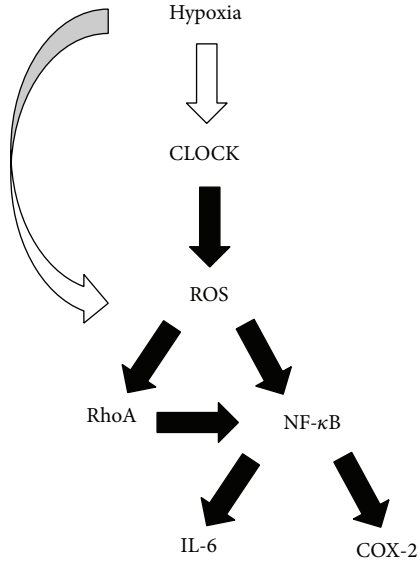

Figure 6: Proposed signaling pathway of the hCLOCK-induced hypoxia response. hCLOCK is the primary inducer of the hypoxia response, leading to ROS production, which in turn induces the RhoA and NF-κB signaling pathways and upregulates key downstream inflammatory effectors IL-6 and COX-2.

finds that (1) expression levels of hCLOCK and RhoA are increased in a hypoxic state, (2) hypoxia induces ROS production via hCLOCK and inhibits HUVEC tube formation, (3) hCLOCK activates the RhoA and NF-κB signaling pathways in HUVECs, (4) inhibition of hCLOCK deactivates the RhoA and NF-κB signaling pathways in HUVECs, (5) inhibition of RhoA attenuates hCLOCK-induced p-P65, ROCK1, IL-6, and COX-2 expression, but not ROS production, and (6) the hCLOCK-induced RhoA and NF-κB pathways are inhibited in the presence of a ROS scavenger. Briefly, hypoxia increases the expression of hCLOCK, which leads to ROS production, which then activates the RhoA and NF-κB pathways.

We pursued these particular pathways on the basis of several areas of prior research linking hCLOCK with the hypoxia response, and the hypoxia and inflammatory responses with tumorigenesis. Additionally, the Rho GTPases and the NF-κB pathway had both been implicated in the inflammatory response. We sought to find the intersection between these pathways.

Our initial experiments confirmed the initial link in the hCLOCK-induced hypoxia response pathway, that hypoxic conditions increase both hCLOCK and RhoA levels. All further experiments were carried out under hypoxic conditions. The hypoxic response pathways are myriad, though hCLOCK had not previously been definitively characterized.

The biochemical involvement of hCLOCK in ROS production has not previously been characterized. By knocking down hCLOCK via a shCLOCK retroviral vector, we confirmed that the hypoxic response of ROS production was mediated by hCLOCK. This resulted in a significant decrease in ROS levels. These findings suggest that although hCLOCK may not be the sole mediator of ROS production, it plays a major role and is thereby a potential target for future research or therapy.

As prior research had shown a link between the Rho GTPases and the NF-κB pathways and the inflammatory response, we then turned our attention to the effectors in these pathways. RhoA and ROCK1, the major effectors in the RhoA pathway, as well as COX-2, IL-6, and p-P65, the major effectors in the NF-κB pathway, were found to be upregulated by hCLOCK. These effectors of both pathways were downregulated with knockdown of hCLOCK, inhibition of RhoA, or decrease in ROS levels.

The ROS scavenger we used, Tiron, is known to also bind metals including iron, copper, uranium, vanadium, beryllium, and chromium; thus it is conceivable that off-target effects may have confounded our study [26]. Of these metals, only iron and copper would be reasonably expected in HUVECs. Copper has previously been shown to activate the NF-κB pathway; however it achieves this via the production

of ROS, similar to hCLOCK [27]. Our shCLOCK knockdown targeted specifically at hCLOCK causes inhibition of this pathway, demonstrating that the two inducers, copper and hCLOCK, have similar though independent roles in inducing ROS production.

The RhoA and NF-κB pathways each have their own profound spheres of influence within the grand world of human biology and are brought together with hCLOCK in the hypoxic inflammatory response. To date, research has been performed on multiple links in a complex chain of biochemical pathways ultimately connecting regulators such as hCLOCK with inflammation and tumorigenesis. Our novel characterization of the hCLOCK-induced hypoxia response helps to complete this chain.

In conclusion, hCLOCK induces Rho GTPase mediated endothelial dysfunction and NF-κB mediated inflammatory responses. This study provides novel insight into the hypoxia response and we hope that these findings may help further elucidate some aspects of the complex biology of inflammation and tumorigenesis.

Conflict of Interests

The authors declare that they have no conflict of interests.

Authors' Contribution

Xiao Tang and Daqiao Guo contributed equally to this paper.

References

[1] B. Paul, K. R. Saradalekshmi, A. M. Alex, and M. Banerjee, "Circadian rhythm of homocysteine is hCLOCK genotype dependent," *Molecular Biology Reports*, vol. 41, no. 6, pp. 3597–3602, 2014.

[2] D. Katzenberg, T. Young, L. Finn et al., "A CLOCK polymorphism associated with human diurnal preference," *Sleep*, vol. 21, no. 6, pp. 569–576, 1998.

[3] M. Doi, J. Hirayama, and P. Sassone-Corsi, "Circadian regulator CLOCK is a histone acetyltransferase," *Cell*, vol. 125, no. 3, pp. 497–508, 2006.

[4] K. Kume, M. J. Zylka, S. Sriram et al., "mCRY1 and mCRY2 are essential components of the negative limb of the circadian clock feedback loop," *Cell*, vol. 98, no. 2, pp. 193–205, 1999.

[5] M. K. Bunger, L. D. Wilsbacher, S. M. Moran et al., "Mop3 is an essential component of the master circadian pacemaker in mammals," *Cell*, vol. 103, no. 7, pp. 1009–1017, 2000.

[6] J. P. DeBruyne, E. Noton, C. M. Lambert, E. S. Maywood, D. R. Weaver, and S. M. Reppert, "A clock shock: mouse CLOCK is not required for circadian oscillator function," *Neuron*, vol. 50, no. 3, pp. 465–477, 2006.

[7] Z. Chen, P. Liu, C. Li et al., "Deregulated expression of the clock genes in gliomas," *Technology in Cancer Research and Treatment*, vol. 12, no. 1, pp. 91–97, 2013.

[8] A. E. Hoffman, C.-H. Yi, T. Zheng et al., "CLOCK in breast tumorigenesis: genetic, epigenetic, and transcriptional profiling analyses," *Cancer Research*, vol. 70, no. 4, pp. 1459–1468, 2010.

[9] G. Mazzoccoli, A. Piepoli, M. Carella et al., "Altered expression of the clock gene machinery in kidney cancer patients," *Biomedicine and Pharmacotherapy*, vol. 66, no. 3, pp. 175–179, 2012.

[10] Y.-M. Lin, J. H. Chang, K.-T. Yeh et al., "Disturbance of circadian gene expression in hepatocellular carcinoma," *Molecular Carcinogenesis*, vol. 47, no. 12, pp. 925–933, 2008.

[11] K. T. Yeh, M. Y. Yang, T. C. Liu et al., "Abnormal expression of period 1 (PER1) in endometrial carcinoma," *Journal of Pathology*, vol. 206, no. 1, pp. 111–120, 2005.

[12] S. S. Sabharwal and P. T. Schumacker, "Mitochondrial ROS in cancer: initiators, amplifiers or an Achilles' heel?" *Nature Reviews Cancer*, vol. 14, no. 11, pp. 709–721, 2014.

[13] G. Waris and H. Ahsan, "Reactive oxygen species: role in the development of cancer and various chronic conditions," *Journal of Carcinogenesis*, vol. 5, article 14, 2006.

[14] W.-L. Lee, J.-Y. Huang, and L.-F. Shyur, "Phytoagents for cancer management: regulation of nucleic acid oxidation, ROS, and related mechanisms," *Oxidative Medicine and Cellular Longevity*, vol. 2013, Article ID 925804, 22 pages, 2013.

[15] J. A. Saunders, L. C. Rogers, C. Klomsiri, L. B. Poole, and L. W. Daniel, "Reactive oxygen species mediate lysophosphatidic acid induced signaling in ovarian cancer cells," *Free Radical Biology and Medicine*, vol. 49, no. 12, pp. 2058–2067, 2010.

[16] L. Tong and V. Tergaonkar, "Rho protein GTPases and their interactions with NFκB: crossroads of inflammation and matrix biology," *Bioscience Reports*, vol. 34, no. 3, pp. 283–295, 2014.

[17] N. D. Perkins, "The diverse and complex roles of NF-κB subunits in cancer," *Nature Reviews Cancer*, vol. 12, no. 2, pp. 121–132, 2012.

[18] M. Pasparakis, "Regulation of tissue homeostasis by NF-kappaB signalling: implications for inflammatory diseases," *Nature Reviews Immunology*, vol. 9, no. 11, pp. 778–788, 2009.

[19] U. C. S. Yadav and K. V. Ramana, "Regulation of NF-kappaB-induced inflammatory signaling by lipid peroxidation-derived aldehydes," *Oxidative Medicine and Cellular Longevity*, vol. 2013, Article ID 690545, 11 pages, 2013.

[20] E. S. Williams, E. Wilson, and K. S. Ramos, "NF-κB and matrix-dependent regulation of osteopontin promoter activity in allylamine-activated vascular smooth muscle cells," *Oxidative Medicine and Cellular Longevity*, vol. 2012, Article ID 496540, 10 pages, 2012.

[21] F. Kheradmand, E. Werner, P. Tremble, M. Symons, and Z. Werb, "Role of rac1 and oxygen radicals in collagenase-1 expression induced by cell shape change," *Science*, vol. 280, no. 5365, pp. 898–902, 1998.

[22] R. Perona, S. Montaner, L. Saniger, I. Sánchez-Pérez, R. Bravo, and J. C. Lacal, "Activation of the nuclear factor-κB by Rho, CDC42, and Rac-1 proteins," *Genes & Development*, vol. 11, no. 4, pp. 463–475, 1997.

[23] M. Perez-Moreno, M. A. Davis, E. Wong, H. A. Pasolli, A. B. Reynolds, and E. Fuchs, "p120-catenin mediates inflammatory responses in the skin," *Cell*, vol. 124, no. 3, pp. 631–644, 2006.

[24] R. Rattan, S. Giri, A. K. Singh, and I. Singh, "Rho a negatively regulates cytokine-mediated inducible nitric oxide synthase expression in brain-derived transformed cell lines: negative regulation of IKKα," *Free Radical Biology and Medicine*, vol. 35, no. 9, pp. 1037–1050, 2003.

[25] X. Cao, C. Voss, B. Zhao, T. Kaneko, and S. S.-C. Li, "Differential regulation of the activity of deleted in liver cancer 1 (DLC1) by tensins controls cell migration and transformation," *Proceedings of the National Academy of Sciences of the United States of America*, vol. 109, no. 5, pp. 1455–1460, 2012.

[26] A. Al Maruf and P. O'Brien, "Flutamide-induced cytotoxicity and oxidative stress in an *in vitro* rat hepatocyte system," *Oxidative Medicine and Cellular Longevity*, vol. 2014, Article ID 398285, 9 pages, 2014.

[27] T. Persichini, Z. Percario, E. Mazzon, M. Colasanti, S. Cuzzocrea, and G. Musci, "Copper activates the NF-κB pathway in vivo," *Antioxidants and Redox Signaling*, vol. 8, no. 9-10, pp. 1897–1904, 2006.